STUDY ON EFFECT OF CLIMATE CHANGE ON SEDIMENT YIELD TO PONG RESERVOIR

Final report

NATIONAL INSTITUTE OF HYDROLOGY
JALVIGYAN BHAWAN
ROORKEE - 247667 (UTTARAKHAND)
2019-2020

Director	**Dr. S. K. Jain**
Division	**Research Management and Outreach Division**
Divisional Head	**Dr. V. C. Goyal, Scientist-G**

STUDY TEAM

Principal Investigator	**Dr. A. R. Senthil Kumar, Scientist-F, RMOD**
Other members of Study Team	**i) Dr. J. V. Tyagi, Sc "G", SWHD** **ii) Dr. Suhas Khobragade, Sc "F", HID** **iii) Dr. Manohar Arora, Sc "D", WRSD** **iv) Sh. R. K. Nema, Sc "B", EHD** **v) Sh. Rohtash, JRF, RMOD**

ABSTRACT

Materials resulting from upland catchments and bedrock through physical and chemical weathering processes are the main supply for sediments. Soil erosion can be induced by natural or manmade activities. Natural erosion is due to landslides, tsunami, earthquakes and floods. Human-induced erosion is due to poor irrigation, improper agriculture practices and deforestation etc. Improper agricultural practices comprise too much tillage operation, make use of heavy cultivator machinery and poor crop cycle scheduling. Erosion accelerates two kinds of problem, one is on-site and another is off-site. On-site effects mainly refer to agricultural and economic losses. The most significant off-site effect of soil erosion is loss of water storage capacity, because of sediment deposition in a reservoir. So, Soil erosion is the major cause of land degradation and reservoir sedimentation. The estimation of sediment yield from watershed is very important for ascertaining the useful life of reservoir for meeting its intended purposes. The sediment process in a watershed is highly random and depends upon the characteristics of basin and river which include climate, land slope and topography, land cover and pattern of land use. The sediment process in the watershed will be increased because of the increase in rainfall intensity due to increased anthropogenic emissions of green house gases. It is imperative to study the effect of climate change on sediment yield to Pong reservoir as the Himalayan watersheds generate more sediment in general.

Climatic variability is multifarious phenomenon of its behavior that is directly associated with uncertainties. Climate describes the average weather conditions of a certain area. In hydrological aspects point of view in the climate change study, it is necessary to identify the input parameters i.e. predictors which is directly or indirectly associated with predictands. The forecasted results are directly associated with the selection of predictors.

The main objective of the study is to develop hydrological model to estimate runoff and sediment yield using SWAT (Soil and Water Assessment Tool) as well as to investigate the impact of likely future changes in climate on sediment yield up to Pong dam using future climatic scenarios. The runoff and sediment yield can be modelled efficiently by Soil and Water Assessment Tool (SWAT) provided all required data are available. Conceptual, distributed and

continuous time, SWAT, 2012 (Soil and Water Assessment Tool) model was selected for the simulation of the runoff and sediment yield from the Beas river basin up to Nadaun bridge, (Pong reservoir, Himachal Pradesh). The input data such as DEM, LULC and soil type were generated from different sources such as National Aeronautics and Space Administration (NASA), USA, Landsat 8 OLI, USGS and National Bureau of Soil Survey and Land Use Planning (NBSSLUP), India. Grid based meteorological data such as daily rainfall, minimum and maximum temperatures were obtained from Indian Meteorological Department (IMD). The model was calibrated using the data of stream flow and sediment yield for the period from 1987 to 1995 and validated with data for the period from 1996 to 2005. The sensitive parameters for streamflow and sediment yield were optimized by SUFI2 algorithm (Sequential Uncertainty Fitting version 2). The simulated values of sediment yield were found to be in good agreement with the observed values. The performance of the model was evaluated on the basis of statistical parameters. The values of coefficient of determination (R^2) for streamflow and sediment yield were found to be 0.82 and 0.64 for calibration period and 0.76 and 0.61 for validation period.

The statistical downscaling model (SDSM) was used to downscale the daily rainfall, minimum and maximum temperature for the location, Nadaun Bridge, Himachal Pradesh from General Circulation Model (GCM) Coupled Model Intercomparison Project Phase 5 (CMIP5): Canadian Earth System Model, CanESM2. In SDSM, the multiple linear regression (MLR) technique was used to derive the statistical relationships between observed small-scale variables and larger GCM scale. The daily rainfall, minimum temperature and maximum temperature data of Indian Meteorological Department (IMD) (1961-2005) of the Nadaun Bridge, Himachal Pradesh was considered as input to the model. This daily rainfall, minimum and maximum temperature data were predictands for the SDSM model. The MLR model was calibrated and validated with the daily rainfall, minimum and maximum temperature for the period of 1961 to1995 and 1996 to 2005 respectively. National Centre for Environmental Prediction (NCEP) reanalysis data (historical) were used as a predictor, which consists of 26 parameters. Monthly rainfall was predicted on the basis of future daily rainfall by MLR model with the predictors from CanESM2 for the period from 2006 to 2100 under the RCP 2.6, RCP 4.5and RCP 8.5 emission scenarios. The same procedure was adopted for the downscaling of the minimum and maximum temperature for the period from 2006 to 2100 under the RCP 2.6, RCP 4.5 and RCP

8.5 emission scenarios. The monthly streamflow and sediment yield for the period from 2006 to 2100 were projected using the monthly projected rainfall, minimum and maximum temperature under the RCP 2.6, RCP 4.5 and RCP 8.5 emission scenarios and the other meteorological data from SWAT website with optimized parameters for streamflow and sediment yield obtained from SWAT-CUP using the hydrometeorological data for the period from 1987 to 2005. The unit weight of deposited sediment in the reservoir was computed from particle size distribution of suspended sediment concentration and the method of reservoir operation by the procedure suggested by USBR, from the sediment volume observed by hydrographic survey and assuming porosity of uniformly distributed sediment in the reservoir. The consolidated unit weights of the sediment were computed by the equation proposed by Miller of USBR and frequency analysis of unit weights derived from particle size distribution. The consolidated unit weights computed by different methods were used to project the sediment volume and the life of the reservoir for the climate scenarios RCP 2.6, RCP 4.5 and RCP 8.5 for 2025, 2050, 2075 and 2100.

Chapter 1 Introduction

1. General

Soil is an important ecosystem component on which all primary productions depend. It has been identified by the International Soil Science Society as a "limited and irreplaceable resource", with natural formation processes requiring 200-400 years to build up 1 cm of top soil (Singh & Phadke, 2006). In India, about 5334 M-tons of soil are being removed annually due to various reasons like soil erosion, excess use of fertilizers and improper irrigation (CSWCRTI, Dehradun). Soil erosion is recognized as a hazard which is more serious in hilly and mountains areas by assessment policy for sustainable agriculture and development. Soil erosion is removal and transportation of soil particles from their original place to further downstream by erosion agents such as water and wind etc. Today, soil erosion is universally recognized as a major environmental and agricultural problem.

Generally, Soil Erosion accelerates two kinds of problems one is on-site and the other off-site. An on-site problem refers to less agricultural productivity and economic losses. The most serious off-site effect of soil erosion is loss of water storage capacity because of sediment deposition in a reservoir. Reservoirs are the main destination of the sediment eroded from upland catchment area. The process of sediments getting deposited in full depth of reservoir is known as sedimentation of reservoir. Sedimentation of a reservoir is natural phenomenon and High sediment rates leads to filling of reservoirs and loss of live storage, which eventually leads to loss of production potential. Furthermore, excavation of sediments from reservoirs is a costly process that can have large environmental impacts. Therefore, assessment and prevention of on-site and off-site erosion problems becomes important. Over the past two decades the focus of scientific investigation is on the impact of climate change on water resources and corresponding counter steps against climate change (Xu et al. (2005) and Jiang et al. (2007)). Future hydrological processes need to be assessed due to the socio-economic importance of water resources. According to some existing studies the historical data and their trends are used to predict future climate scenario (Araujo and New, 2007). General Circulation Models (GCMs) used to predict future climate scenarios have been followed as the important mechanism for accessing the future climate data (Bates et al., 2008; Whitehead et al., 2009)), and many researchers have applied it for new investigation (Mo et al., 2013; Zhang et al., 2011). Future

climate change has a clear impact on hydrological processes, soil water content and vegetation evapotranspiration in arid and semi-arid regions((Brown and Rosenberg, 1994)). The Pong reservoir is major water infrastructure for irrigation, water supply and power generation to the states, Himachal Pradesh, Punjab, Haryana and Rajasthan. The climate of area surrounded Pong reservoir is sub-tropical with monsoons in the months of July to September. The water resource plays an important role for territorial development of the villages nearby Pong dam depends primarily on agriculture for their income as well as has got a big business community mostly involved in small to medium size businesses. Therefore, the research of the influence of future climate change on hydrological process in this region is important.

Hydrological modelling is a powerful technique of hydrologic system investigation for both the research hydrologists and the practicing water resources engineers involved in the planning and development of integrated approach for management of water resources (Schultz, G.A., 1993).The study evaluate the possible influence of climate change on discharge and sediment yield of Beas river basin up to Pong dam using Geographical Information System (GIS) and hydrological modelling tools, namely ,Soil and Water Assessment Tool (SWAT). To run the model, the required spatial input data layers are Digital Elevation model (DEM), land use data, soil data and weather data. The DEM used to delineate boundary of the watershed and analyze the drainage patterns of the terrain was obtained from the global U.S. Geological Survey (USGS) in the format of SRTM (Shuttle Radar Topography Mission) with a spatial resolution of 30 m x 30 m. The DEM was used to derive slope gradient, slope length and stream network characteristics such as channel slope, length and width. Whereas soil properties were prepared from National Bureau of Soil Survey and Land Use Planning (NBSSLUP) map at 1:250,000 scale. Model calibration and uncertainty analysis performed by SUFI-2 have the potential to examine a large number of parameters and observed data obtained by many gauging stations simultaneously and the same was considered in this study . For achieving good calibration and uncertainty results ArcSWAT requires less number of model run and can be easily linked to SWAT-CUP through an interface.

1.1 Statement of the Problem

The developmental activities in the catchment area contribute high sediment load which affects the expected performance of the reservoir. Increase of anthropogenic emissions of green house gases will aggravate climate change and thus average temperature of atmosphere, no of extreme events of rainfall and intensity will increase. In Himalayan region, the increase in high intensity rainfall will contribute more sediment to the reservoir. The development of a procedure is imperative to assess future sediment rates and the life of the Pong reservoir on the account of climate change which will help reservoir authorities in planning for irrigation, water supply, flood control and hydro power generation in future.

The sedimentation in the reservoir is a continuous process and it reduces the performance of the reservoir slowly in meeting the demands over the time during the life of the reservoir (Morris and Fan, 1997). Survey of Indian reservoirs shows that sediment yield from the catchment due to unpredicted land use changes has been many fold than the sediment inflow considered during the design of the reservoirs (Tejwani, 1984). Consideration of sediment yield from the catchment area over the life period of the reservoir in view of the high sediment inflow has become important to evolve future operating policy to maximize the benefits from the water releases for various sectors.

The recent IPPC's summary report for policymakers confirms the human interference with the climate system based on the data of anthropogenic emissions of green house gases observed for many decades (IPCC WGII AR5, 2014). Increased level of green house gases in the atmosphere has increased average surface temperature of the earth and it will continue to increase in the 21st century. Increased average surface temperature results in extreme events and high intensity of precipitation. The high intensity rainfall will dislodge the sediment and generate more sediment from the catchment and the sediment will get deposited in the reservoir in due course. So it is imperative to estimate the sediment yield at the upstream of Pong reservoir under different future climate scenarios considered by the IPCC summary report and the elevation-area-capacity will be revised by considering the increased sediment yield.

1.2 Soil Erosion Process and Types:

In India, the soil erosion is observed to be more severe in, Northeastern states, Himalayan ranges and Western Ghats which are affected by serious soil erosion due to improper irrigation, excessive use of fertilizer, pesticide and crop growing pattern. India has about 2.45% of global geographic land area, which is 329 million hectares (Mha), among that, 147 Mha of land is affected by soil degradation. According to global assessment of human induced soil degradation, 32.8 Mha area is affected by water erosion in India. The extent of water erosion in India is presented in Table 1.1. The National Bureau of Soil Survey & Land Use Planning (NBSS&LUP, 2005) has given the state wise extent of soil erosion due to wind as well as water. The total extant of water erosion in India as per NBSS&LUP, (2005) is 93.68 Mha.

Table 1.1 Water erosion in India

Region	Light Mha	Moderate Mha	Strong Mha	Total Mha
India	**2.936**	**17.217**	**12.620**	**32.773**
India, dry region	**1.177**	**0**	**1.676**	**2.853**
India, humid region	**1.759**	**17.217**	**10.944**	**29.920**

Soil erosion is caused by detachment and removal soil particles from land surface. It has been classified based on natural occurrence of erosion namely geologic erosion and accelerated erosion. Geologic erosion of soil is caused due to effects of rainfall, runoff, topography, velocity and gravity. Accelerated erosion of soil is caused mainly due to by improper management practices such as raising crops without adopting any soil conservation measures, deforestation etc. The process of soil erosion consists of two main stages namely detachment of soil particle and their transportation. The principle agents responsible for these two stages of activities are wind, water and gravity.

1.2.1 Wind Erosion

When the soil particles are transported by the forces of moving wind, it known as wind erosion. In regions where precipitation is low and the velocity of wind is high invariably, the erosion is very high. Such climatic conditions are generally common in semiarid and arid

regions. For example in India, Rajasthan state, wind erosion is higher than in Jammu &Kashmir etc.

1.2.2 Water Erosion

Erosion of soil by water is caused by liquid (water) and solid (glaciers). In reality, running water is the most common cause of soil erosion. Water erosion may further be classified, based on different actions of water responsible for erosion, as: Raindrop erosion, Sheet erosion, Rill erosion, Gully erosion, Pipe erosion and Stream bank erosion.

1.2.3 Glacial Erosion

Glacial erosion also called as ice erosion occurs mostly in cold regions at high altitudes. The glacial erosion causes heavy landslides. Glacial erosions, in India are mostly confined to mountains and hilly Himalayan regions. The different type of soil erosion is given in figure 1.1. Some of the soil erosion processes are illustrated in figures 1.2 to 1.7

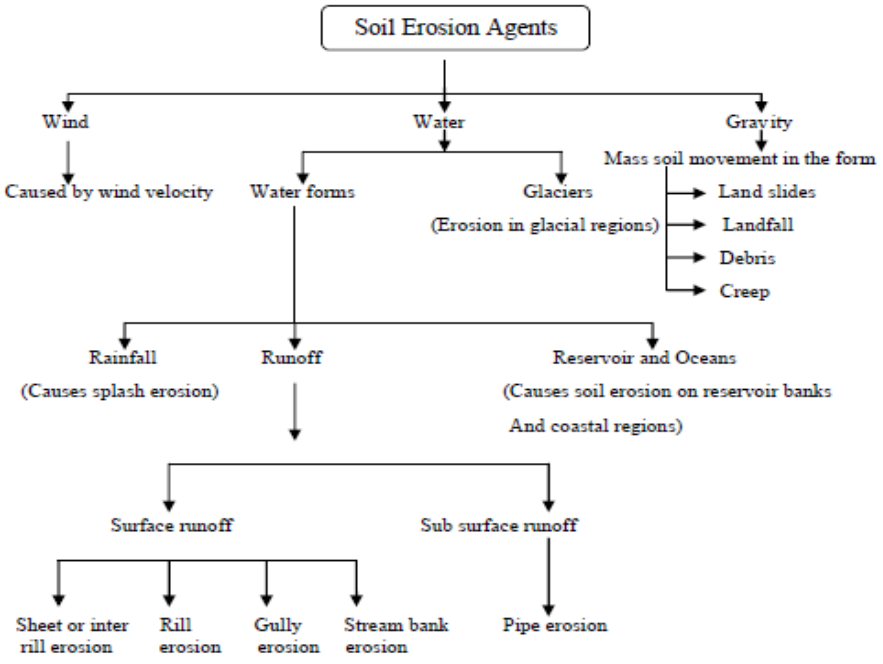

Fig. 1.1 Different type of soil erosion

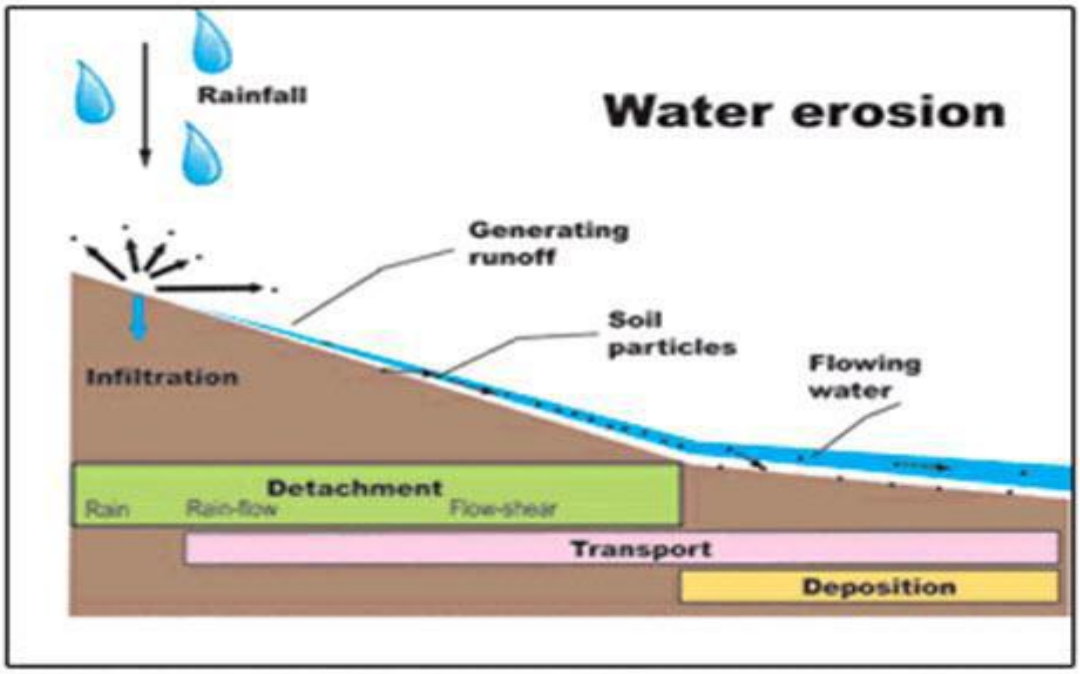

Fig. 1.2 Soil Erosion Agents

Process of Water Erosion

(Source: http://www.weru.ksu.edu)

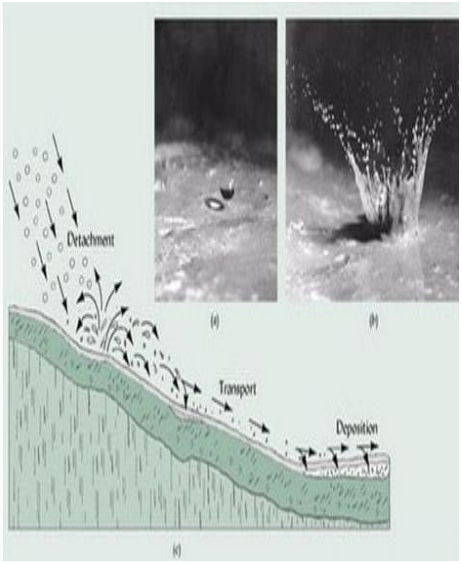

Fig. 1.3 Splash erosion

Source: http://restoringutopia.blogspot.in/

Fig. 1.4 Sheet erosion

(Source: http://soer.justice.tas.gov.au

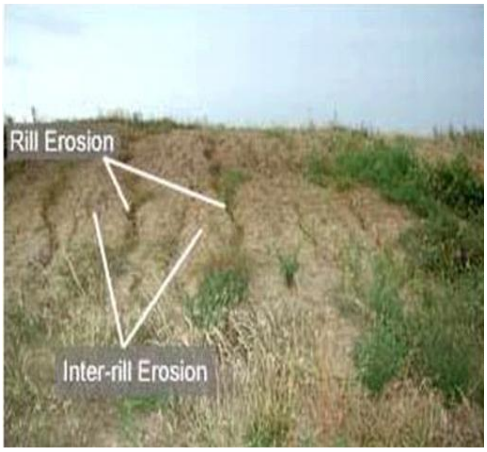

Fig. 1. 5 Rill formations from sheet erosion) **Fig. 1.6 Gully erosion**

(Source: http://passel.unl.edu) (Source: CSWCRTI, Dehradun)

Fig. 1.7 Stream bank erosion in mid Himalayan region of India

(Source: https://www.flickr.com)

1.2.4 Gravitational Erosion:

When there is mass movement of soil erosion under the effect of gravity e.g. landslides, landfalls etc. it leads to gravitational erosion. This type of erosion is observed in areas that are near to pits, roads, rivers etc.,

1.3 Objective of the study

The main objective of this study is to develop a hydrological model to estimate Sediment yield using SWAT (Soil and Water Assessment Tool). The objectives of the study are given as follows:

- To model sediment yield at Pong dam.
- To investigate the impact of likely future changes in climate on sediment yield up to Pong dam using future climatic scenarios.
- To assess the life of the reservoir for the likely sediment yield under the projected different climatic scenarios.

Chapter 2 Literature Review

2.1 General

Estimation of sediment load has become important in river engineering practices, river training, river management and the design, maintenance and operation of hydraulic structures mainly power plants. Another important use is in water quality monitoring (Nagy et al., 2002). The estimation of sediment from the catchment has been the subject of research for several decades and has been difficult task due to the complex nature of the sedimentation process. The sedimentation process depends upon the characteristics of basin and river which include climate, land slope and topography, land cover and pattern of land use (Shahin, 1993). Measurement of sediment load in some of the rivers dates back to the last century. Recent publications reveal that sediment load has been observed to understand sediment process in the watershed as well as to predict the sediment load (Nagle et al., 2007;Woodward and Walling, 2007; Kido et al., 2007; Smith, 2008; Horowitz et al., 2008; Mano et al., 2009; Deasy et al., 2009; Dugan et al., 2009; Tomas D. Reyes, JR. 2017; Gao et al. 2017; Mathlouthi and Lebdi, 2018).

Several methods have been proposed to predict sediment load based on the properties of flow and sediment. Models such as black box models, regression based models and physically based models have been developed for computing the sediment yield (Garde and Rangaraju, 1985; Graf, 1984; Rijn, 1984 a,b,c; Arnold et al. 1998; Tayfur, 2002; Gao and Pasternack, 2007; Doomen et al., 2008; Parajuli et al., 2009; Tomas D. Reyes, JR. 2017;). During 1945 to 1965, an empirical method for computing the upland soil losses was evolved based on statistical analysis from the experiment conducted from many small plots in the states of USA, which was named as Universal Soil Loss Equation (USLE) (Schwab, et al. 1993). It has been widely used in many countries to estimate the sediment yield from the watersheds despite its simplification of many variables involved. The USLE is given as

$$A = RKLSCP \tag{2.1}$$

where A is average annual soil loss per unit area, R is rainfall and runoff erosivity index for geographic location, K is soil erodibility factor, L is slope length factor, S is slope steepness factor, C is cover management factor and P is conservation practice factor. USLE predicts average annual gross erosion as a function of rainfall energy. To improve the prediction

capability of USLE, the rainfall energy factor is replaced with a runoff factor and this is called as modified universal soil loss equation (MUSLE). Sediment yield prediction is improved because runoff is a function of antecedent moisture condition as well as rainfall energy. MUSLE eliminates the need for delivery ratio and it allows the equation to be applied to individual storm events. The MUSLE is given as

$$Y = 11.8\left(Qq\right)^{0.56} KLSCP \qquad (2.2)$$

where Y is the single storm sediment yield (*tons*), Q is the runoff (m^3), q is peak storm discharge (m^3/s) and K, L, S, C and P are the standard USLE terms used in equation in (2.1) (Neitsch et al., 2005).

Physically based semi distributed models such as Soil and Water Assessment Tool (SWAT) and Annualized Agricultural Non Point Source (AnnAGNPS) have been developed to estimate the sediment load wherein modified USLE is used for the estimation of sediment yield (Parajuli et al., 2009).

Development of many process-based physical models for computing soil erosion and deposition in the basin are reported in the literature. The models developed are 1D, 2D, 3D considering numerical solution of differential conservation equations of mass and momentum of flow along with sediment mass continuity equation. The models applied to different basins are HEC-6, MOBED, IALLUVIAL, FLUVIAL 11, CHARIMA, SEDICOUP, OTIS, EFDCID, MIKE3, HEC-RAS, 3ST1D, SERATRA, SUTRENCH-2D, MOBED2, FLUVIAL 12, MIKE 21, DELFT 2D, ECOMSED, CH3D-SED, MIKE 3, DELFT 3D and TELEMAC (Papanicolaou et al., 2008). Water Erosion Prediction Project (WEPP) model is a process-based model based on infiltration theory, hydrology, soil physics, plant science, hydraulics and erosion mechanics (Pandey et al., 2009).

Discrepancies between physically based sediment transport models and measurements are observed due to the oversimplification of the problem by using an inappropriate model, inappropriate input data, lack of appropriate data for model calibration, unfamiliarity with the limitations of the sediment transport equations and computational errors of numerical schemes.

The applicability of these models to all rivers is limited due to the simplification of important parameters and boundary conditions considered (Nagy et al., 2002). Moreover, these models warrant huge amount of data and require substantial computational time to implement. Models such as black box models like Autoregressive (AR), Autoregressive Moving Average (ARMA) and Autoregressive Integrated Moving Average (ARIMA); and regression based models like Multiple Linear Regression (MLR) have been applied under limited data availability conditions.

A comprehensive review of the research work on sediment yield assessment using SWAT model was carried out and are presented as follows:

2.2 SWAT Model

Arnold et al. (1998) explained about SWAT model development, operation, limitations and assumptions. Hydrologic modeling is the basic tool for integrated watershed managements. They explained model development from the basic assumptions of various models like standard watershed model (Crawford and Linsley, 1966), SSARR (Rockwood et al., 1972), the tank model (Sugawara et al., 1976) etc. In these models, processes are described by differential equation, empirical algebraic equations, conservation of mass, energy and momentum. Based on the above mentioned model process studies, they developed the model to estimate the impact of land management on runoff, sediments and pollutants.

Shrivastava et al. (2004) tested SWAT model for estimating runoff and sediment yield on monthly basis from small watershed in eastern India. They showed that if daily rainfall and air temperature data were not available the weather generator attached with the SWAT model could simulate daily rainfall, air temperature and other weather parameters also. They concluded that SWAT model was capable of generating monthly rainfall for 10 years (1992 – 2001) using weather generator and verified with help of observed monthly rainfall data.

Tripathi et al. (2006) studied the effect of watershed subdivision on the water balance mechanism for Nagwan watershed in eastern India. Their study showed that the number and size of sub-watersheds did not significantly affect surface runoff but had noticeable effect on other

components like evapotranspiration, percolation of water and soil water content. Therefore, they concluded that the watershed subdivision had an effect on the water balance in general. The number and size of sub-watersheds for a given catchment depends on the resolution of spatial data used in the model. It was reported that high resolution data resulted in higher number of sub-watersheds and in that way improved the water balance prediction of the model.

Moriasi et al. (2007) reviewed several research papers about SWAT model performance analysis and discussed about various statistical and graphical techniques to evaluate model performance. These parameters were namely NSE, PBAIS, and R^2 etc. Based on the review they recommended that three statistical values were sufficient for stream flow, sediment and nutrients for evaluating the performance of the model. SWAT model simulation was considered satisfactory if NSE is greater than 0.5 and RSR is less than 0.7 and if PBAIS 25 % for stream flow and PBAIS 55 % for sediment and PBAIS 70% for N &P.

Setegn et al. (2008) made his study for Lake Tana Basin to assess the hydrological water balance using SWAT model. The objective of his study was to test the applicability of SWAT model for prediction of stream flow in the basin. The model was effectively applied to the basin in simulating the daily and monthly stream flows and they concluded that stream flow was more sensitive to the HRU definition compared to sub basin categorization.

Mengistu et al. (2008) had done his study to see the effects of variation of spatial resolution of soil data on stream flow and sediment using SWAT model. The state soil geographic maps (STATSGO-1:250000) were compared with soil survey geographic maps (SSURGO - 1:120000) in ArcSWAT model. Similar sub-basins were used for watershed delineation and during HRU classification they used SSURGO and STATSGO. They observed that high resolution soil map (SSURGO) delineating more HRU compared to low resolution soil map (SSURGO). Finally they concluded that predicting accuracy of stream flow and sediment loading was high in case of SSURGO compared to STATESGO.

Xu et al. (2009) applied SWAT model to simulate the runoff and sediment yield in Miyun river catchment, China. The model accurately predicted the daily and monthly runoff and sediment yield with the value of Nash-Sutcliffe efficiency of greater than 0.6. During their study,

the sensitivity analysis was carried out to identify parameters which affect runoff and sediment yield from the watershed showed that runoff was most sensitive to curve number (CN) and Base flow alpha factor (ALPHA_BF) and sediment yield was sensitive to curve number (CN) and channel re-entrainment linear parameter (SPCON).

Easton et al. (2010) applied SWAT model to a Blue Nile Basin, Ethiopia and they observed that the SWAT model was incapable of practically modelling gully erosion. Their study showed that SWAT model under predicted the sediment from a basin where gully erosion was high. To compensate for this the USLE soil erodability factor (USLE_K) in MUSLE (Modified Universal Soil Loss Equation) was increased.

Lin et al. (2010) did his work to observe the effect of Digital Elevation Model (DEMs) resolution on runoff and sediment yield. The DEMs they considered were DLG5 - local Digital Line Graph for 5m interval, ASTER - 30m resolution, and SRTM - 90m resolution. Based on the results they concluded that the runoff was not sensitive to different spatial resolution. But the sediment yield was slightly sensitive (decreased) with coarser resolution.

Raneesh et al. (2010) carried out work for prediction of stream flow and sediment yield in chaliyar river basin, Kerala, India. The model performance was reasonably high during calibration (1995 to 2001) and validation (2002 to 2004). The NSE and R^2 value were found to be 0.99 and 0.99 during calibration of runoff and NSE and R^2 value were found to be 0.93 and 0.77 during calibration of sediment yield. They observed that model slightly underestimated the runoff. They concluded that the model was able to simulate sediment yield with reasonable accuracy.

Patil et al. (2014) carried out work for simulation of runoff using SWAT model in Bhima River, Krishna basin**.** They divided ten years discharge data into two equal parts for calibration and validation. The flow was auto-calibrated using monthly observed and simulated flows from 1974 to 1978. Validation was carried out for flows from 1979 to 1983. The calibration result showed that there was a good agreement (R^2=0.89, NSE=0.81) between the calibrated and observed monthly flows. For validation, the R^2 was found to be 0.74 and NSE was estimated as 0.77. They concluded that SWAT model was applicable for simulating runoff for small

watershed.

Tyagi et al. (2014) had done his work to examine the applicability of SWAT model in two mountainous forest watersheds in Himalaya, India. The two forest watersheds are Bansigad, Arnigad. They run the model on daily time step scale and calibrated model from 2008 to 2010 and validated model from 2010 to 2012. They assessed impact of degraded oak forest cover, dense oak forest on stream flow and sediment yield. They concluded that Arnigad watershed had higher ET and lower surface runoff compared to Bansigad watershed. Because Arnigad watershed has dense oak forest and more canopy cover.

Omani et al. (2015) simulated the effect of management practices on surface runoff and sediment yielding in Gharasu watershed using SWAT model. The model was calibrated from 1991 to 1996 and validated 1997 to 2000. They identified critical erosion prone watersheds based on average sediment yield at sub basin level and recommended for soil conservation measures such as terracing and afforestation. Generally, developing land practices in hilly and mountains areas are impracticable, land cover change of these areas is recommended for soil conservation. The results showed that land use conversion had best effect on sediment yield reduction at hillsides sub basins and wherever mountainous sub basins are negligible. Because in mountainous areas, main factor is steep slope. Finally their study showed that SWAT was capable tool for simulating the effect of management practices.

Kumar et al. (2015) carried out work towards identification of critical watersheds prone to soil erosion in Damodar river catchment, located in Jharkhand. Damodar watershed has two gauge station mentioned by CWC and model was calibrated, validated at those two gauge station using observed data. They obtained acceptable statistical value for developed SWAT model. After rewriting model with calibrated value again they run the model from 1993 to 2003. Watersheds were classified based on annual soil erosion loss into six categories, recommended by Singh et al. (1992). And they compared these classes with manually prepared map by DVC. Comparison was reasonable to accept the model for identifying erosion prone watershed.

Gupta et al.(2015) carried out their study work on different watershed model approaches, techniques in hydrology and watershed management. They described various

empirical model and computer model such as HEC-HMS, the EPA-SWMM and ARS-SWAT. The basic governing equations used in those models such as SCS-CN methods, MUSLE equation, Hargreave method, Penman-Monteith methods are common and accurate methods for watershed modelling.

Thawait et al. (2015) predicted sediment yield from Mohgaon Watershed of Narmada River Basin using SWAT model. They used SUFI2 in SWAT-cup to calibrate the model parameters and 5 years sediment load data were used for calibration purpose. They finally concluded that the swat model was capable of predicting sediment yield and hence could be used as a tool for water resource planning and management of watersheds.

Chandra et al. (2016) used SWAT model for prediction of sediment erosion pattern in upper Tapti basin and calibrated, validated model for twelve years with good NSE, PBIAS. Most sensitive parameters were Surlag, Curve number CN2, USLE_P, USLE_C and overland manning's n during sediment calibration in upper Tapti basin. Based on erosion pattern they identified critical watersheds and adopted BMPs in SWAT model. Simulated results from SWAT model indicated that Burhanpur sub catchment at Tapi River is much more erosion-prone than the adjoining Yerli sub catchment at Purna River, and contributes nearly 80% of sedimentation in Hathnur reservoir.

Tomas D. Reyes, JR. (2017) applied the Soil and Water Assessment Tool (SWAT) model to predict streamflow and sedimentation in Wahig-Inabanga Watershed, Bohol, Philippines. The applicability of the SWAT model was evaluated and its output was integrated to GIS to generate sedimentation hazard map. The result of the SWAT model performance evaluation on stream flows was satisfactory. However, the model did not provide precise estimates of sediment yield in subbasins and hydrological response units (HRU) especially with corn as single land use or one of the landuses even on flat to gently rolling terrain. Inaccuracy issue on sediment yield prediction deferred further analysis including the sedimentation risk valuation which supposed to provide baseline information for watershed management and land use planning.

2.3 GCM models and Climate scenarios

The recent IPPC's summary report for policymakers confirms the human interference with the climate system based on the data of anthropogenic emissions of green house gases observed for many decades (IPCC WGII AR5, 2014). Increased level of green house gases in the atmosphere has increased average surface temperature of the earth and it will continue to increase in the 21st century. Increased average surface temperature results in increase of extreme events, quantity and high intensity of precipitation. The high intensity rainfall will dislodge the sediment and generate more sediment from the catchment and the sediment will get deposited in the reservoir in due course. So it is imperative to estimate the sediment yield at the upstream of Pong reservoir under different future climate scenarios considered by the IPCC summary report and the life of the reservoir is determined by considering the predicted sediment yield by different climate scenarios.

According to IPCC, (2012) any detectable change in the state of climate which persists over a considerable period of time (more than a decade) can be referred to as climate change. Both natural (such as periodic changes in solar irradiance) and man-made (such as GHG emissions, changes in land-use patterns etc.) sources can be responsible for it. However, role of anthropogenic factors towards climate change has been found to be significant as compared to other sources (Huber & Knutti, 2011; IPCC,2007).

Carbon-di-oxide (C02) is an important greenhouse gas, whose concentration in the atmosphere has increased significantly since the industrial revolution, primarily due to increased consumption of fossil fuels and rapid land use change. According to IPCC, (2007) atmospheric concentration of C02 in 2005 was higher than that experienced in the past 6,50,000 years and annual C02 growth rate continues to increase each passing year. Similar trends have also been recorded for other greenhouse gases such as methane and nitrous oxide. Due to the changes in environmental chemistry, changes in the mean, standard deviation and extremes of key climate variables are being observed. There has been an unprecedented increase in global mean temperatures in the last 25 years. Changes in precipitation patterns have also been noted worldwide. A change in climate variables other than precipitation and temperature have also been reported (IPCC, 2007).

In India, few extreme events of rainfall were experienced and were very well measured in terms of quantity. Lakshadweep received 1168 mm rainfall on May 6, 2004. Mumbai received 942 mm rainfall on July 26, 2005. Chennai received 494 mm on December 1, 2015. All these rainfall were received over a period of twenty four hours. Jammu and Kashmir received heavy rainfall during September 3-5, 2014 which led to severe flooding in Srinagar. Kerala received 2346.6 mm of rainfall from 1 June 2018 to 19 August 2018 in contrast to an expected 1649.5 mm of rainfall in Uttarakhand, the rainfall received between 15th and 18th June 2013 was 385.1 mm against the normal of 71.3 mm which was in excess by 440 percent. Kedarnath disaster occurred during this period of rainfall. In addition to the quantity, the intensity of rainfall has also increased which leads to severe flooding and soil erosion and deposition of sediment in storage structures such as reservoirs, ponds and lakes.

Since hydrologic behaviour of a catchment is governed by feedbacks from various climatic and ecologic variables, relationships between them are difficult to formulate. An extensive Canada-wide study highlighting this relationship has been performed by Whitfield & Cannon, (2000). They grouped changes observed in precipitation, temperature and streamflow between the decades 1976-1985 and 1986-1995 into different classes or clusters. After analysing the spatial distribution of these climatic and hydrologic clusters obtained from temperature, precipitation and hydrology stations, they noted distinct linkages between climate variables, hydrologic responses of streams and ecozones within Canada. The study also highlights that even small changes in climate variables may result in significant changes in a region's hydrologic characteristics. General circulation models (GCMs) are used worldwide to analyse the effect of change in climate variables on the different hydrologic responses such as streamflow, evaporation, evapotranspiration and sediment yield.

A general circulation model (GCM) is a type of climate model. It employs a mathematical model of the general circulation of a planetary atmosphere or ocean. It uses the Navier–Stokes equations on a rotating sphere with thermodynamic terms for various energy sources (radiation, latent heat). These equations are the basis for computer programs used to simulate the Earth's atmosphere or oceans. Atmospheric and oceanic GCMs (AGCM and OGCM) are key components along with sea ice and land-surface components. GCMs and global climate models are used for weather forecasting, understanding the climate and

forecasting climate change. Atmospheric (AGCMs) and oceanic GCMs (OGCMs) can be coupled to form an atmosphere-ocean coupled general circulation model (CGCM or AOGCM). With the addition of submodels such as a sea ice model or a model for evapotranspiration over land, AOGCMs become the basis for a full climate model.

A single AOGCM have been used by most of the studies related to climate change impacts for predicting future climate. It is recognized that there is a great deal of uncertainty involved in the estimation of future extreme events under climate change (e.g. Prudhomme et al., 2003; Mareuil et al., 2006; Minville, 2008). The utilization of a single AOGCM may only represent a single realization out of a multiplicity of possible realizations and therefore cannot be representative of future. Therefore, for a reliable assessment of future changes in extremes, it is important to use collective information by utilizing all available climate models and by synthesizing the projections and uncertainties in a probabilistic manner.

A Representative Concentration Pathway (RCP) is a greenhouse gas concentration (not emissions) trajectory adopted by the IPCC for its fifth Assessment Report (AR5) in 2014. It supersedes Special Report on Emissions Scenarios (SRES) projections published in 2000. Four pathways have been selected for climate modeling and research, which describe different climate futures, all of which are considered possible depending on how much greenhouse gases are emitted in the years to come. The four RCPs, namely RCP2.6, RCP4.5, RCP6, and RCP8.5, are labelled after a possible range of radiative forcing values in the year 2100 (2.6, 4.5, 6.0, and 8.5 W/m^2, respectively). The RCPs are consistent with a wide range of possible changes in future anthropogenic (i.e., human) greenhouse gas (GHG) emissions, and aim to represent their atmospheric concentrations. RCP 2.6 assumes that global annual GHG emissions (measured in CO2-equivalents) peak between 2010–2020, with emissions declining substantially thereafter. Emissions in RCP 4.5 peak around 2040, then decline. In RCP 6, emissions peak around 2080, then decline. In RCP 8.5, emissions continue to rise throughout the 21st century. Despite characterizing RCPs in terms of inputs, a key change from the 2007 to the 2014 IPCC report is that the RCPs ignore the carbon cycle by focusing on concentrations of greenhouse gases, not greenhouse gas inputs. The IPCC studies the carbon cycle separately, predicting higher ocean

uptake of carbon corresponding to higher concentration pathways, but land carbon uptake is much more uncertain due to the combined effect of climate change and land use changes.

Combining of hydrological model with GCM is a common modelling technique to analyze the effect of climate variables on hydrologic responses such as streamflow, evaporation, evapotranspiration and sediment yield using climate scenarios such as RCP2.6, RCP4.5, RCP6 and RCP8.5. Many Coupled Model Intercomparison Project Phase 5 (CMIP5) models are available worldwide for obtaining RCP2.6, RCP4.5, RCP6 and RCP8.5 climate scenarios. Few of the GCMs under CMIP5 model are bcc_csm1_1, bcc_csm_1_1_m, canesm2, cccma_canesm2, ccma_cgcm2_0, cesm1_cam5, csiro_mk2, csiro_mk3_0, ec_earth, fio_earth, gfdl_cm2_0, hadcm_cntrl, hadcm_midi, ispl_cm4, miroc3_2_hires, miroc_esm, miroc_miroc5, mpi_echam4, mpi_esm_lr, ncar_ccsm3, ncar_pcm1, ncep_r2 and ukmo_hadgem1. CanESM2 is a CMIP5 model gives four climate scenarios RCP2.6, RCP4.5, RCP6 and RCP8.5 for all regions worldwide and widely used in all climate change studies. The second generation Canadian Earth System Model (CanESM2) consists of the physical coupled atmosphere-ocean model CanCM4 coupled to a terrestrial carbon model (CTEM) and an ocean carbon model (CMOC).

Shrestha et al. (2013) evaluated the impact of climate change on sediment yield in the Nam Ou basin located in northern Laos using SWAT and GCM. The temperature and precipitation were projected by four CGMs: CCCMA CGCM3.1, CNRM-CM3, MPI ECHAM5 , NCAR CCSM3 and regional circulation model (PRECIS) for three emission scenarios A2 (870 ppm of GHG at the end of 21st century), A1b (GHG of 720 ppm stabilization) and B1 scenario (GHG of 550 ppm stabilization). The Soil and Water Assessment Tool (SWAT) was used to simulate sediment flux attributable with projected temperature and participation for all four GCMs and RCM for all the three scenarios. Projected temperature showed an increasing trend for all the climate models under the considered scenarios. But the trend of projected precipitation varied depending on the greenhouse gas emission scenarios (GHGES), climate models, prediction period and season. The simulation results of SWAT with projected temperature and precipitation from all GCMs and RCM showed the changes in annual stream discharges with a range from 17 % decrease to 66 % increase in the future, which led to predicted changes in annual sediment yield ranging from a 27 % decrease to about 160 %

increase. They concluded that the uncertainty in the projection of sediment flux should be taken into account in both sediment management and climate change adaptation.

Principe J. A. (2012) examined the impact of climate change in Philippines' largest basin—the Cagayan River Basin—by predicting its sediment yield for a long period of time using Soil and Water Assessment Tool (SWAT) model, Remote Sensing (RS) and Geographic Information System (GIS). The impact of climate change was assessed by varying air surface temperature and amount of precipitation as predicted in the Intergovernmental Panel on Climate Change (IPCC) scenarios. A Nash-Sutcliff efficiency (NSE) > 0.4 and coefficient of determination (R2) > 0.5 for both the calibration and validation of the model showed that SWAT model can realistically simulate the hydrological processes in the study area. The model was then utilized for land cover change and climate change analyses and their influence on sediment yield. Results showed a significant relationship exists among the changes in the climate regime, land cover distributions and sediment yield. Finally, the study suggested land cover distribution that can potentially mitigate the serious negative effects of climate change to a regional watershed's sediment yield.

Paul and Mishra (2014) carried out uncertainty analysis of the future climate change impacts on sediment yield in Brahmani river basin using well calibrated and validated ArcSWAT model for stream flow and sediment yield. Future climate change of rainfall and temperature (minimum and maximum) were projected using change factor (CF) projection for two GCMs UKMO-HADCM3 and MPIM-ECHAM5 for three scenarios A1B, A2 and B1, and three future time periods: 2010-39, 2040-69 and 2070-99 with respect to the 1961-1990 as base period. Uncertainty in projected sediment yield of river basin was estimated by applying GLUE (Generalized Likelihood Uncertainty Analysis) and SUFI-2 (Sequential Uncertainty Fitting-2) methodology of SWAT-CUP. The results show a most probabilistic future behavior of sediment yield of the river basin. The process uncertainty of sediment yield show comparatively lower uncertainty while used SUFI-2 method for both the GCMs under A1B scenario, whereas all results of GLUE were showing much more uncertainty under two GCMs and three scenarios.

Awotwl et al. (2015) used an ensemble of Regional Climate Model (REMO) (GCM ECHAM4) to simulate and project the climate at local scale in order to investigate the hydrological impact of possible future climate change in White Volta Catchment (West Africa). The results obtained from the REMO climate model were compared to the observational datasets for precipitation and temperature for the period 1995-2008. The projected meteorological variables for the period 2030-2043 were used as input to the Soil and Water Assessment Tool (SWAT) hydrological model which was calibrated with historical data to investigate the possible impact of climate change in the catchment. The results obtained from the investigation revealed that catchment was sensitive to climate change.

Rodriguez-Blanco et al. (2016) evaluated the potential medium (2031–2060) and long-term (2069–2098) impacts of projected changes of temperature, rainfall and CO2 concentration on sediment yield in a small rural catchment located in NW Spain using the Soil and Water Assessment Tool (SWAT) model. Climate change scenarios were created using future climate data projected by regional climate models from the ENSEMBLES project and two CO2 concentration scenarios (550 and 660 ppm) under A1B scenarios. The simulation results from SWAT using the projected climate variables temperature and rainfall under considered scenarios showed that the suspended sediment was expected to decrease (2031–2060: −11%,2069–2098: −8%) compared to the baseline period (1981–2010), mainly due to decreased streamflow. However, an increase in sediment transport in winter was predicted, possibly associated with increased erosion in cultivated areas (11%–17%), suggesting that, at this time of the year, the effect of soil detachment prevails over sediment transport capacity.

Janapriya et al. (2016) evaluated the impacts of possible future climate change scenarios on the hydrology of the catchment area of the Manjalar sub basin of River Vaigai, Tamil Nadu, India using Soil and Water Assessment Tool (SWAT). The output of bias corrected Earth System Models of the Coupled Model Intercomparison Project Phase 5 (CMIP5): HadGEM2 under scenarios RCP 4.5 and RCP 8.5 was used to simulate hydrological response using the calibrated parameters of SWAT. Three future periods: 2012–2039, 2040–2069, and 2070–2098 were considered under the scenarios RCP 4.5 and RCP 8.5. The projected maximum and minimum temperature, rainfall for both the scenarios showed an increasing trend. They concluded that the

soil water storage and stream flow contribution to ground water were likely to increase in RCP 4.5 scenario and it would decline for RCP 8.5 scenario. The increase in annual rainfall, evapotranspiration and surface runoff would be more in RCP 8.5 scenario compared to RCP 4.5 scenario.

Azari et al. (2016) assessed the impacts of climate change on streamflow and sediment yield from the Gorganroud river basin in North of Iran using SWAT and GCM models. SWAT model was implemented with historical data (1972-1994) and the parameters were optimized by SUFI-2 algorithm. Three SRES scenarios A1F1, A2 and B1 of three GCMs: CGCM2 (coupled global climate model) from the Canadian Centre for Climate Modelling and Analysis; HadCM3 from the Hadley Centre for Climate Prediction and Research; and CSIRO2 from the Australian Commonwealth Scientific and Industrial Research Organization Scenarios with the highest (A1FI scenario—970 ppm by 2100), lowest (B1 scenario—550 ppm by 2100) and plausible (A2 scenario—845 ppm by 2100) projected CO2 concentrations were considered for simulating the streamflow and sediment yield. Simulated streamflow and sediment yield showed increasing trend under the considered scenarios for the period from 2040 to 2069. They found that the impact of climate change on sediment yield was greater than on streamflow.

Fengping et al. (2016) conducted a modelling assessment on the potential change of water resources in Songhua River Basin (SRB) in Northeast China using SWAT under global climate change. The SWAT was calibrated and validated with the historical streamflow records (1980-2009) in the basin. Projected and downscaled climate data under two emission scenarios RCP 4.5 and RCP 8.5 for the period from 2020 to 2049 were used in SWAT model with calibrated parameters to simulate future streamflow in the basin. They observed that SWAT model performed very well during the calibration and validation periods in SRB. Projected temperature showed an increasing trend under both the scenarios in sub-basins, Nenjiang River Basin (NRB) and lower SRB (LSRB). Projected precipitation under both scenarios showed decreasing trend in NRB and LSRB, increasing trend in Upper Songhua River Basin (USRB). They found that the simulated streamflow with projected temperature and precipitation showed a decreasing trend in LSRB and NRB and increasing trend in USRB.

Sharanya et al. (2018) used SWAT model with the outputs from regional climate model (RCM), COordinated Regional climate Downscaling EXperiment (CORDEX) for baseline (1951-2005) and future RCP 4.5 scenario (2006-2060) data of rainfall and temperature to evaluate the impact of climate change on rainfall, temperature and streamflow in a west flowing river originating in the Western Ghats of India. They found that the rainfall followed decreasing trend, average temperature followed increasing trend, annual streamflow followed deceasing trend for baseline and RCP 4.5 scenario. They also investigated the capability of SWAT to simulate the groundwater flow. The simulated results were compared with the recession limb of the hydrograph and were found to be reasonably accurate.

Monteclos-Zamora et al. (2018) applied the SWAT model first time in Cuba to assess the potential impacts of climate change on water availability in the Cauto River basin. SWAT model was calibrated and validated with the historical data for the period from 2001 to 2010 at a monthly timescale in two sub-basins La Fuente and Las Coloradas. The output available from regional climate model RegCM4.3 was used with calibrated parameters of SWAT to simulate baseline (1970–2000) period and near-future (2015–2039) hydrologic regimes under the representative concentration pathway RCP 8.5 emission scenario. The projected mean annual temperature showed an increasing trend and projected mean annual precipitation showed a decreasing trend. The simulated streamflow with the calibrated parameters of SWAT showed a decreasing trend for both baseline and near future period.

2.3 Conclusions

Based literature review on various studies, selection of proper input parameters is most important for model calibration and those parameters have to be considered separately for runoff and sediment. It is observed from the above review that SWAT model is capable of simulating streamflow and sediment on daily and monthly, but model accuracy depends on spatial resolution of input data. The studies related to SWAT model carried out by many researchers indicate that SWAT model is applicable to Beas basin located in Himachal Pradesh, India to simulate runoff and sediment yield. The review on CGM models with climate scenarios RCP 2.6, RCP 4.5 and RCP 8.5 with hydrological model SWAT in general is capable of analyzing the

effect of climate change on future streamflow and sediment yield. The three emission scenarios RCP 2.6, RCP 4.5 and RCP 8.5 from CanESM2 (CMIP5) were considered for studying the effect of climate on future streamflow and sediment yield from Beas basin, Himachal Pradesh.

Chapter 3 Soil and Water Assessment Tool (SWAT)

3.1 General

The main objective of model development is to simulate the impact of land management practices on water, sediment and water quality (nutrient, phosphorous loss) in large and complex watersheds having varying soils, land uses and different management conditions over a long period of time.

3.2 SWAT model Description

The SWAT (Soil and Water Assessment Tool) model is a river scale model developed for the USDA- Agricultural Related Research Service in Texas. SWAT can be classified in number of ways. It can be classified as a deterministic model based on the input and uncertainty. It can be classified as a distributed model based on spatial representation of the catchment. It is a physically based model based on nature wise. It is continuous time scale event model based on storm event. SWAT is a comprehensive model and it has features of various agricultural research service models namely CREAMS, EPIC and GLEAMS.

3.2.1 Model Components

The main components of SWAT can be classified into weather, hydrology, soil temperature, sedimentation, agricultural management and crop growth (Figure 3.1). The hydrology components of SWAT model is based on the water balance equation. The weather parameters such as precipitation, air temperature, solar radiation, relative humidity and wind speed are required to run the SWAT. These variables can be entered directly in to the SWAT model as daily or sub-daily values. SWAT generates the sediment from the watershed using Modified Universal Soil Loss Equation (MUSLE). Surface water movement on the ground is controlled by soil temperature.

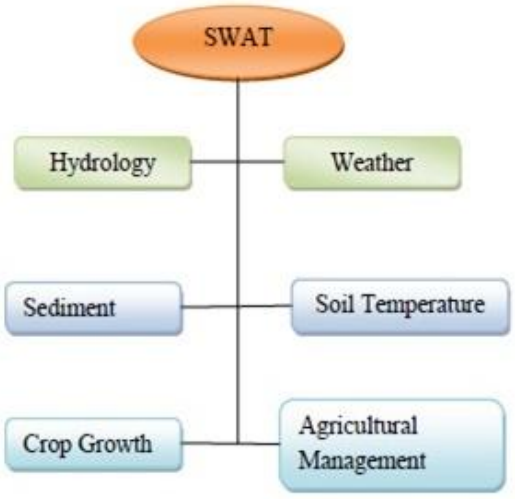

Fig. 3.1 Components of SWAT model

3.2.2 Hydrological processes in SWAT

SWAT simulates surface runoff and sediment in a watershed by considering a number of different physical processes. The physical processes include evaporation, runoff, infiltration process, potential and actual evapotranspiration, lateral flow and ground water contribution. The accuracy of prediction of the movement of sediment, pesticides or nutrients depends on accuracy of prediction components of hydrologic cycle, because these are transported through stream flow from upland watershed. In SWAT model, simulation of the hydrology can be divided by two major parts; one is land phase and the other one is routing phase of the hydrologic cycle.

3.2.3 Land phase of hydrologic cycle

The land phase of hydrologic cycle estimates the quantity of water, sediment and water quality loadings which is coming from land surface to main reach of the each basin. The land phase of hydrologic cycle is simulated by following the water balance equation:

$$SW_t = SW_o + \sum_{i=1}^{N} (R_{day} - Q_{surf} - E_a - W_{seep} - Q_{gw})$$

(3.1)

Where, SW_t = final soil water content, SW_o = initial soil water content, t = time in days, R_{day} = amount of precipitation of *i*th day, Q_{surf} = amount of surface runoff of *i*th day, E_a= amount of evaporation of $_i$th day, W_{seep} = amount of water entering the unsaturated zone from the top soil profile of *i*th day, Q_{gw} = amount of return flow of *i*th day

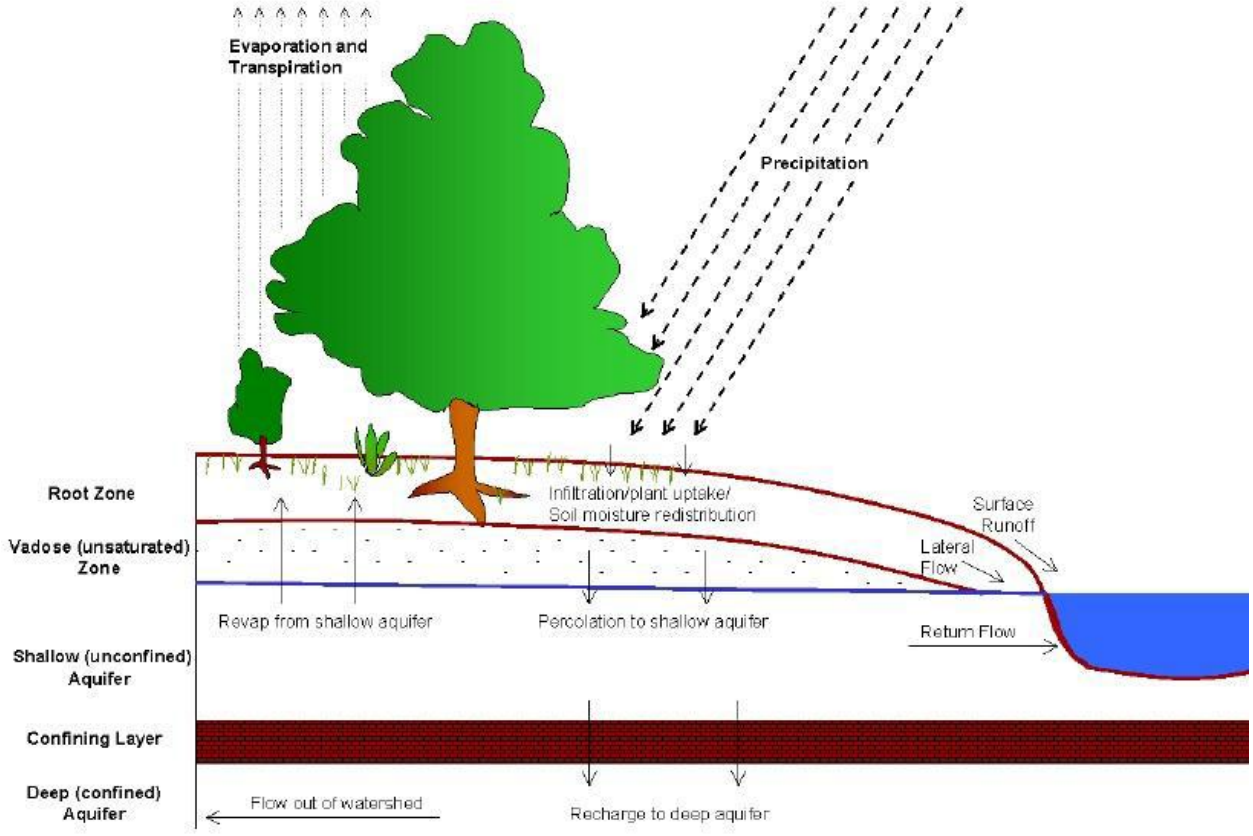

Fig. 3.2 Land phase Hydrologic cycle

(i) Surface Runoff

Runoff is that portion of rain which ultimately joins the stream and rivers. It is the output produced by the catchment for the given input of rainfall after satisfying various losses. SWAT model provides two methods for simulating surface runoff; one is SCS curve number (SCS,

1972) and another one is Green and Ampt infiltration method (Green and Ampt equation, 1911). The SCS curve number method includes the permeability of soils, antecedent moisture conditions, soil hydrological group, varying land use and soil type whereas the Green and Ampt infiltration method calculates surface runoff as a function of effective hydraulic conductivity assuming that above wetting front, the soil is completely saturated. SWAT allows the user to calculate the surface runoff in daily and hourly time steps of rainfall data. In case of daily time basis, SWAT model uses the SCS curve number (CN) method and for hourly time steps SWAT model uses the Green and Ampt equation. In this study, the SCS curve number was adopted for the simulation of surface runoff in SWAT since daily precipitation data was readily available. According to the Soil Conservation Service equation

$$Q_{surf} = \frac{(R_{day} - Ia)^2}{(R_{day} - Ia + S)} \tag{3.2}$$

Where Q_{surf} is the accumulated runoff or excess rainfall, R_{day} = depth of precipitation of *i*th day in mm of water, S = retention parameter

$$S = 25.4\left[\frac{100}{CN} - 10\right] \tag{3.3}$$

Where, CN is the curve number I_a = initial abstraction which includes surface storage and interception, I_a is commonly approximated as 0.2S

$$Q_{surf} = \frac{(R_{day} - 0.2S)^2}{(R_{day} + 0.8S)} \tag{3.4}$$

ii) Sediment modeling

Generally, Sediment transport in catchment consists of two components: landscape component, channel component. SWAT model simulates the sediment based on these two components. On the basis of landscape component, SWAT keeps track of the particle size distribution of eroded sediment particles and routes them through reservoirs, ponds and surface water bodies. Generally Sediment particle transported in canal or channel network depends on two processes, one is degradation and another one is deposition. Degradation phenomenon will occur when sediment transporting capacity of river is more than sediment load being transported

by a river and vice versa for deposition. Both deposition and degradation is a function of stream velocity and contact portion of the channel sides and bottom surface to the stream erosive force. Sediment yield reaching the stream channel from landscape component is the sum of total sediment yield calculated by MUSLE minus the sediment lagged or stored in surface runoff and the sediment trapped in grassed way, filter strips etc.

Landscape contribution SWAT model estimates the sediment yield from the upland catchments by Modified Universal Soil Loss Equation developed by Williams (1975). The MUSLE empirical equation is a modified form of Universal Soil Loss Equation (USLE) developed by Wischmeier and Smith (1965, 1978).

$$SED = 11.8\,(Q_{surface}\ \ q_{peak}\ \ Area_{Hru})^{0.56}\,.K_{USLE}\,.C_{USLE}\,.P_{USLE}\,.LS_{USLE}\,.CFRG \tag{3.5}$$

3.4 Sensitivity Analysis

Sensitivity analysis is a process of testing and identifying the most sensitive model parameters that affects most the output from the model when the input is changed. This is an initial step before calibrating SWAT model. The current version of SWAT model, SWAT2012, provides two types of sensitivity analysis and are performed when using SUFI2 (Sequential Uncertainty Fitting version 2). Those are Global Sensitivity and One-at-a-time sensitivity analysis. Global sensitivity analysis performs the sensitivity of one parameter while the value of other related parameters are also changing. The main problem related to global sensitivity analysis is that it needs a large number of simulations.

3.5 Model Calibration and Validation

SWAT-CUP (SWAT Calibration and Uncertainty Procedure) is used for the calibration of SWAT model as it is automated model calibration that requires the uncertain model parameters and corresponding to measured data are extracted from the model output files. SWAT-CUP is an interface of SWAT model and that has been developed for calibration

purpose. The interaction between calibration programs of SWAT in SWAT-Cup are as shown in the figure 3.3.

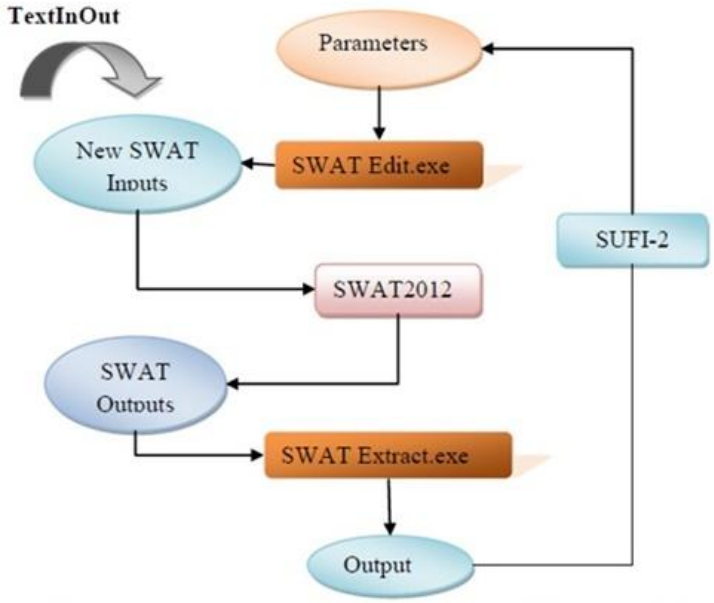

Fig. 3.3 Interactions between Calibration Programs of SWAT in SWAT-CUP

SWAT-CUP has the interface which contains the program PSO, SUFI-2, GLUE and Para Sol and run for SWAT version 2000, 2005, 2009, 2012. In this model setup, calibration and validation process were conducted by using the SUFI2 (Sequential Uncertainty Fitting Version 2) in SWAT-CUP. SUFI-2 (Sequential Uncertainty Fitting) contains uncertainty in parameters, expressed as ranges (uniform distributions), accounts for all sources of uncertainties.

3.6 Evaluation of Model Performance

The systematic and dynamic behavior of the SWAT model can be visualized by drawing graph between time and simulated flow, observed flow on the same coordinate system. To assess the goodness of the model; three methods have been used normally during the calibration and validation periods. These are coefficient of determination (R2), the Nash-Sutcliffe efficiency (NSE) and Percent bias (PBIAS). These three statistical parameters are used to measure the model performance.

3.6.1 Coefficient of determination (R^2)

The coefficient of determination R^2 measures the fraction of the variation in the measured data that is replicated in the simulated model results.

$$R^2 = \frac{\left[\sum_i (Q_{m,i} - \bar{Q}_m)(Q_{s,i} - \bar{Q}_s)\right]^2}{\sum_i (Q_{m,i} - \bar{Q}_m)^2 \sum_i (Q_{s,i} - \bar{Q}_s)^2} \quad (3.6)$$

Where, Q is the Discharge, *m* and *s* stand for measured and simulated data, *i* is the *i*th measured and simulated data. R^2 values ranges from 0 to 1, R^2 value more than 0.5 then model performance is considered acceptable and values close to one indicates less error variance. The main drawback of R^2 is that it only quantifies dispersion.

3.6.2 Nash-Sutcliffe Efficiency

The Nash-Sutcliffe efficiency is used for analyzing the predictive power of any hydrological model.

$$NSE = 1 - \frac{\sum_i (Q_m - Q_s)_i^2}{\sum_i (Q_{m,i} - \bar{Q}_m)^2} \quad (3.7)$$

Where, Q is the Discharge, m and s stand for measured and simulated data, i is the i*th* measured and simulated data. Generally, NSE coefficient ranges various from - ∞ to 1.0 and coefficient values between 0.5 and 1.0 are acceptable levels of performance, whereas values less than 0.5 indicate unacceptable performance.

3.6.3 Percent bias (PBIAS)

PBIAS defined as it shows the approximation tendency of the simulated data to be smaller or larger observed data. Generally, the optimal value of PBIAS is 0.0; value near to zero indicates

model performance is good. A negative value indicates model simulation is overestimated and Positive value indicates model simulation is underestimated (Gupta et al., 1999).

$$\text{PBIAS} = 100 * \frac{\sum_{i=1}^{n}(Q_m - Q_s)_i}{\sum_{i=1}^{n} Q_{m,i}} \tag{3.8}$$

Where, Q is the Discharge, *m* and *s* stand for measured and simulated data, *i* is the *i*th measured and simulated data. The general setup of the SWAT model for the simulation of surface runoff and sediment yield is given in the figure 3.4.

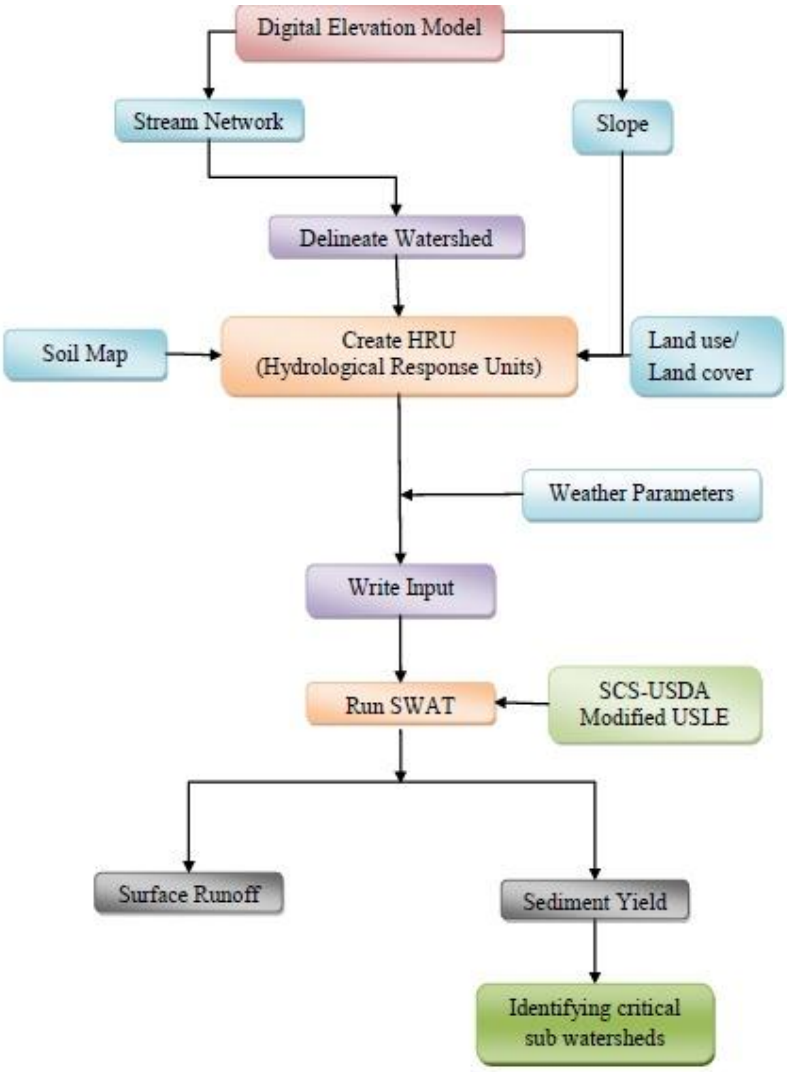

Fig. 3.4 General setup of SWAT Model

3.7 Data requirement and preparation

The results of any hydrological modeling study depend to a large extent on the quality and length of data used. To Run SWAT model minimum four input data set is required namely digital elevation model, land use and land cover map, soil map and weather data. The following paragraphs are described about the preprocessing of SWAT input file. The spatial and temporal resolution of data used in modeling will greatly influence the model performance. SWAT (Soil and Water Assessment Tool) needs high resolution Digital Elevation Model (DEM) and spatial data such as Soil and Land use/land cover data for accurate generation of HRUs. The length of period of weather and climatic data is important for calibrating and validating the model performance.

3.8 Description of study area

The Beas river basin up to Pong dam is located in Himachal Pradesh state of India (Figure 3.5). The river Beas flows from the Beas Kund near Rohtang Pass in the upper Himalayas and traverses a total length of about 116 km from the source to the Pong Dam. It lies between Northern latitude of 31°15' to 32°30" and Eastern longitude of 75°30' to 78°15'. Area of the watershed is about 12,562 km^2 out of which the permanent snow catchment is 780 km^2 and water spread area of the reservoir is 260 sqkm. The Pong reservoir is a major water infrastructure for irrigation water supply to Himachal Pradesh, Punjab, Haryana and Rajasthan. The climate of area surrounded Pong reservoir is sub-tropical with monsoons in the months of July–August. Monsoon rainfall is a major source of water supply to the reservoir, apart from snow and glacier melt. The dam acts as a sponge for flood flows, and reservoir regulation prevents the inundation of surrounding upland areas from routine flooding during the monsoon season. The reservoir stretch is 42 km long with a maximum width of 19 km, and with a mean depth of 35.7 m. The designed maximum flood discharge of (12,400 m^3/s is discharged through a gated chute spillway located on the left abutment of the dam. The Beas river along with its tributaries generate lot of sediments while flowing through hilly regions and transports the sediment into the Pong reservoir. The water resource play an important role for territorial

development of the villages nearby Pong dam depend primarily on Agriculture for their income as well as has got a big business community mostly involved in small to medium size businesses.

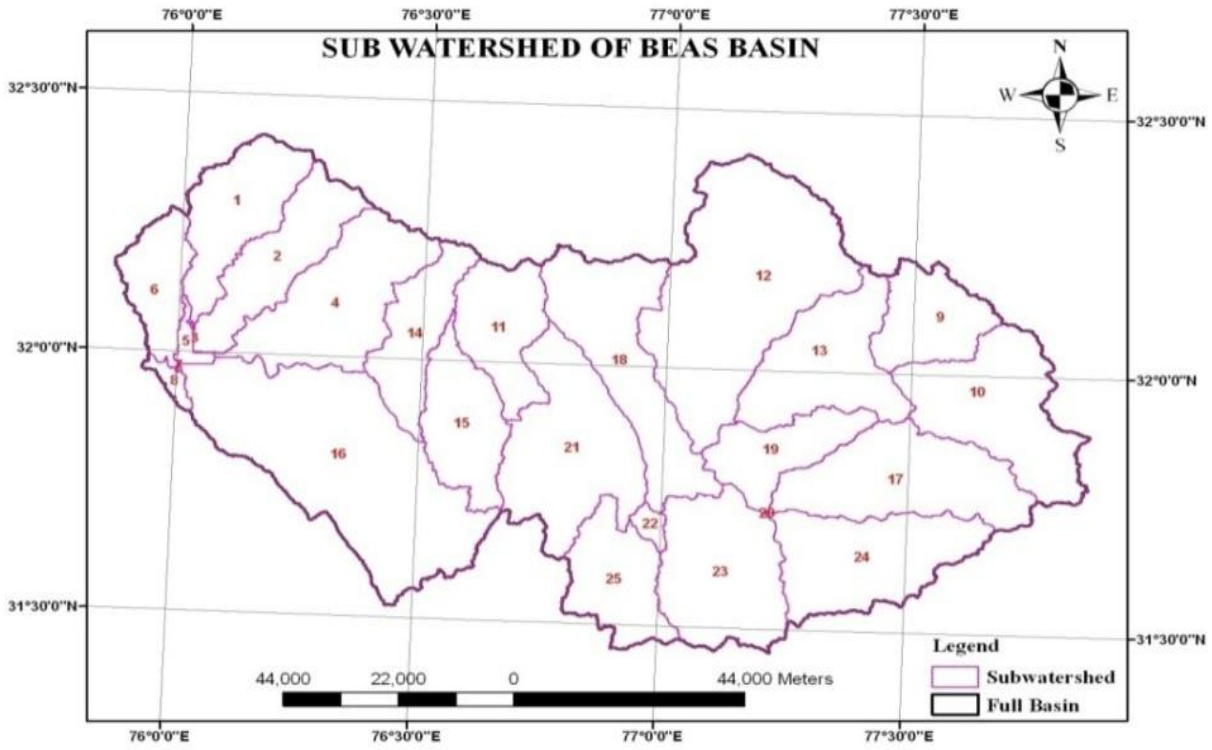

Fig. 3.5 Study area of Beas basin upto Pong reservoir

There are four seasons in watershed namely, winter, spring, summer, and autumn. Observed average (1981-2010) Tmax, Tmin and Precipitation in winter are 10.9°C, 0.3°C, 370 mm, in spring are 20.8°C, 8.4°C, 438 mm, in summer are 29.5°C, 17°C, 406 mm and in autumn are 22.7°C, 9.1°C, 160 mm. Summer consists of (JJAA) June, July, August and Autumn, Winter consists of (DJF) December, January and February, Spring consists of (MAM) March, April and May, Autumn consists of (SON) September, October and November. The following table shows the data type, period of records and source of data.

Table 3.1 Data type, period of records and source of data

S.No.	Data Type	Period of records	Source
1	DEM	2014	USGS Earth Explorer (SRTM)
2	LULC	2014	Landsat 8 OLI
3	SOIL Map	2014	NBSSLUP
4	Meteorological Data(Rainfall, Temperature RH,SR,Wind)	1961-2005	IMD(0.25*0.25grid) for Rainfall, minimum and maximum temperature SWAT.tamu for other Meteorological Data
5	Reanalysis Data	1961-2005	NCEP
6	Discharge	1987-2005	BBMB
7	Sediment load	1987-2005	BBMB

The gridded rainfall data obtained from IMD was converted into point rainfall by Thiessen polygon of 31 subwatersheds and is given in figure 3.6. The gridded minimum and maximum temperature data obtained from IMD were converted into point data by averaging the grid values and are given in figures 3.7 and 3.8. The discharge and sediment load obtained from BBMB are given in figures 3.9 and 3.10.

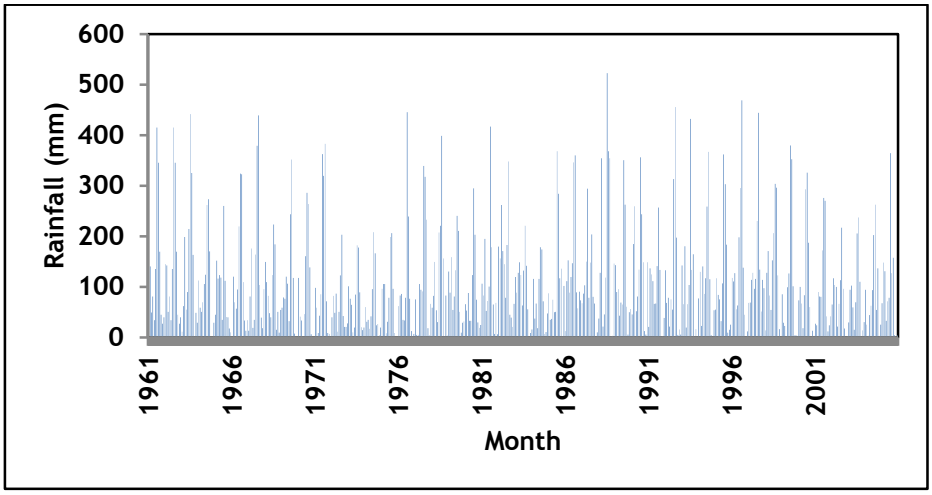

Fig. 3.6 Rainfall (IMD) from 1961 to 2005

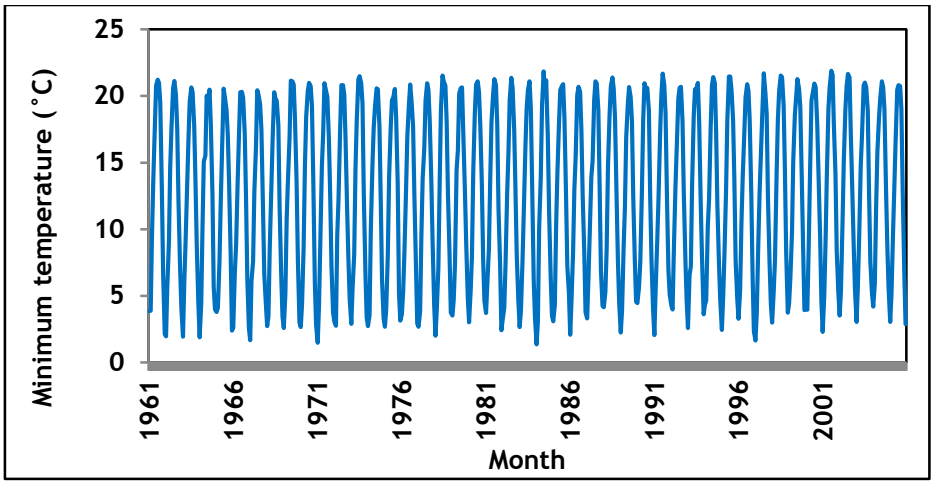

Fig. 3.7 Minimum temperature (IMD) from 1961 to 2005

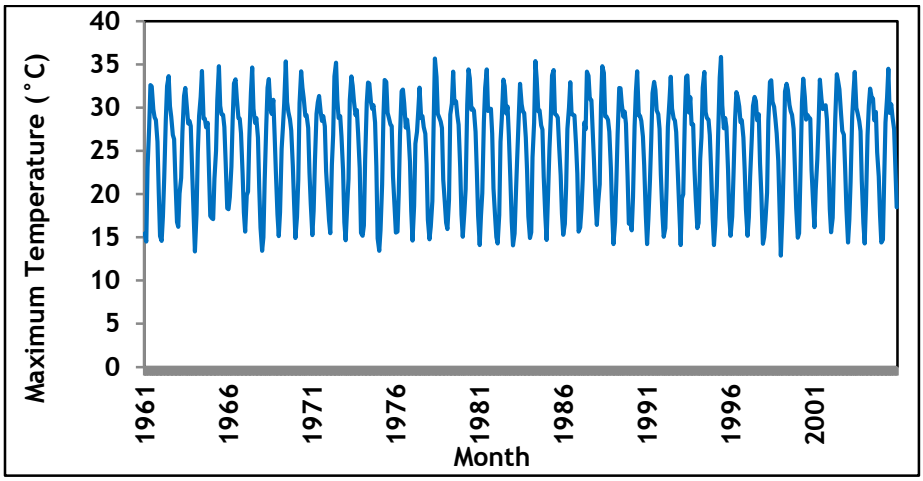

Fig. 3.8 Maximum temperature (IMD) from 1961 to 2005

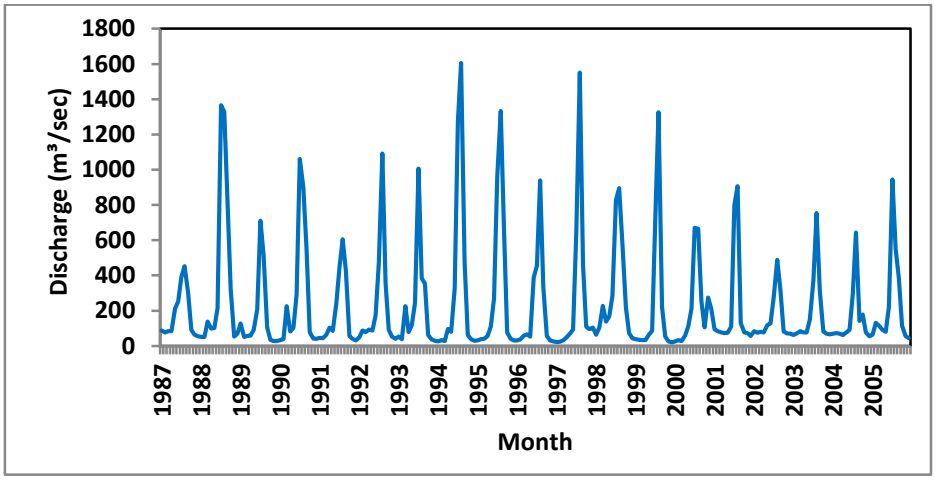

Fig. 3.9 Discharge at Nadaun Bridge (1987 to 2005)

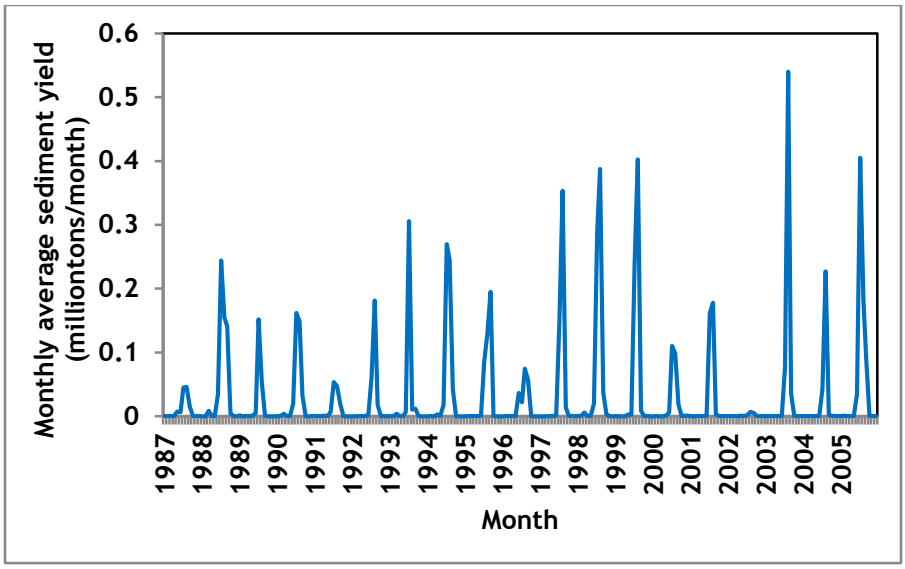

Fig. 3.10 Sediment yield at Nadaun Bridge (1987 to 2005)

3.9 SWAT Model Inputs

SWAT is a comprehensive model that requires information provided by the user to simulate runoff and sediment yield. In the present study SWAT 2012 model was applied on Beas river basin up to Pong dam located in Himachal Pradesh state of India to simulate the surface runoff and sediment yield with topography, land use, soil, and climatic condition.

3.9.1 Digital Elevation model

Digital Elevation Model (DEM) is one of the main and initial inputs of the SWAT (Soil and Water Assessment Tool) model. DEM is used in the SWAT model along with soil and land use/land cover data to delineate the watershed and to further divide the watershed into sub-watersheds and hydrologic response units (HRUs). For this study, the digital elevation model (DEM) was extracted from the global U.S. Geological Survey (USGS) in the format of SRTM (Shuttle Radar Topography Mission) with a spatial resolution of 30 m x 30 m. The DEM was downloaded in geographic co-ordinate system, then was converted to projected coordinate system (WGS1984 UTM Zone 43N) using the raster re-projection tool in ArcGIS before it was imported to ArcSWAT. The projected map was used for watershed delineation. The DEM is presented in figure 3.11

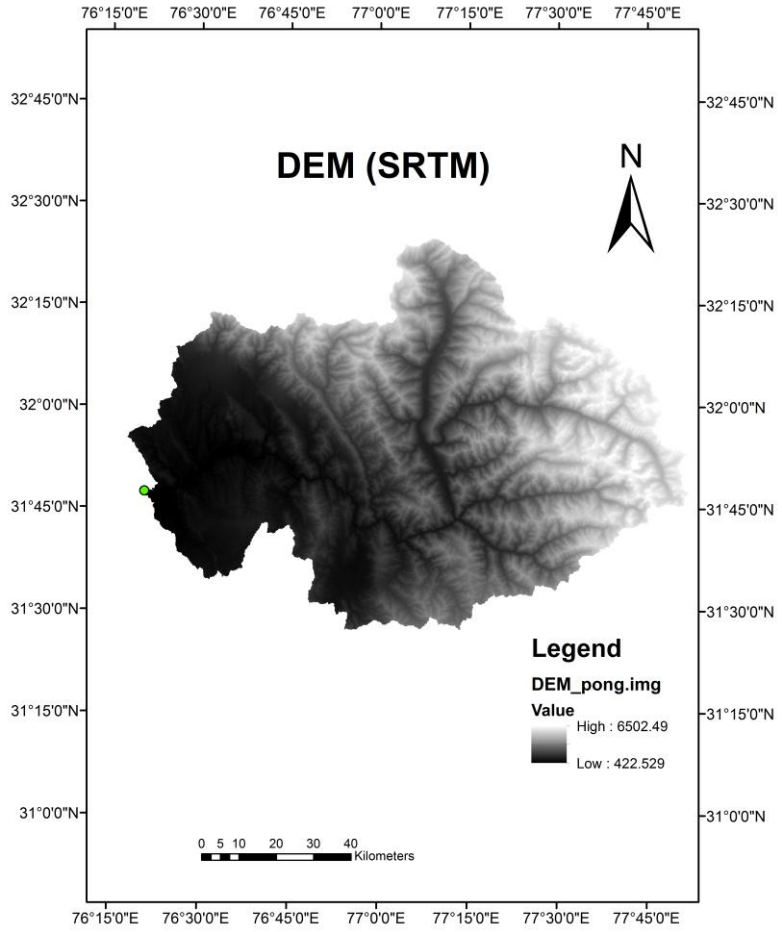

Fig. 3.11 Digital Elevation Model of Beas upto Nadaun bridge

3.9.2 Land use/ land cover map

Land use pattern of watershed is very important in generation of runoff and soil loss, as it affects the distribution of precipitation on the watershed. Land use/land cover data has also a significant effect on the hydrological modelling. For the present study land use/land cover data was obtained from USGS earth explorer Landsat 8 OLI image. The land use/land cover map (30 km resolution) was projected to WGS1984 UTM Zone 43N according to Bias river watershed study area using the raster re-projection tool in ArcGIS. The Projected LULC map was reclassified into different classification which distinguishes seven land use/land cover classes and their percent coverage in the basin is presented in Table 3.2. The land use map of the Beas river basin up to Pong dam is shown in figure 3.12.

Table 3.2 Landuse reclassification and percentage area

S. No.	Landuse	Landuse reclassification	Percentage area
1	Forest-Deciduous	FRSD	36.5
2	Forest-Evergreen	FRSE	26.66
3	ROCK	ROCK	10.01
4	SNOW	SNOW	10.01
5	WATR	WATR	2.11
6	URBAN	URBAN	2.73
7	Agricultural	AGRL	11.99

3.9.3 Soil map

Like the Digital Elevation Model (DEM), soil data resolution has also a significant impact on the modelling of stream flow, sediment load and nutrient content. Soil data is used for assessing the soil type while generating HRUs. Different types of soils have different soil erodability factor, hydraulic conductivity, infiltration capacity etc. which affect the water yield and sediment yield from the watershed. Therefore, using fine spatial resolution soil map will increase the prediction accuracy of the model. The soil map used for the study was obtained from National Bureau of Soil Survey and Land Use Planning (NBSSLUP). The soil map (30 arc-second raster resolution) was projected to WGS1984 UTM Zone43N according to Beas river watershed using the raster re-projection tool in ArcGIS. The soil map is given in figure 3.13.

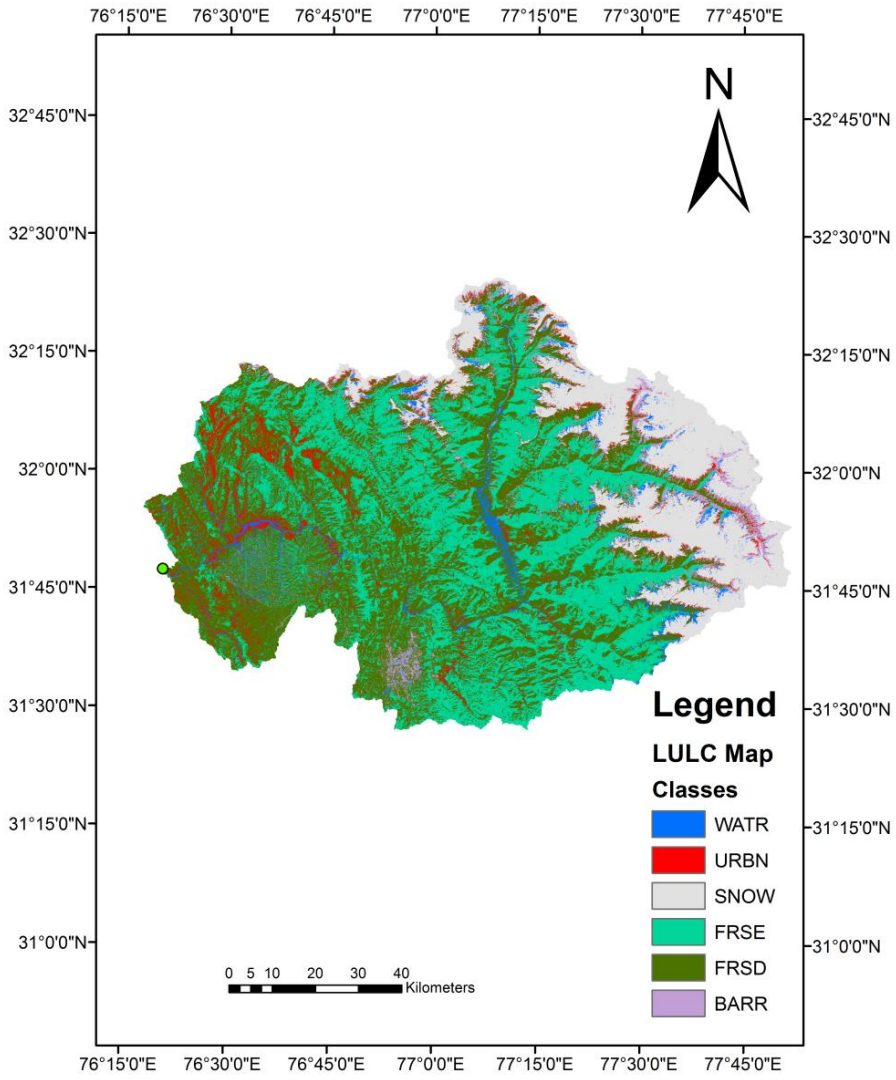

Fig. 3.12 LULC map of Beas upto Nadaun bridge

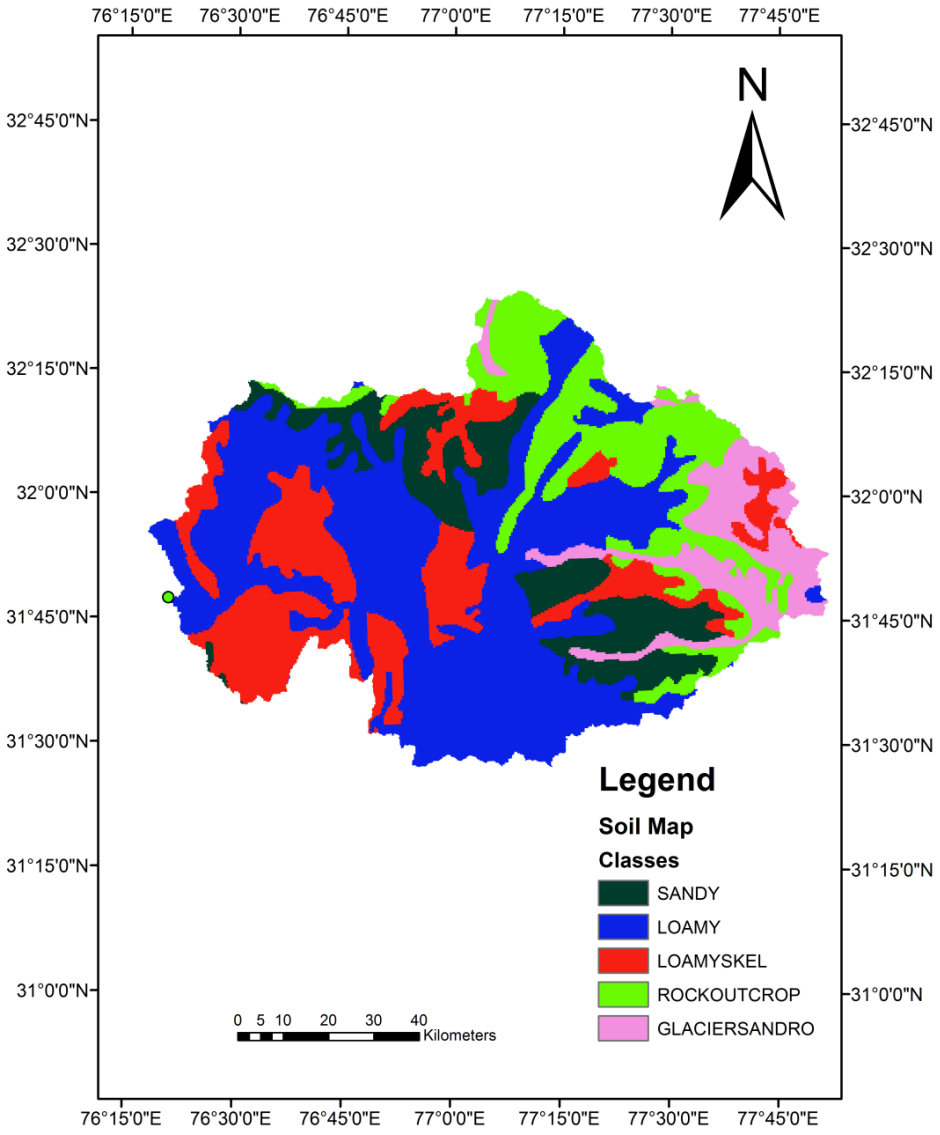

Fig. 3.13 Soil map of Beas upto Nadaun bridge

Based on the soil map, the soil was classified into five categories as shown in Table 3.3. The major soil type in the catchment is loam covering about 42.93 % of the area.

Table 3.3 Soil type and percentage area

S. no.	Soil type	Percentage (area)
1	LOAMY	42.93
2	ROCKOUTCROP	15.23
3	GLACIERSANDRO	8.61
4	LOAMYSKEL	20.10
5	SANDY	13.13

3.9.4 Slope map

Slope map of the basin/watershed represent the rate of change of elevation with respect to the distance along the principal flow path. Slope map of the watershed is important spatial data as required by the SWAT model for HRU creation. The slope map for Beas basin up to Nadaun Bridge was generated from DEM of the basin. The slope map is given in figure 3.14.

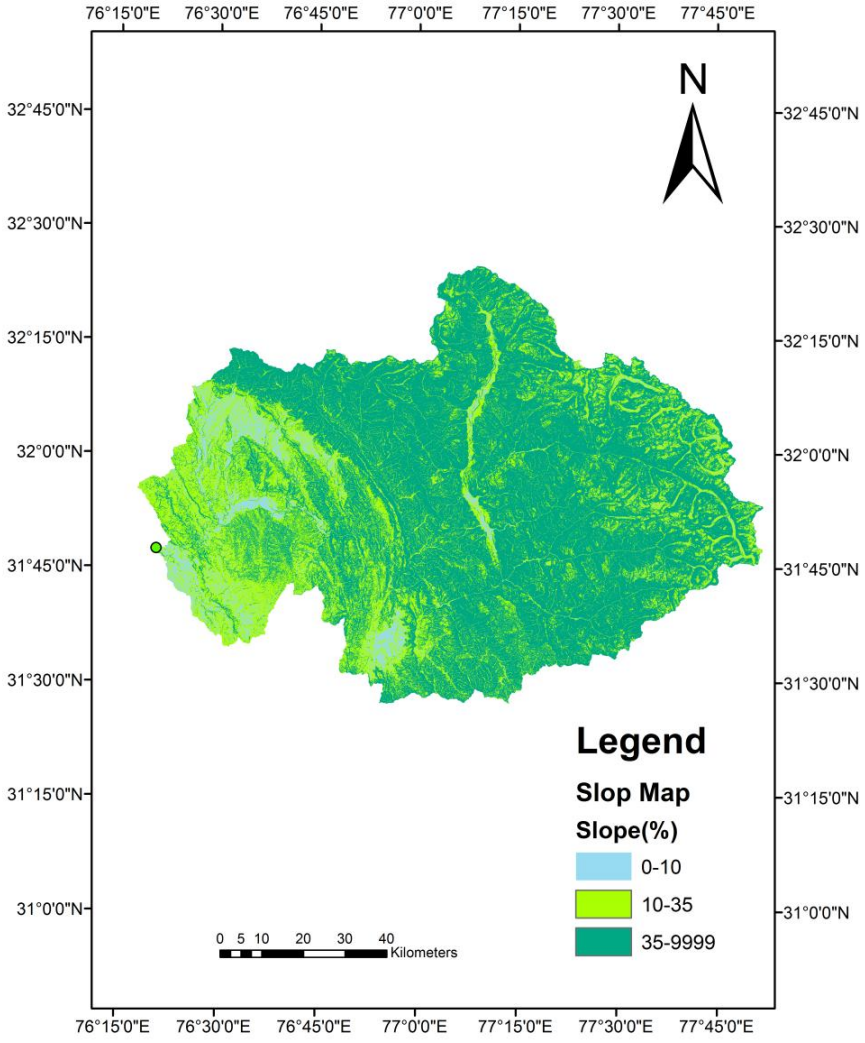

Fig. 3.14 Slope map of Beas upto Nadaun bridge

3.9.5 Meteorological data

Meteorological data is the most important data required for the SWAT model to run. SWAT model requires at least one observed metrological parameter like daily rainfall data to get accurate runoff and sediment while the other metrological parameters can be simulated by SWAT model using weather generator. The rainfall and minimum and maximum temperature data required for the study were obtained from IMD for 0.25x0.25 Deg gird. The other meteorological parameters i.e. solar radiation, relative humidity, wind speed were simulated by SWAT model with help of weather generator. NCEP Reanalysis data (historical period) were used for statistical downscaling of rainfall, minimum and maximum temperature. The probability of exceedence method was used to bias correct the statistically downscaled data.

3.10 SWAT model Setup

The first step in model set up was creating the new SWAT project in ArcSWAT. Then the projected DEM map was imported in to ArcSWAT. Next the area of interest was delineated by selecting a point at the outlet of the watershed and found to be 959742.0900 ha. The drainage network, flow accumulation and flow direction were automatically processed in ArcSWAT. 21 number of sub basins were delineated by Arc SWAT for Beas river up to pong watershed. Projected Land use and soil map were imported in to the ArcSWAT model for hydrologic response unit (HRU) analysis. The watershed/sub basins further are divided into hydrologic response units and HRU are part of sub basins possess unique land use/soil/slope. The benefits of HRU are for more accuracy in prediction of sediment load from sub basins. Both the LULC and soil maps were classified in ArcSWAT. The land slope of the study area was classified into four slope classes and made to overlay with land use and soil maps to subdivide the study watershed into hydrologic response units. A total of 190 HRUs were defined for the whole catchment. After HRUs were defined, the nest step was to import the weather data into SWAT project. Weather data is the most important input for simulating the hydrological parameters and sediment load in SWAT model. So weather data were prepared in text (.txt) format and added using weather station input option in the SWAT model. Then the various SWAT input tables were written into the model namely configuration file, soil data, land use, management file etc. SWAT input

parameters were edited using SWAT editor before the model was run for simulation. Penman-Monteith equation method was selected for calculating the potential evapotranspiration, SCS curve number was chosen to calculate surface runoff, initial curve number was estimated using soil moisture method, and Muskingum method was selected for channel routing. Finally, the model was run for the year from 1987 to 2005 by fixing the warm up period of five years. Generally, warm up period is recommended 3–5 years for SWAT model to reach at hydrological equilibrium. The sensitivity parameters for runoff and sediment yield were optimized by SUFI2 algorithm (Sequential Uncertainty Fitting version 2).

Chapter 4.0 The statistical downscaling model (SDSM)

The statistical downscaling model (SDSM) is a multiple regression-based tool for generating future scenarios to assess the impact of climate change on different hydrological variables. It has the ability to capture the inter-annual variability better than other statistical downscaling approaches. This approach involves three sub-classes such as weather typing, weather generator and regression/transform function. The model requires two types of daily data, i.e., (i) the local data known as 'Predictand' (rainfall, minimum and maximum temperature) and (ii) the different atmospheric variables known as 'Predictors'. Formulating an empirical relationship between predictand and predictor is central to the downscaling technique. This can be derived by various methods such as parametric (multiple linear regression) and non-parametric (artificial neural network; support vector machine). This study used the Multiple Linear Regression method which falls under parametric methods. The downscaling was carried out using SDSM tool version 4.2.9. The predictors were obtained from National Centres for Environmental Protection (NCEP) reanalysis data for the period from 1961-2005. The NCEP reanalysis data were downloaded from CanESM2 website. The reanalysis data consists of 26 parameters (predictors) related to various atmospheric variables. SDSM tool was used to find out significant predictors out of 26 predictors using the NCEP reanalysis data and the IMD data for rainfall, minimum and maximum temperature for the period from 1961 to 2005 by correlation analysis. The averaged gridded data for rainfall, minimum and maximum temperature were considered for the downscaling of data. The gridded rainfall data from IMD was for the period from 1961 to 2013. The gridded maximum and minimum temperature from IMD were for period from 1961 to 2005. The gridded rainfall was converted into point rainfall by Thiessen polygon of 31 subwatersheds. The gridded maximum and minimum temperature were converted into point data by averaging all the gridded data. The significant predictors extracted from SDSM tool for rainfall, maximum and minimum temperature were used to get regression equation with the IMD data for the period from 1961 to 1995. The multiple regression equations obtained using the significant predictors and the IMD data were calibrated and validated for the period from 1961 to 1995 and from 1996 to 2005 respectively. The significant parameters for rainfall, minimum and maximum temperature are given as follows:

4.1 Significant predictors out of 26 predictors for rainfall

- ncepmslpgl.dat - mean sea level pressure (pa)
- ncepprcpgl.dat -total precipitation (mm)
- ncepp1_fgl.dat - surface airflow strength (m/s)
- ncepr500gl.dat- surface specific humidity at 500 hPa (%)
- ncpshumgl.dat -surface specific humidity (%)

4.2 Significant predictors out of 26 predictors for Minimum temperature

- ncepmslpgl.dat -mean sea level pressure (pa)
- ncepp1zhgl.dat- wind direction at 500 hPa
- ncepp5_zgl.dat- vorticity at 500 hPa
- ncepp500gl.dat- geopotential height (m) at 500 hPa
- ncpshumgl.dat- surface specific humidity (%)

4.3 Significant predictors out of 26 predictors for Maximum temperature

- ncepmslpgl.dat -mean sea level pressure (pa)
- ncepp1zhgl.dat- wind direction at 500 hPa
- ncepp5_fgl.dat- surface airflow strength (m/s) at 500 hPa
- ncepp5_zgl.dat- vorticity at 500 hPa
- ncepp500gl.dat- geopotential height (m) at 500 hPa
- nceptempgl.dat- Mean Temp (˚C)

The scatter plot for calibration and validation of rainfall using the multiple regression equation for downscaling obtained from the significant predictors and the IMD data are presented in figures 4.1 and 4.2. The coefficient of determination (R^2) for calibration (1961-1995) and validation (1996 – 2005) of rainfall were found to be 0.98 and 0.96 respectively. The scatter plot for calibration and validation of maximum temperature using the multiple regression equation for downscaling obtained from the significant predictors and the IMD data are presented in figures 4.3 and 4.4. The coefficient of determination (R^2) for calibration (1961-1995) and validation (1996 – 2005) of maximum temperature were found to be 1.0 and 1.0 respectively. The scatter plot for calibration and validation of minimum temperature using the

multiple regression equation for downscaling obtained from the significant predictors and the IMD data are presented in figures 4.5 and 4.6. The coefficient of determination (R^2) for calibration (1961-1995) and validation (1996 – 2005) of minimum temperature were found to be 1.0 and 1.0 respectively.

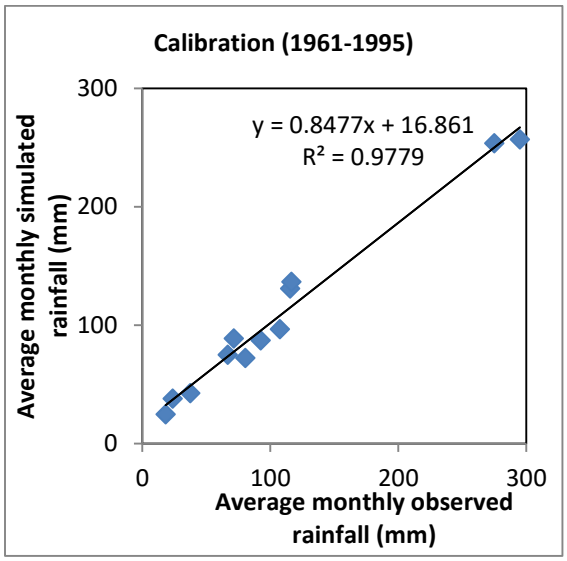

Fig. 4.1 Scatter plot of rainfall during calibration for 1961-1995

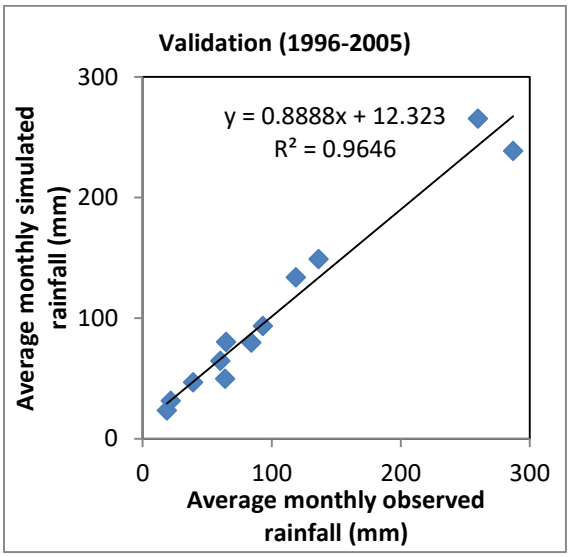

Fig. 4.2 Scatter plot of rainfall during validation for 1996-2005

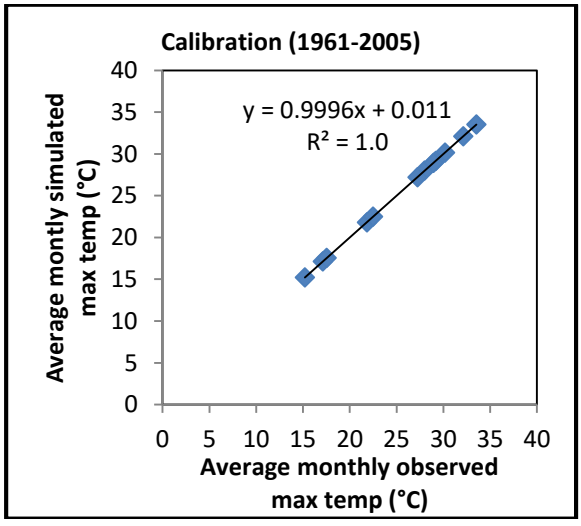

Fig. 4.3 Scatter plot of maximum temperature during calibration for 1961-1995

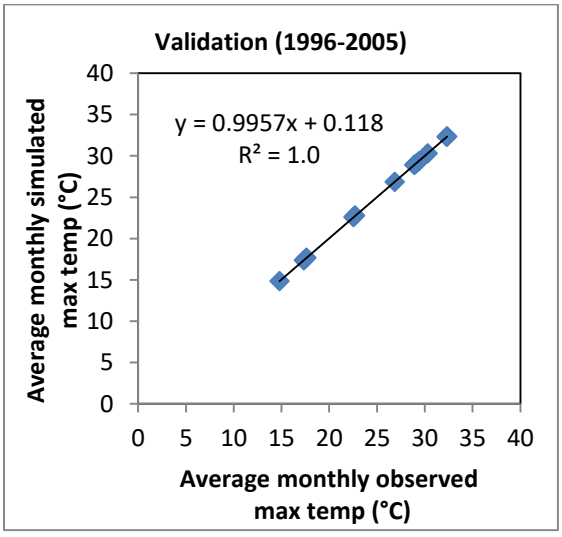

Fig. 4.4 Scatter plot of maximum temperature during validation for 1996-2005

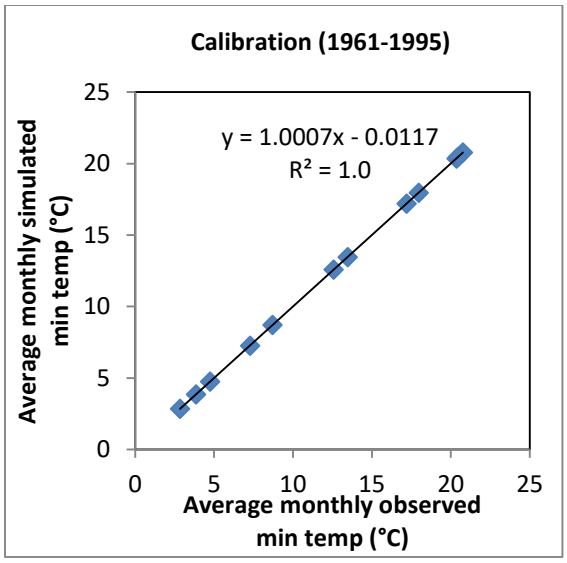

Fig. 4.5 Scatter plot of minimum temperature during calibration for 1961-1995

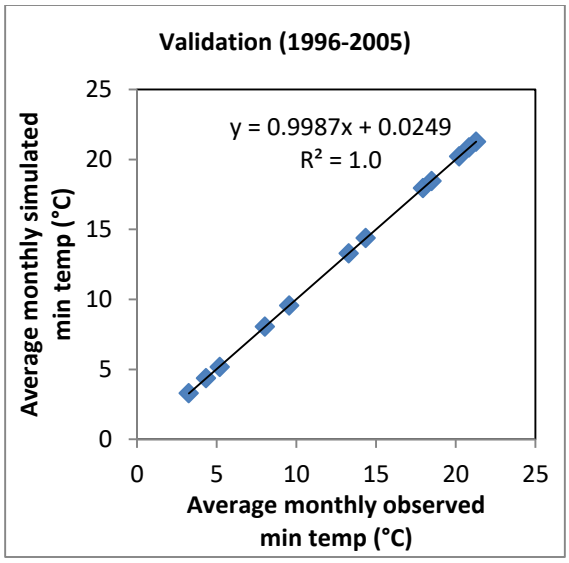

Fig. 4.6 Scatter plot of minimum temperature during validation for 1996-2005

Table 4.1 Performance of linear regression model for rainfall, maximum and minimum temperature

	Rainfall	Maximum temperature	Minimum temperature
Calibration results – R^2	0.98	1.0	1.0
Validation results – R^2	0.96	1.0	1.0

The multiple linear regression models developed using SDSM with NCEP reanalysis and IMD data for rainfall, maximum and minimum temperature could be used for the downscaling of data from CanESM2 CMIP5 model for the scenarios RCP 2.6, RCP 4.5 and RCP 8.5 based on the performance of the models during calibration and validation as mentioned in Table 4.1

4.6 Downscaling of data

The significant predictors of rainfall, maximum and minimum temperature from CanESM2 for climate scenarios RCP 2.6, RCP 4.5 and RCP 8.5 were downloaded from the website of Canadian Centre for Climate Modelling and Analysis for the period from 2006-2100. The multiple linear regression models developed using SDSM with NCEP reanalysis and IMD

data for rainfall, maximum and minimum temperature were used to downscale the data with the significant predictors downloaded from CanESM2 for climate scenarios RCP 2.6, RCP 4.5 and RCP 8.5. The downscaled data of rainfall, maximum and minimum temperature were bias corrected by the method of probability of exceedence as mentioned in the following section 4.5

4.5 Bias correction method

The goal of the bias correction method is to use the probability of exceedence of monthly projected values and match this probability to the historical observed climate value (Wood et al. 2007). The steps followed for the bias correction are explained below.

1. Compute empirical probability of exceedance curve Pobs(P) from observed predictand values at particular month.

2. Compute empirical probability of exceedence curve PGCM (P) for a GCM results, for the same period and same month as from predictand values at particular month historical values of step 1

3. Do bias correction approach, i=1, number of observations

   (a) Select a given value PGCM

   (b) For this particular value PGCM, compute its probability of exceedence from the curve derived in step 2.

   Using the probability obtained in step 3b, go to the probability of exceedance curve Pobs(P) and assume PGCM(TGCM)=Pobs(PGCM)

   (d) Using the probability Pobs(PGCM), compute Pobs

   (e) Do this for all months.

The downscaled rainfall, maximum and minimum temperature from CanESM2 for climate scenarios RCP 2.6, RCP 4.5 and RCP 8.5 with the significant predictors were bias corrected by the method of probability of exceedence as explained above. The bias corrected avearge monthly rainfall and bias corrected monthly rainfall for the scenario RCP 2.6 for 2006-2100 are presented in figures 4.7 and 4.8 respectively. The bias corrected avearge monthly

rainfall and bias corrected monthly rainfall for the scenario RCP 4.5 for 2006-2100 are presented in figures 4.9 and 4.10 respectively. The bias corrected avearge monthly rainfall and bias corrected monthly rainfall for the scenario RCP 8.5 for 2006-2100 are presented in figures 4.11 and 4.12 respectively. The bias corrected average monthly rainfall values for the scenarios RCP 2.6, RCP 4.5 and RCP 8.5 are given in Table 4.2. The bias corrected avearge monthly maximum temperature and bias corrected monthly maximum temperaure for the scenario RCP 2.6 for 2006-2100 are presented in figures 4.13 and 4.14 respectively. The bias corrected avearge monthly maximum temperature and bias corrected monthly maximum temperaure for the scenario RCP 4.5 for 2006-2100 are presented in figures 4.15 and 4.16 respectively. The bias corrected avearge monthly maximum temperature and bias corrected monthly maximum temperaure for the scenario RCP 8.5 for 2006-2100 are presented in figures 4.17 and 4.18 respectively. The bias corrected average monthly maximum temperature values for the scenarios RCP 2.6, RCP 4.5 and RCP 8.5 are given in Table 4.3.The bias corrected avearge monthly minimum temperature and bias corrected monthly minimum temperaure for the scenario RCP 2.6 for 2006-2100 are presented in figures 4.19 and 4.20 respectively. The bias corrected avearge monthly minimum temperature and bias corrected monthly minimum temperaure for the scenario RCP 4.5 for 2006-2100 are presented in figures 4.21 and 4.22 respectively. The bias corrected avearge monthly minimum temperature and bias corrected monthly minimum temperaure for the scenario RCP 8.5 for 2006-2100 are presented in figures 4.23 and 4.24 respectively. The bias corrected average monthly minimum temperature values for the scenarios RCP 2.6, RCP 4.5 and RCP 8.5 are given in Table 4.4.

Table 4.2 Bias corrected average monthly rainfall values (mm) for the scenarios RCP 2.6, RCP 4.5 and RCP 8.5

Month	RCP 2.6	RCP 4.5	RCP 8.5
Jan	62.07	53.80	61.96
Feb	58.96	57.87	59.13
Mar	83.13	75.91	77.40
Apr	78.17	78.71	83.95
May	82.81	87.53	86.41
Jun	110.86	114.01	130.32
Jul	181.05	168.12	231.03
Aug	193.33	171.17	211.38
Sep	110.87	121.20	113.30
Oct	71.32	69.14	70.24
Nov	70.29	63.60	61.70
Dec	57.56	60.96	61.96

Table 4.3 Bias corrected average monthly maximum temperature values (°C) for the scenarios RCP 2.6, RCP 4.5 and RCP 8.5

Month	RCP 2.6	RCP 4.5	RCP 8.5
Jan	16.2	16.4	17.1
Feb	19.2	19.2	19.9
Mar	23.4	23.9	24.8
Apr	29.8	30.6	32.1
May	38.7	39.4	41.3
Jun	34.5	35.2	35.7
Jul	30.3	30.4	30.7
Aug	30.0	30.2	30.6
Sep	29.8	30.1	30.6
Oct	28.2	28.5	29.2
Nov	23.5	24.0	24.5
Dec	18.5	19.1	19.4

Table 4.4 Bias corrected average monthly minimum temperature values (°C) for the scenarios RCP 2.6, RCP 4.5 and RCP 8.5

Month	RCP 2.6	RCP 4.5	RCP 8.5
Jan	3.1	3.2	3.5
Feb	5.5	5.6	6.1
Mar	9.5	9.8	10.4
Apr	14.7	15.1	16.0
May	20.4	20.9	22.2
Jun	23.4	23.9	24.7
Jul	23.2	23.5	24.2
Aug	22.0	22.4	23.3
Sep	18.8	19.2	20.1
Oct	13.2	13.6	14.1
Nov	8.1	8.4	8.9
Dec	4.0	4.3	4.6

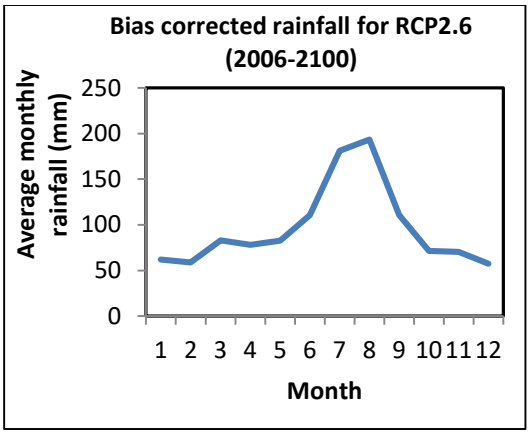

Fig 4.7 Bias corrected average monthly rainfall for the scenario RCP 2.6 for 2006-2100

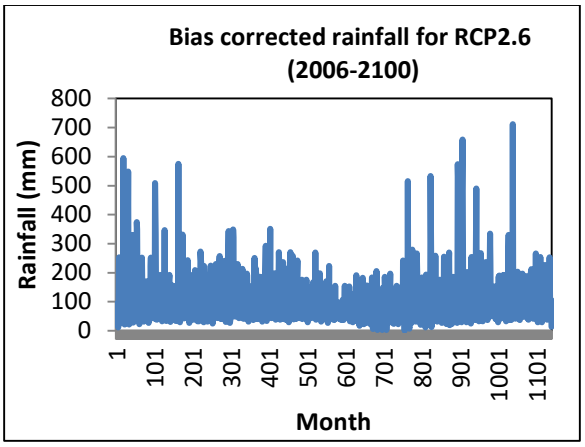

Fig 4.8 Bias corrected monthly rainfall for the scenario RCP 2.6 for 2006-2100

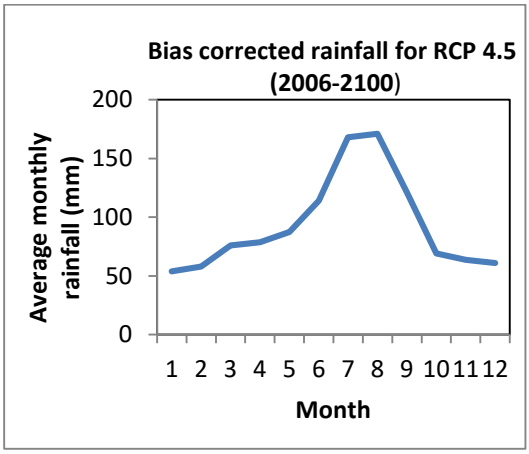

Fig 4.9 Bias corrected average monthly rainfall for the scenario RCP 4.5 for 2006-2100

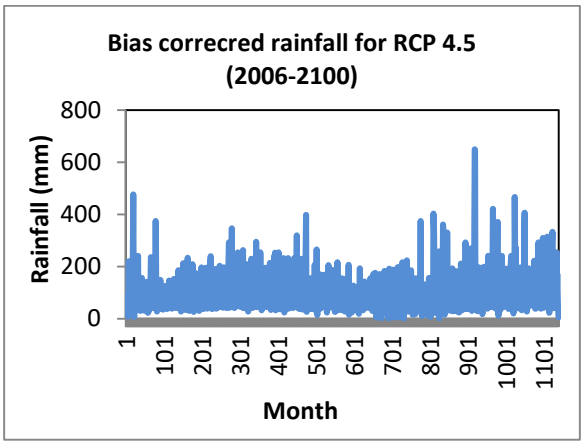

Fig 4.10 Bias corrected monthly rainfall for the scenario RCP 4.5 for 2006-2100

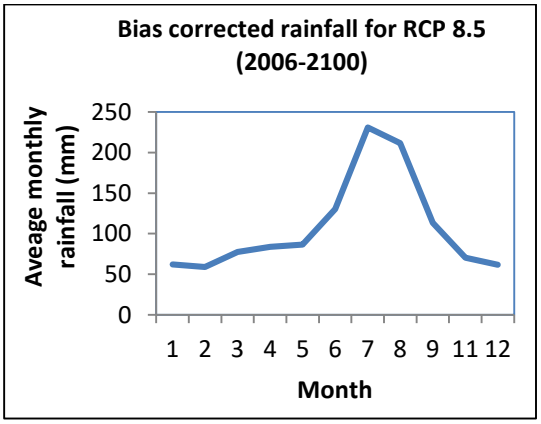

Fig 4.11 Bias corrected average monthly rainfall for the scenario RCP 8.5 for 2006-2100

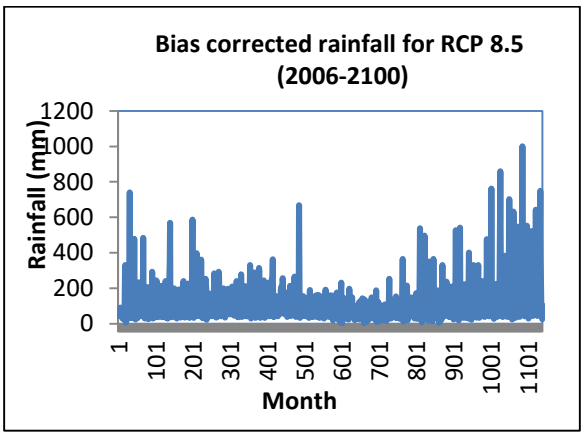

Fig 4.12 Bias corrected monthly rainfall for the scenario RCP 8.5 for 2006-2100

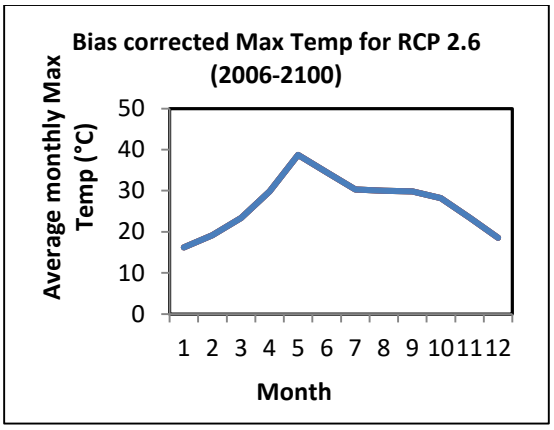

Fig 4.13 Bias corrected average monthly maximum temperature for the scenario RCP 2.6 for 2006-2100

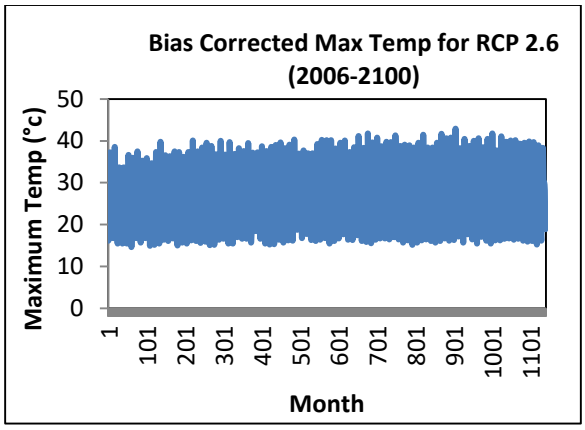

Fig 4.14 Bias corrected monthly maximum temperature for the scenario RCP 2.6 for 2006-2100

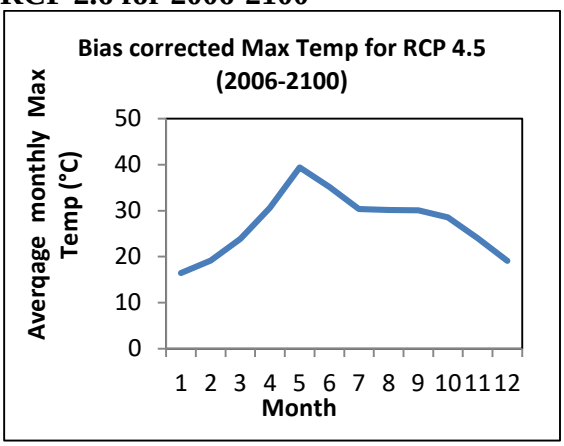

Fig 4.15 Bias corrected average monthly maximum temperature for the scenario RCP 4.5 for 2006-2100

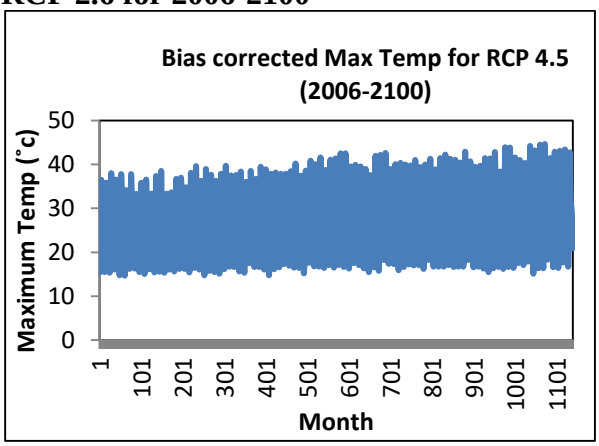

Fig 4.16 Bias corrected monthly maximum temperature for the scenario RCP 4.5 for 2006-2100

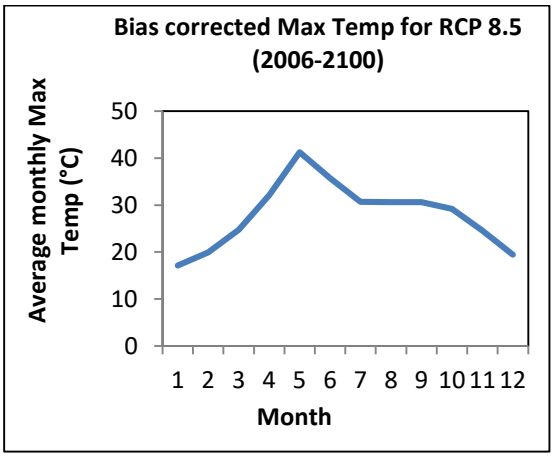

Fig 4.17 Bias corrected average monthly maximum temperature for the scenario RCP 8.5 for 2006-2100

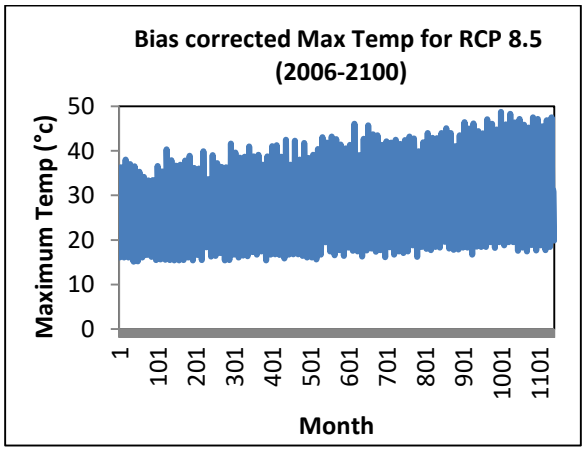

Fig 4.18 Bias corrected monthly maximum temperature for the scenario RCP 8.5 for 2006-2100

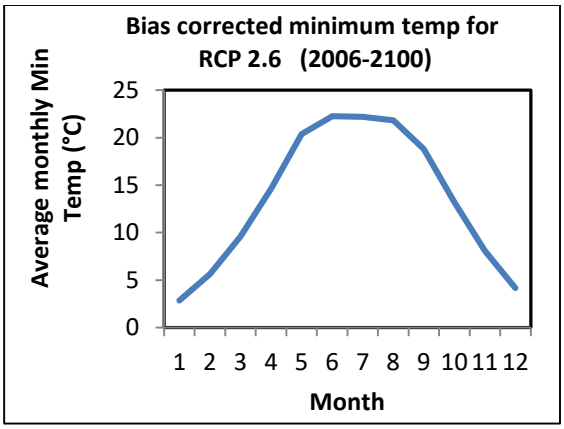

Fig 4.19 Bias corrected average monthly minimum temperature for the scenario RCP 2.6 for 2006-2100

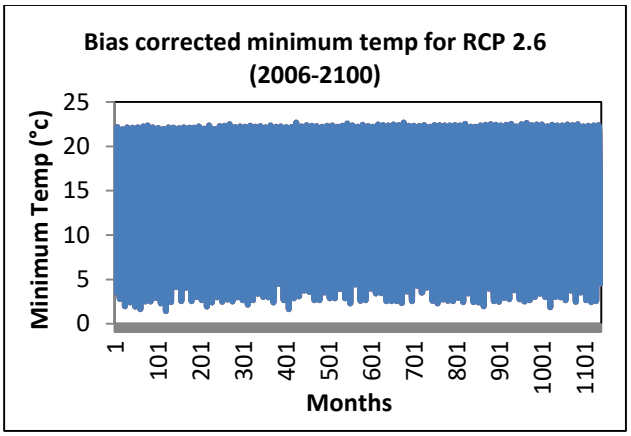

Fig 4.20 Bias corrected monthly minimum temperature for the scenario RCP 2.6 for 2006-2100

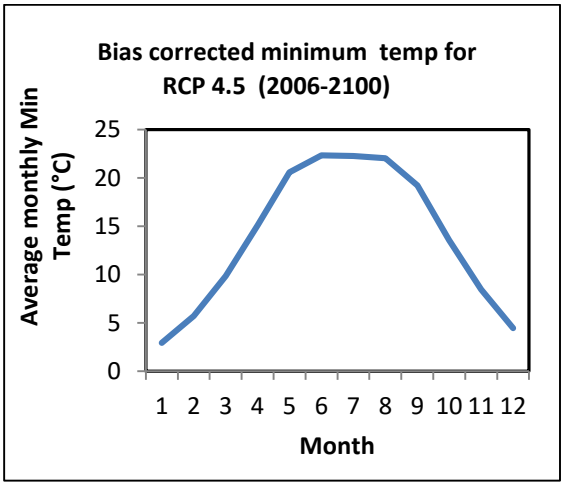

Fig 4.21 Bias corrected average monthly minimum temperature for the scenario RCP 4.5 for 2006-2100

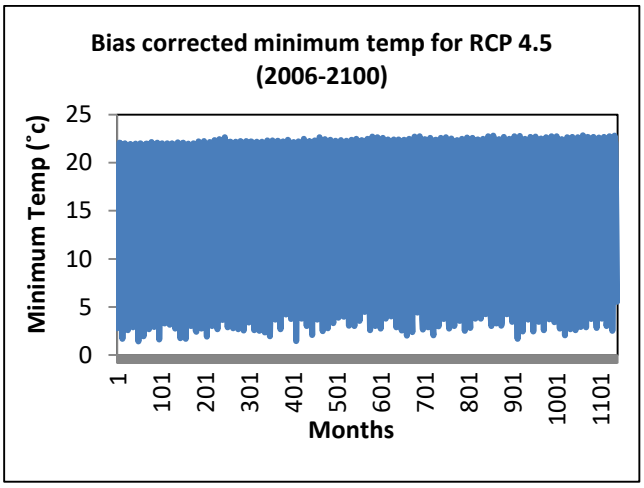

Fig 4.22 Bias corrected monthly minimum temperature for the scenario RCP 4.5 for 2006-2100

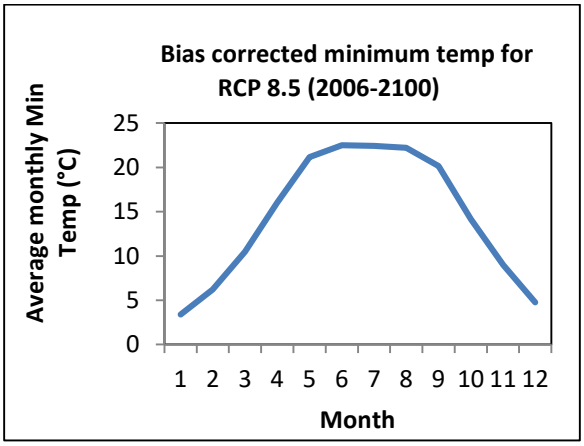

Fig 4.23 Bias corrected average monthly minimum temperature for the scenario RCP 8.5 for 2006-2100

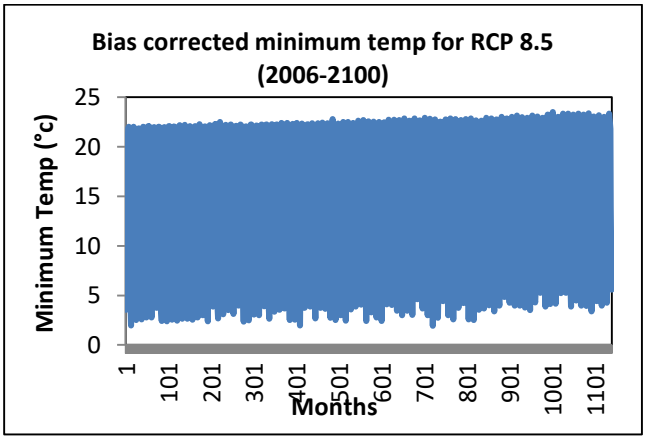

Fig 4.24 Bias corrected monthly minimum temperature for the scenario RCP 8.5 for 2006-2100

Chapter 5.0 Projected life of the reservoir

The discharge and sediment yield for the climate scenarios RCP 2.6, RCP 4.5 and RCP 8.5 for 2006-2100 can be simulated using SWAT with the input such as DEM, slope map, LULC, soil map, bias corrected rainfall, maximum and minimum temperature for the climate scenarios RCP 2.6, RCP 4.5 and RCP 8.5 for 2006-2100. The consolidated unit weight of the sediment to be deposited in the reservoir for the period 2025, 2050, 2075 and 2100 is required to be estimated to find out the projected life of the reservoir. The unit weight of the sediment is estimated from the properties of the suspended sediment load as explained in section 5.1. The consolidated unit weight of the sediment is estimated by empirical formula proposed by Miller (1953) using the unit weight of the sediment estimated from the properties of suspended sediment load as explained in section 5.2. The consolidated unit weight of the sediment can be obtained by the porosity of the deposited sediment and frequency analysis of the suspended sediment load. The following sections explain to find out the consolidated unit weight of the sediment for 2025, 2050, 2075 and 2100.

5.1 Unit Weight of Deposited Sediment in Reservoir

The computation of unit weight of deposited sediment in reservoir is essential to arrive at the consolidated volume of sediment for required periods using the generated series of sediment yield. The best method of estimation of unit-weight of sediment is from the observation of sediment load at upstream of the reservoir and the volume of sediment in the reservoir by hydrographic survey. But the operation condition of the reservoir sometimes prevents to carry out the hydrographic survey to compute the most accurate value of the unit-weight of the deposited sediment. In such case, the equation proposed by Lara and Pemberton (Strand and Pemberton 1987) can be used to estimate the unit-weight of the sediment from the proportion of particle size distribution of suspended sediment concentration and the method of reservoir operation and it is given as:

$$W = W_C P_C + W_m P_m + W_S P_S \tag{5.1}$$

where W is unit weight in kg/m^3, P_c, P_m, P_s are percentages of clay, silt and sand of the incoming sediment respectively and W_c, W_m, W_s are initial unit weights of clay, silt and sand respectively.

The classification of sediment according to size as proposed by the American Geophysical Union can be used to estimate the percentages of clay, silt and sand and is given in Table 5.1. The values of W_c, W_m and W_s are obtained from the Table 5.2.

Table 5.1 Soil classification by American Geophysical union

Sediment type	**Size range (*mm*)**
Clay	**Less than 0.004**
Silt	**0.004 to 0.0625**
Sand	**0.0625 to 2.0**

Table 5.2 Coefficient values for Lara-Pemberton equation

Operational Condition of the reservoir	**Initial weight, *kg/m³***		
	W_c	W_m	W_S
Continuously submerged	**416**	**1120**	**1150**
Periodic drawdown	**561**	**1140**	**1150**
Normally empty reservoir	**641**	**1150**	**1150**
Riverbed sediment	**961**	**1170**	**1550**

5.2 Estimation of Consolidated Unit Weight of Sediment

5.2.1 *Consolidated Unit Weight of Sediment by Empirical Method*

The average unit weight of all sediment deposited during t years of consolidation is computed using the equation presented by Miller (1953) and is given as

$$W_t = W_1 + 0.4343B\left[\frac{t}{t-1}(\ln t) - 1\right] \tag{5.2}$$

where W_t is the average unit weight after t years of consolation, W_1 is the initial unit weight and B is a constant and is given as

$$B = B_C P_C + B_m P_m + B_S P_S \tag{5.3}$$

where P_c, P_m, P_s are percentages of clay, silt and sand of the incoming sediment respectively and B_c, B_m, B_s are unit weights of clay, silt and sand respectively. The values of B_c, B_m and B_s are obtained from Table 5.3.

Table 5.3 Coefficient values for the calculation of consolidated unit weights

Operational Condition	B, kg/m^3		
	Sand	Silt	Clay
Continuously submerged	0	91	256
Periodic drawdown	0	43	171
Considerable drawdown	0	16	96
Normally empty reservoir	0	0	0

5.2.1 *Consolidated Unit Weight of Sediment by Porosity of the Sediment*

Swamee (2001) have analyzed number of soil samples of the reservoirs and have found the value of initial (λ_i) and ultimate (λ_∞) porosity of uniformly distributed sediment as 0.523 and 0.355 respectively. The following equation can be used to find the initial and ultimate unit weight of the sediment by assuming initial and ultimate porosity as 0.523 and 0.355.

$$\lambda = 1 - \frac{\rho_{bulk}}{\rho_{particle}} \tag{5.4}$$

where ρ_{bulk} is unit weight of the sediment and $\rho_{particle}$ is particle density which is 2650 kg/m^3. If the time for which the reservoir gets silted up is known, the unit weight of the sediment can be interpolated linearly for any particular year.

5.2.2 *Consolidated Unit Weight of Sediment by Frequency Analysis*

Frequency analysis helps to identify the statistical population of random variable from which the sample measurements have come from (Ojha et al. 2008). Probability statements about the future occurrences of random variable can be made once the population distribution is identified. The possible distribution to represent any hydrological random variable includes Generalized logistic (*GLO*), Generalized extreme value (*GEV*), Generalized normal, Pearson type III and generalized Pareto, all are three parameter distributions. The parent distribution, four parameter Kappa distribution, is considered to simulate large sample from the measurement values and from which the suitable population distribution can be identified from goodness of fit measures of each possible distribution considered. The probability density function *f(x)*,

cumulative distribution function *F(x)* and quintile function *x(F)* of Kappa distribution is given as follows (Hosking and Wallis 1997):

$$f(x) = \alpha^{-1}\left\{1-\frac{k(x-\xi)}{\alpha}\right\}^{\frac{1}{k-1}}\{F(x)\}^{1-h} \tag{5.5}$$

$$F(x) = \left[1-h\left\{1-\frac{k(x-\xi)}{\alpha}\right\}^{\frac{1}{k}}\right]^{\frac{1}{h}} \tag{5.6}$$

$$x(F) = \xi + \frac{\alpha}{k}\left\{1-\left(\frac{1-F^{h}}{h}\right)^{k}\right\} \tag{5.7}$$

where ξ (location), α (scale), k, h are parameters and F is the probability of non exceedence.

The parameters of any distribution can be estimated by Graphical method, Method of Moments (*MOM*), Probability Weighted Moments (*PWM*) and L-moments. If *PDF* be denoted by $F = F(x) = P[X \le x]$, then *PWM*s are the moment of the function *x(F)*,and they are expressed as

$$M_{i,j,k} \equiv E\left[x^{i}F^{j}(1-F)^{k}\right] = \int_{0}^{1}\left[x(F)^{i}F^{j}(1-F)^{k}\right]dF \tag{5.8}$$

where $M_{i,j,k}$ is the *PWM* of the order of *i, j* and *k*; and *E* is the expectation operator.

L-moments are linear combination of order statistics which are robust to outliers and are unbiased for small samples. L-moments are identified as linear combination of probability weighted moment (*PWM*) and first four L-moments are given as

$$\lambda_1 = \beta_0 \tag{5.9a}$$

$$\lambda_2 = 2\beta_1 - \beta_0 \tag{5.9b}$$

$$\lambda_3 = 6\beta_2 - 6\beta_1 + \beta_0 \tag{5.9c}$$

$$\lambda_4 = 20\beta_3 - 30\beta_2 + 12\beta_1 + \beta_0 \tag{5.9d}$$

L-moments produce quintile estimates with lower root mean squared error than unbiased alternatives. The unbiased estimates of *PWMs* for any distribution can be computed as follows:

$$b_o = \frac{1}{n} \sum_{j=1}^{n} x_j \tag{5.10a}$$

$$b_1 = \sum_{j=1}^{n-1} \left[\frac{(n-j)}{(n)(n-1)} \right] x_j \tag{5.10b}$$

$$b_2 = \sum_{j=1}^{n-2} \left[\frac{(n-j)(n-j-1)}{(n)(n-1)(n-2)} \right] x_j \tag{5.10c}$$

$$b_3 = \sum_{j=1}^{n-3} \left[\frac{(n-j)(n-j-1)(n-j-2)}{(n)(n-1)(n-2)(n-3)} \right] x_j \tag{5.10d}$$

where x_j represents the order values of random variable with x_1 as the largest value and x_n as the smallest value. The L-moment ratios which are used for expressing the parameter estimates are expressed as L-coefficient of variation $(\tau) = \lambda_1$; L-skewness $(\tau_3) = \frac{\lambda_3}{\lambda_2}$ and L-kurtosis $(\tau_4) = \frac{\lambda_4}{\lambda_3}$. The sample estimates of L-moments are calculated by replacing b_0, b_1, b_2 and b_3 for $\beta_0, \beta_1, \beta_2$ and β_3 in equations 5.9a to 5.9d. The goodness-of-fit measure for each distribution is given as

$$Z^{DIST} = \left(\tau_4^{DIST} - \tau_4^R + B4 \right) / \sigma_4 \tag{5.11}$$

where *DIST* can be any of the three parameter distributions such as generalized logistic (GLO), Generalized extreme value (GEV), Generalized normal, Pearson type III and generalized Pareto; τ_4^{DIST} is L-kurtosis of the fitted distribution; τ_4^R is regional average of L-kurtosis; $B4$ is the bias of τ_4^R. The standard deviation of τ_4^R is given as

$$\sigma_4 = \left[\left(N_{sim} - 1 \right)^{-1} \left\{ \sum_{m=1}^{N_{sim}} \left(\tau_4^{[m]} - \tau_4^R \right)^2 - N_{sim} B_4^2 \right\} \right]^{\frac{1}{2}} \tag{5.12}$$

The bias of τ_4^R is given as

$$B_4 = N_{sim} - 1 \sum_{m=1}^{N_{sim}} \left(\tau_4^{[m]} - \tau_4^R \right) \tag{5.13}$$

where $\tau_4^{[m]}$ is L-kurtosis for N_{sim} of realizations of a region with *N* sites by fitting kappa distribution to the regional average L-moment ratios, τ^R (L-Coefficient of Variation), τ_3^R (L-Skewness), and τ_4^R (L-kurtosis). If $\left| Z^{DIST} \right| \leq \pm 1.64$, the fitness of the considered distribution is adequate. If any of the considered distribution is not satisfying the goodness-of-fit, Wakebey distribution is selected as best distribution for the measured data. The quantile estimate of Wakebey distribution is given as

$$x(F) = \xi + \frac{\alpha}{\beta} \left\{ 1 - \left(1 - F \right)^{\beta} \right\} - \frac{\gamma}{\delta} \left\{ 1 - \left(1 - F \right)^{-\delta} \right\} \tag{5.14}$$

where ξ (location), α , β , γ , δ are parameters of the distribution. Once the parameters of the distribution are estimated the quantile estimate of any return period can be obtained from the equation of *x(F).* This method is valid up to the maximum possible consolidation of the sediment in the reservoir.

5.3 Trap efficiency of the reservoir

Swamee (2001) proposed the following equation for the estimation of the trap efficiency of the reservoir

$$\eta = \left[\left(\frac{t}{t*} \right)^{\frac{1}{q}} + 1 \right]^{-(q+1)} \tag{5.15}$$

where t is the year for which the trap efficiency is to be computed; t_* is the time for which the reservoir gets silted up; q is transition exponent and can be obtained from the following equation

$$q = 1.4427 \ln\left(\frac{V_i}{v*}\right) \tag{5.16}$$

where V_i is the initial storage capacity of the reservoir and v_* is the storage capacity at t_* which is obtained from the plot of cumulative volume of deposition *V*s time.

5.4 Sediment volume prediction

The simulated sediment yield at the reservoir is converted into sediment volume by the consolidated unit weight of the sediment. The simulated sediment volume is compared with the volume computed by the empirical formulae given by Swamee (2001) and are given as follows:

$$v = V_i \left[\left(\frac{t*}{t}\right)^{\frac{1}{q}} + 1 \right]^{-q} \tag{5.17}$$

$$V = V_i - v \tag{5.18}$$

where *v* is the reservoir capacity for any year *t*. The sediment volume is computed from equation (5.18). The consolidated unit weights of sediment after 25, 50, 75, 100 years computed by all three methods mentioned in the above sections, trap efficiency of the reservoir and sediment yield simulated at the reservoir for 2025, 2050, 2075, 2100 for RCP 2.6, RCP 4.5 and RCP 8.5 are used to find out possible range of sediment volumes for future 2025, 2050, 2075 and 2100 for 2.6, RCP 4.5 and RCP 8.5.

Chapter 6.0 Results and discussion

6.1 General

In the present work, identification of 21 sub watersheds for Beas river basin up to Pong dam basin having whole watershed outlet point in watershed 9 and their ranking was done based on the sediment yield at sub basin level using SWAT model. The SWAT model was setup with the input data such as DEM, LULC map, soil map, slope map, rainfall, maximum and minimum temperature estimated from IMD gridded data and other meteorological parameters from SWAT. tamu website. The rainfall, maximum and minimum temperature data were for the period from 1987 -2005. The runoff and sediment yield was simulated with the SWAT setup and the required input data and default parameters. Then the simulated runoff and sediment yield was taken into SWAT-CUP for sensitivity analysis of the parameters and optimization of the most sensitive selected parameters. The parameter optimization was done by SUFI2 algorithm (Sequential Uncertainty Fitting version 2). Initially sensitivity analysis was performed for runoff and the parameters were optimized with the data from 1987-1995. Then the model with the optimized parameters was calibrated and validated for data from 1987-1995 and 1996-2005. Then the sensitivity analysis for sediment yield was carried out using the data from 1987-1995 and the parameters were optimized in SWAT-CUP as done for the runoff. The model was then calibrated and validated with the observed sediment yield at the watershed outlet. The streamflow and sediment yield for the period from 2006-2100 were simulated with optimized parameters for streamflow and sediment yield, the bias corrected projected data for rainfall, maximum and minimum temperatures for the scenarios RCP 2.6, RCP 4.5 and RCP 8.5 for the period from 2006-2100 and other meteorological data from SWAT.tamu website.

6.2 Sensitive Parameters

Since SWAT model has several parameters to deal with. Sensitive analysis helps us to identify those parameters which affect the model output most during calibration. The sensitivity analysis is done separately for flow parameters and sediment parameters since some parameters are sensitive only for flow and some other parameters are sensitive only for sediment. Therefore,

it is better to do separate sensitivity analysis for flow and sediment. In order to identify the most sensitive parameters initially SWAT-Cup is run with a large number of tentative parameters for simulation. Once the sensitive parameters have been identified they can be used for better convergence of simulation during calibration of the model.

The streamflow was simulated for the period from 1987 to 2005 with default parameters and the data of rainfall, minimum and maximum temperature estimated from the gridded IMD data. The monthly observed and simulated discharge is presented figure 6.1 and the scatter plot of monthly observed and simulated discharge is given in figure 6.2. The coefficient of determination (R^2) is 0.75.

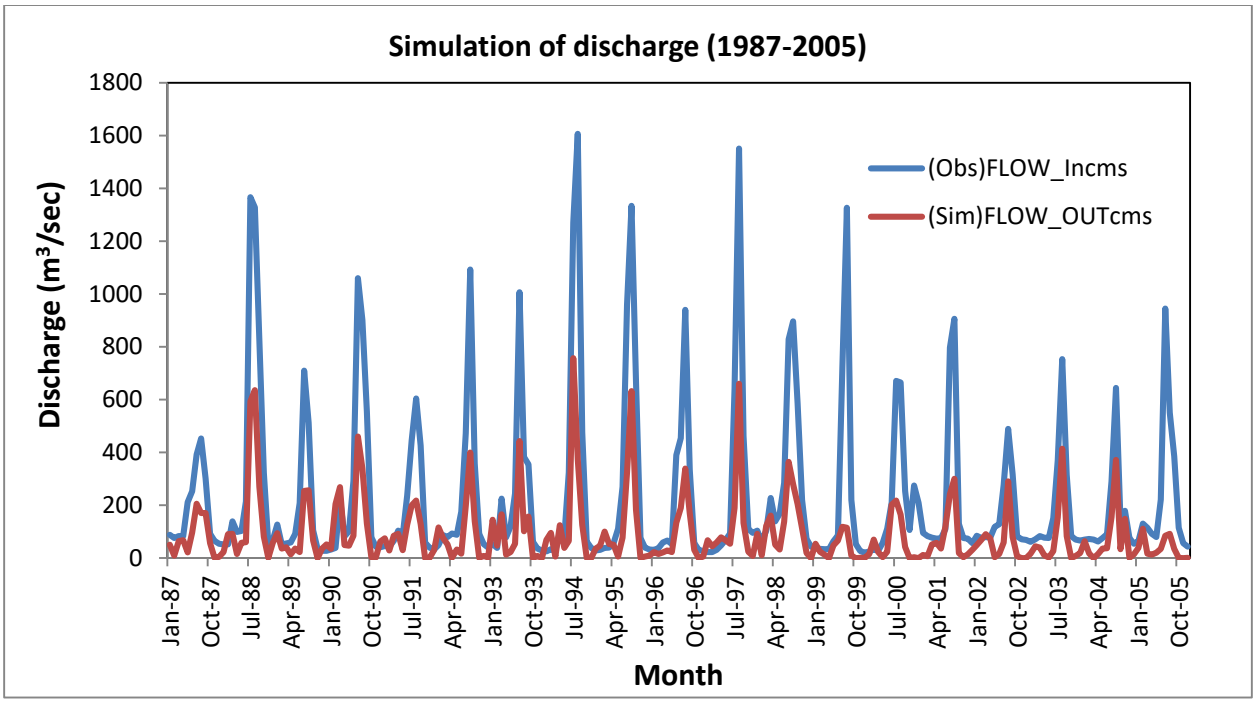

Fig. 6.1 Observed and simulated discharge for the period from 1987 to 2005

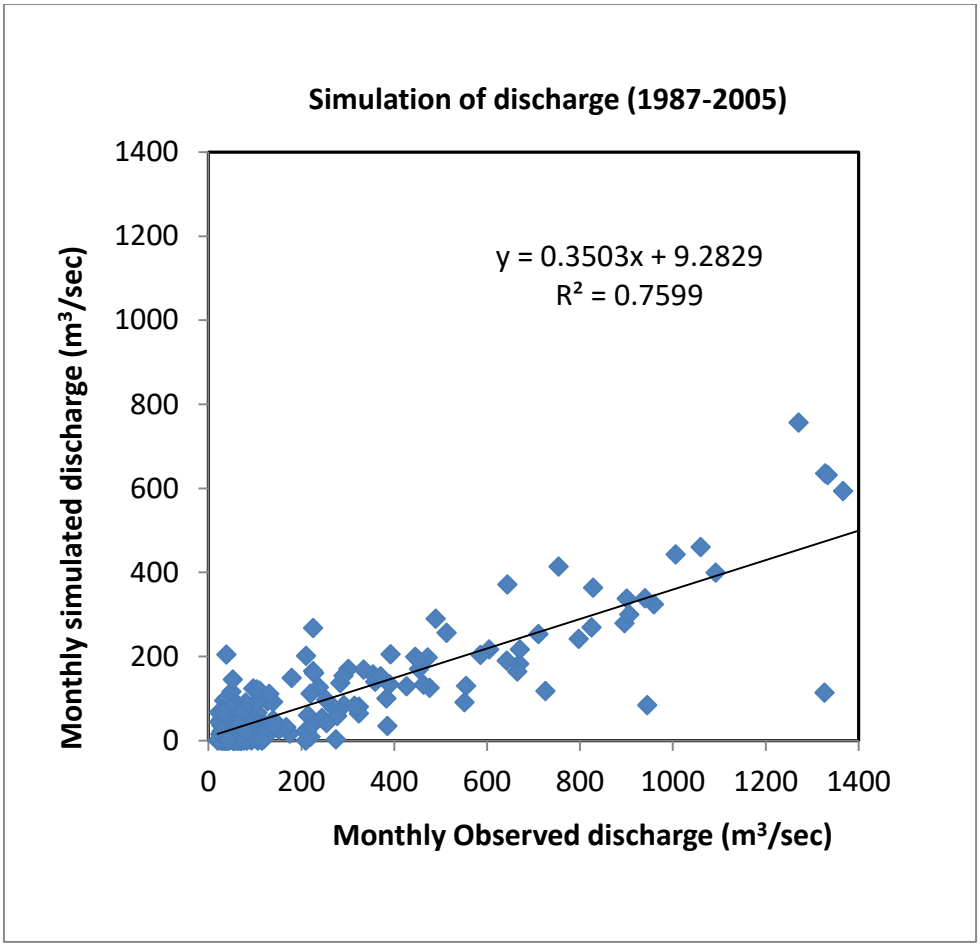

Fig. 6.2 Scatter plot of observed and simulated discharge for the period from 1987 to 2005

6.3 Calibration and validation of model for streamflow

Based on literature review 16 parameters listed in Table 6.1 were identified for sensitivity analysis of runoff. Then SWAT-Cup was run and P-value & t-Stat were obtained and are given in table 6.1. The parameters were ranked based on the P-value & t-Stat vales. The parameter snowfall temperature (R_SFTMP.bsn) was the most sensitive among all. All the sixteen parameters were considered for the optimization using the data of streamflow from 1987 to 1995. The simulated streamflow with the optimized parameter for the period from 1987 to 1995 is compared with the observed streamflow.

After the getting satisfactory result of SWAT run with coefficient of determination of 0.75, the calibration of parameters of for streamflow runoff was done in SWAT_CUP with the

monthly observed streamflow at Naduan Bridge for the period from 1987 to 1995. Since SWAT model was run on monthly interval so the daily observed runoff was converted into monthly average flow. The model was calibrated by using the values of 16 parameters that were identified as highly sensitive to streamflow. The fitted, minimum and maximum values of the selected parameters for streamflow are given in Table 6.2. The optimized values of the parameters were obtained with 1000 iterations. The observed and simulated streamflow were compared for the calibration and is presented in figure 6.3. The scatter plot of observed and simulated streamflow is given in 6.4. The coefficient of determination (R^2) for the calibration was 0.82. The validation of the parameters was done with the streamflow data for the period from 1996 to 2005 and the coefficient of determination (R^2) was 0.76. The observed and simulated streamflow were compared for the validation and is presented in figure 6.5. The scatter plot of observed and simulated streamflow is given in figure 6.6.

Table 6.1 sensitivity analysis of the selected parameters

Sl.No.	Parameter Name	t-Stat	P-Value
1	R_SFTMP.bsn	19.557919030	0.000000000
2	R_SOL_AWC(..).sol	1.680028307	0.094658083
3	R_GW_REVAP.gw	-1.380619860	0.169079797
4	R_CH_K2.rte	-1.227167166	0.221336123
5	R_SMTMP.bsn	-0.980110192	0.328325672
6	V_CH_N2.rte	-0.846874882	0.398170996
7	R_CH_COV1.rte	0.804648943	0.422066417
8	V_ESCO.hru	-0.498192649	0.618946462
9	R_REVAPMN.gw	0.458208467	0.647346321
10	R_SNOCOVMX.bsn	-0.352924043	0.724551562
11	V_GWQMN.gw	-0.318723720	0.750299505
12	R_ALPHA_BF_.gw	0.274475303	0.784028981
13	V_GW_DELAY.gw	-0.222590410	0.824102539
14	V_ALPHA_BF_.gw	-0.184539466	0.853794613
15	R_CH_COV2.rte	0.118510925	0.905792824
16	R_CN2.mgt	0.092673154	0.926264601

Table 6.2 Fitted, minimum and maximum values of the selected parameters for streamflow simulation

Parameter_Name	Fitted_Value	Min_value	Max_value
1:R__SNOCOVMX.bsn	674.255249	587.65686	852.079346
2:R__SMTMP.bsn	-18.97625	-25.928091	-10.217714
3:R__SFTMP.bsn	17.866707	9.016929	26.454914
4:R__SOL_AWC(..).sol	0.452369	0.221586	0.509166
5:R__CH_COV2.rte	0.062325	-0.24978	0.48893
6:R__CH_COV1.rte	0.248923	0.166008	0.459512
7:R__CH_K2.rte	-24.793098	-201.314102	-4.633314
8:R__ALPHA_BF.gw	1.387996	0.875349	1.446543
9:R__REVAPMN.gw	-133.970215	-308.705048	-88.219444
10:R__GW_REVAP.gw	0.062249	0.061104	0.152686
11:V__ESCO.hru	0.836426	0.814077	0.881293
12:R__CN2.mgt	-0.220127	-0.310812	-0.172888
13:V__ALPHA_BF.gw	-0.555729	-0.68702	-0.167056
14:V__GW_DELAY.gw	339.874359	328.806763	436.783264
15:V__GWQMN.gw	4577.772949	3264.193359	7401.452148
16:V__CH_N2.rte	0.13517	0.084141	0.148531

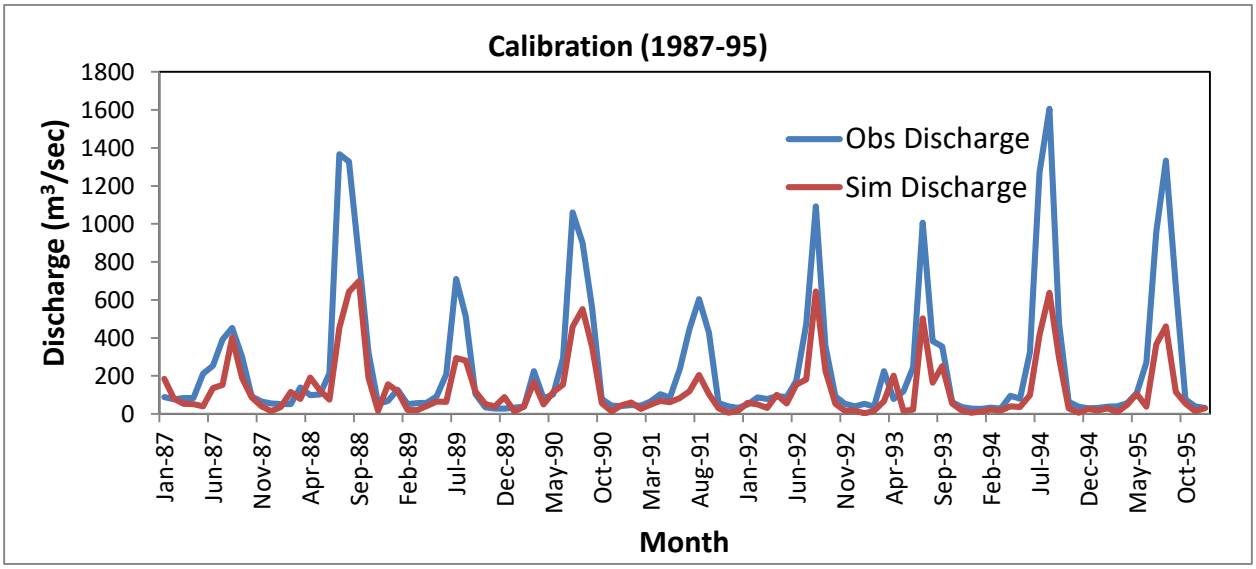

Fig. 6.3 Observed and simulated streamflow for the calibration (1987-1995)

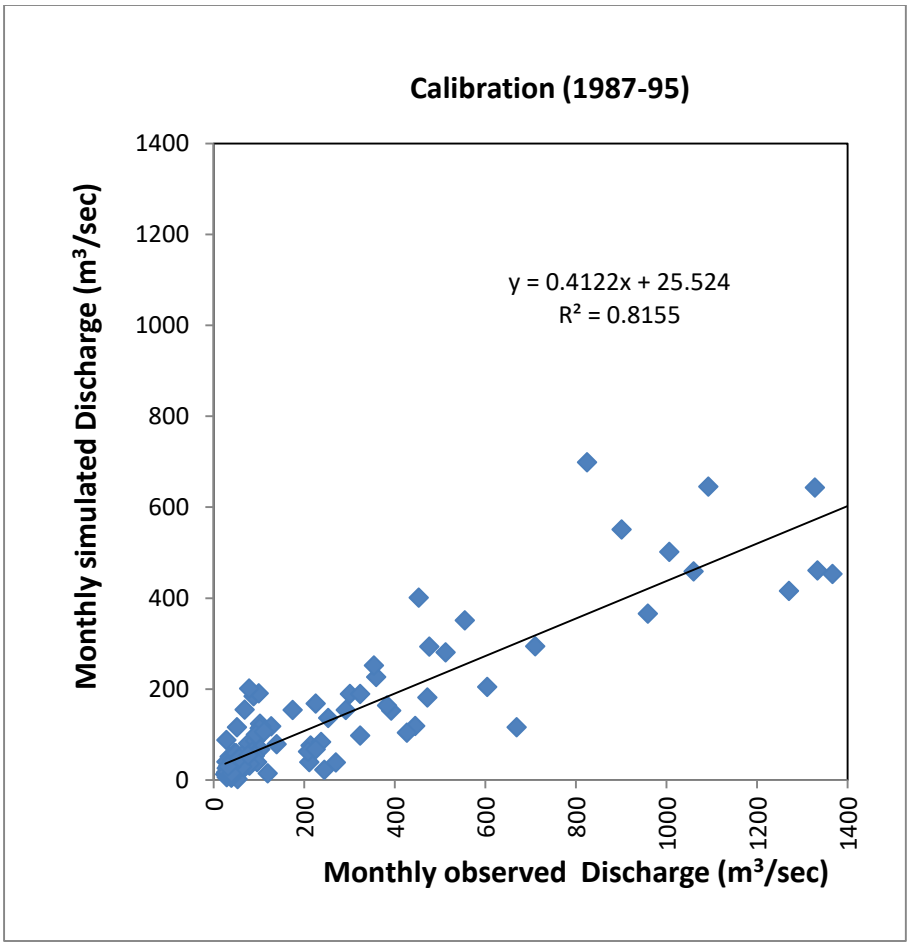

Fig. 6.4 Scatter plot of observed and simulated streamflow for the calibration (1987-1995)

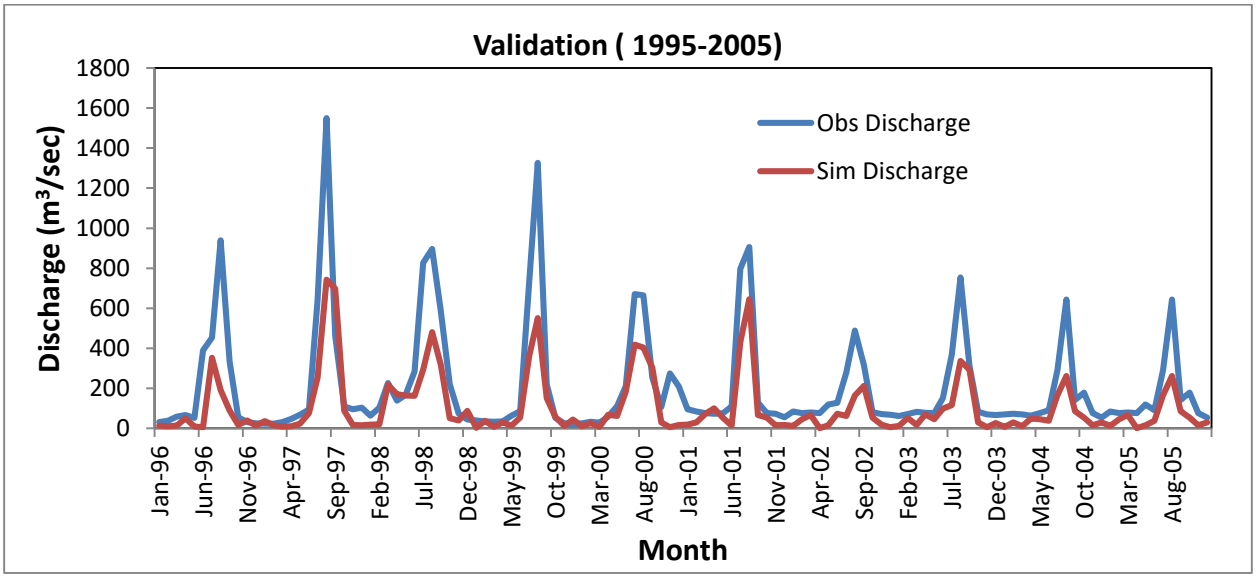

Fig. 6.5 Observed and simulated streamflow for the validation (1996-2005)

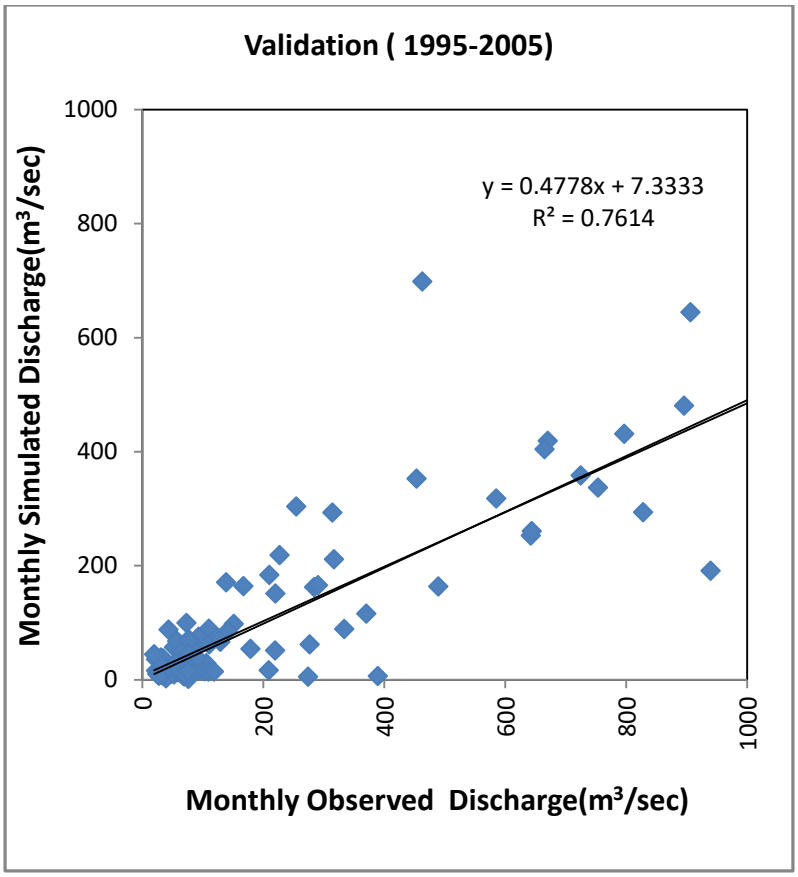

Fig. 6.6 Scatter plot of observed and simulated streamflow for the validation (1996-2005)

6.4 Calibration and validation of model for sediment yield

The sediment yield for the period was simulated with default parameters, the observed sediment yield at Nadaun bridge and other input data in SWAT for the period from 1987 to 2005. The monthly observed and simulated sediment yield is presented figure 6.7 and the scatter plot of monthly observed and simulated sediment yield is given in figure 6.8. The coefficient of determination (R^2) is 0.44. Eight parameters were considered for the simulation of sediment yield based on the literature review and the sensitivity analysis was carried in SWAT-CUP with the data of observed sediment yield for the period from 1987-2005. The parameters used in the sediment sensitivity analysis can be categorized as upland factors which affect the landscape component of the sediment transport and channel factors which affect the channel component of the sediment transport. The fitted, minimum and maximum values of the selected parameters for sediment yield are given in Table 6.3. The sediment data was available in the form of daily

concentration of total suspended solids (TSS) in g/lit. As SWAT does not take into account the bed load concentration, the total sediment load was calculated on the basics of only TSS. The calibration of SWAT model for sediment was done by using the daily observed total suspended sediment concentration (g/lit) data at Nadaun bridge for the years 1987 to 1995. SWAT Model was run on monthly basis and hence daily observed TSS(g/lit) was converted into monthly total sediment load (tons).

$$\text{Sediment load per day} = TSS * Qobservedflow * 1000 * 3600 * 24 \quad (6.1)$$

Where, TSS is the Total suspended sediment (g/lit), Q is corresponding the observed flow ($m3$/sec). The simulated sediment load was correlated with this observed sediment load by adjusting the identified sensitive upland erosion parameters and channel erosion parameters. The optimized values of the parameters were obtained with 1000 iterations. The observed and simulated sediment yield were compared for the calibration and is presented in figure 6.9. The scatter plot of observed and simulated sediment yield is given in 6.10. The coefficient of determination (R^2) for the calibration was 0.64. The validation of the parameters was done with the sediment yield data for the period from 1996 to 2005 and the coefficient of determination (R^2) was 0.61. The observed and simulated sediment yield were compared for the validation and is presented in figure 6.11. The scatter plot of observed and simulated streamflow is given in figure 6.12.

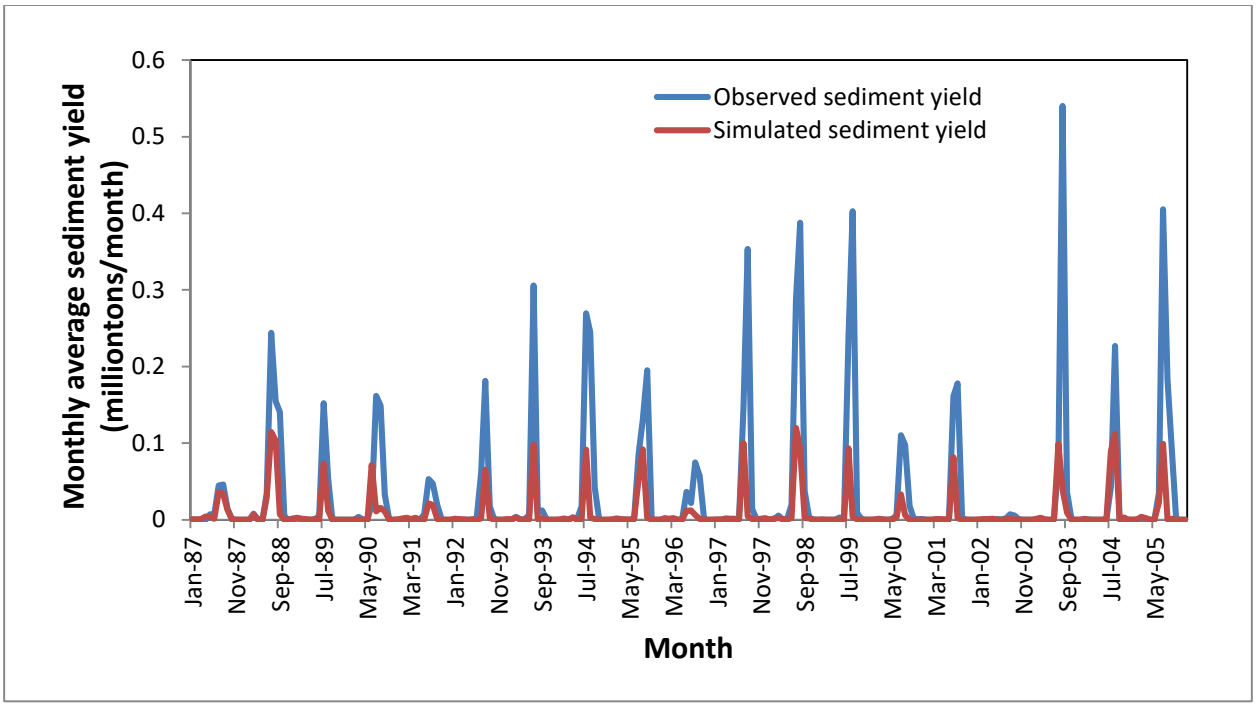

Fig. 6.7 Observed and simulated sediment yield for the period from 1987 to 2005

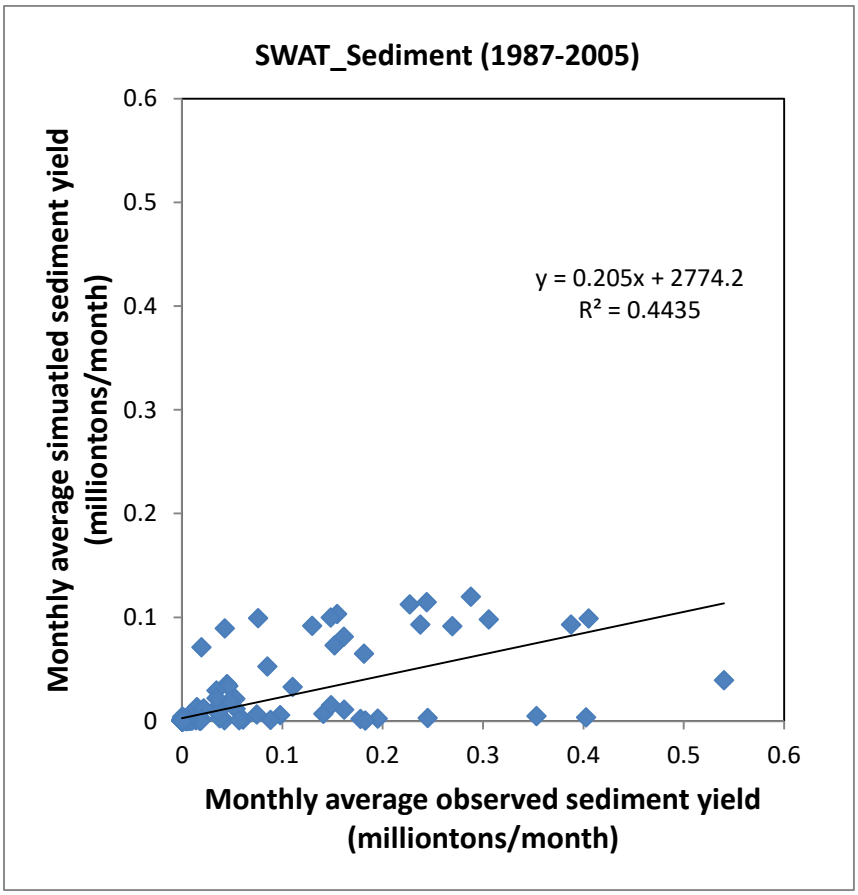

Fig. 6.8 Scatter plot of observed and simulated sediment for the period from 1987 to 2005

Table 6.3 Fitted, minimum and maximum values of the selected parameters for sediment yield

Parameter_Name	Fitted_Value	Min_value	Max_value
1:R__CH_COV2.rte	0.553972	0.481879	0.570609
2:R__RSDIN.hru	2471.274658	2306.497314	2555.218018
3:R__HRU_SLP.hru	1.79737	1.643528	1.877508
4:V__CH_COV1.rte	0.321132	0.303974	0.32422
5:V__USLE_P.mgt	0.966766	0.961907	0.986511
6:V__SPEXP.bsn	1.457055	1.43957	1.466998
7:V__SED_CON.hru	213.01857	201.847107	221.707489
8:R__USLE_K(..).sol	0.445569	0.442898	0.466638

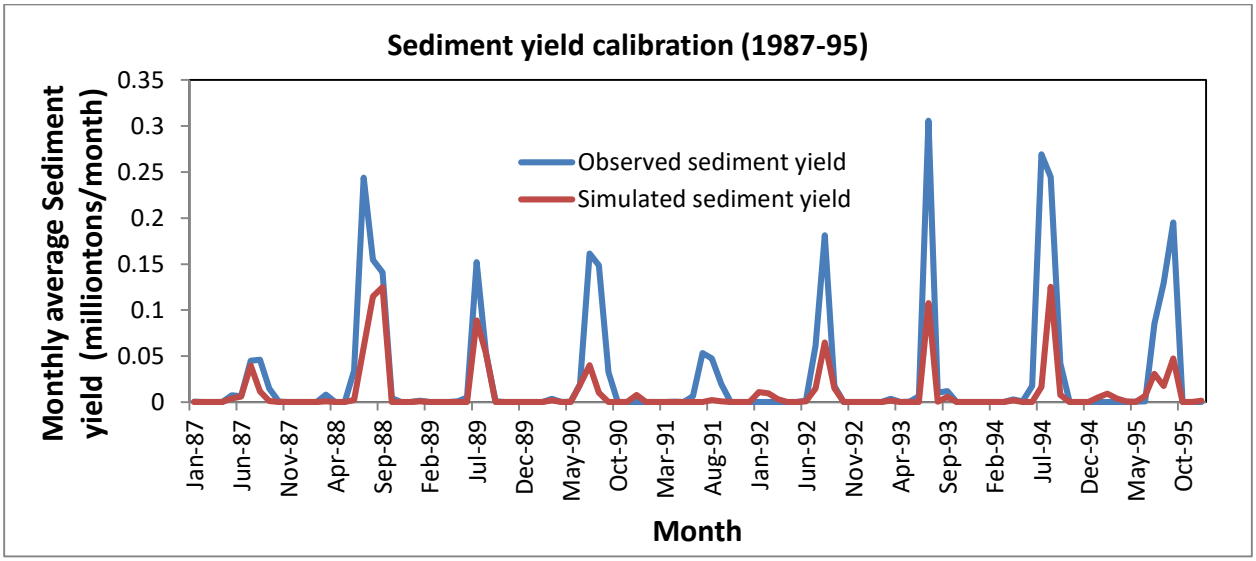

Fig. 6.9 Observed and simulated sediment yield for the calibration (1987-1995)

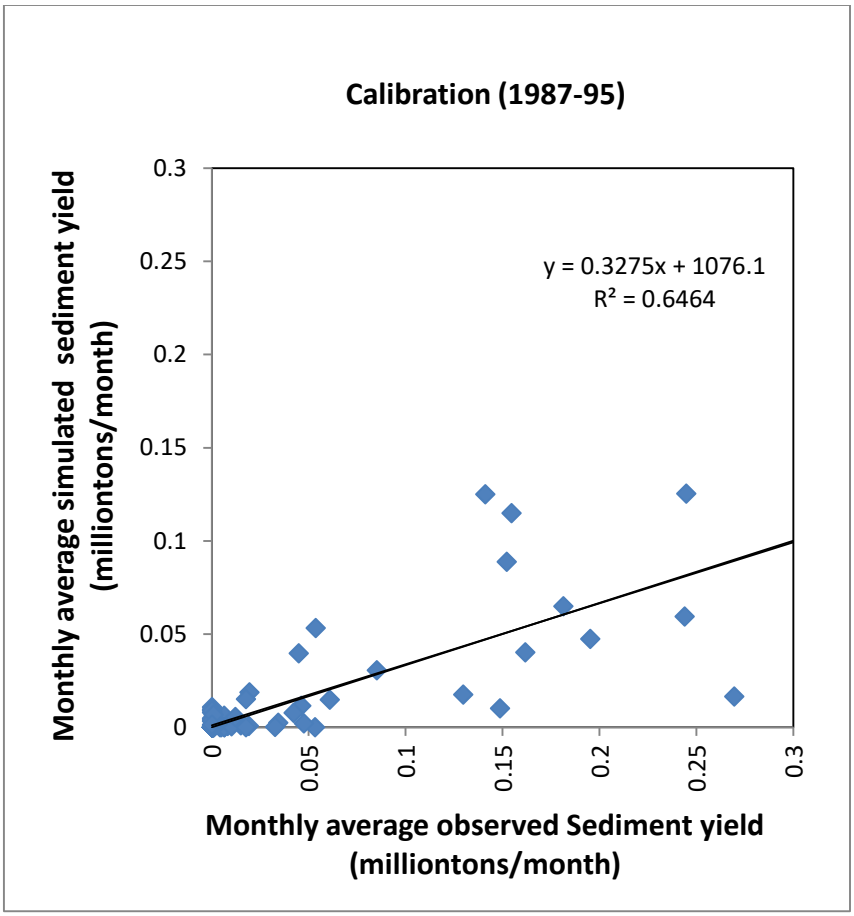

Fig. 6.10 Scatter plot of observed and simulated sediment yield for the calibration (1987-1995)

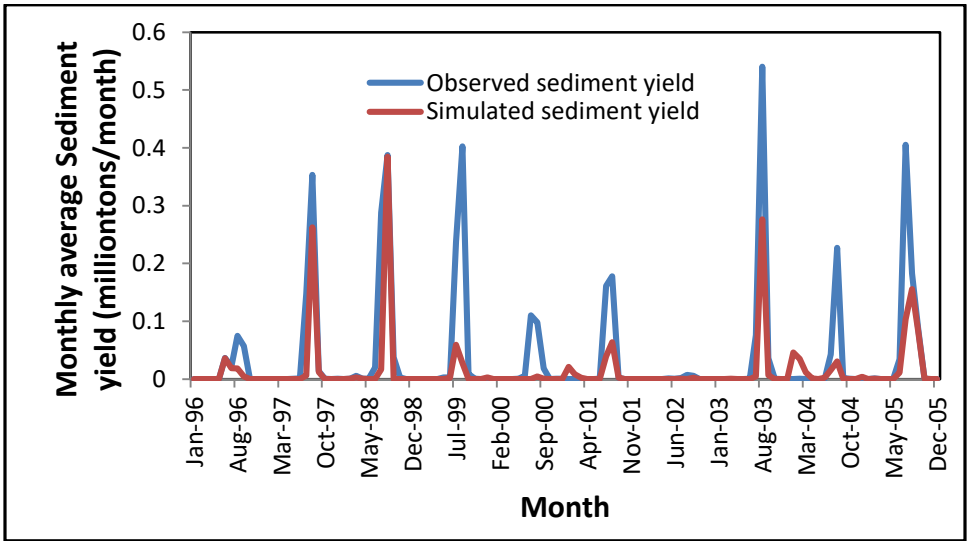

Fig. 6.11 Observed and simulated sediment yield for the validation (1996-2005)

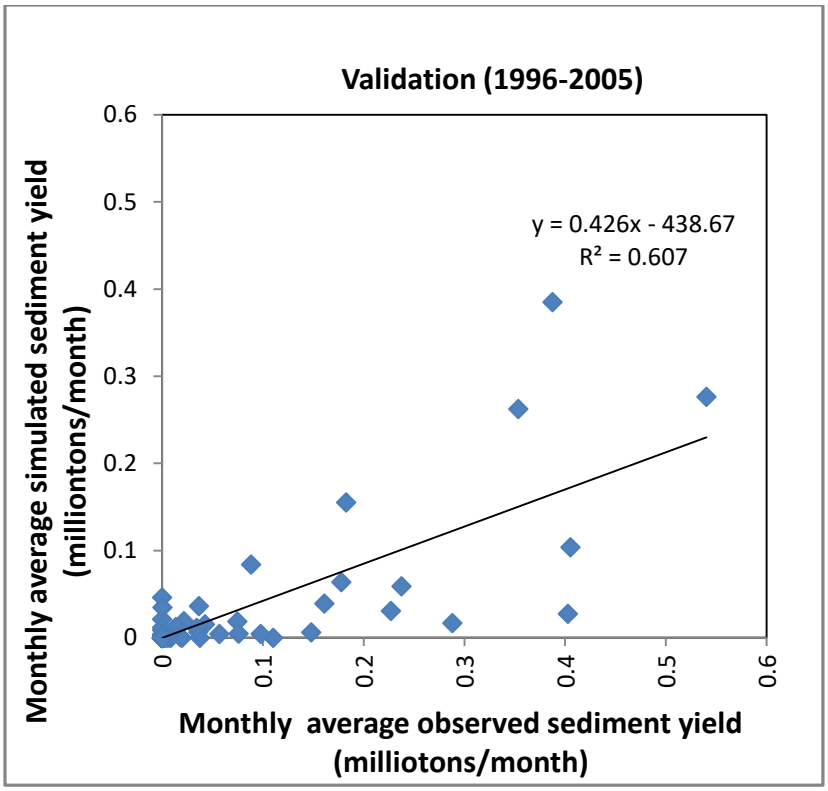

Fig. 6.12 Scatter plot of observed and simulated sediment yield for the validation (1996-2005)

The streamflow and sediment yield for climate scenarios RCP 2.6, RCP 4.5 and RCP 8.5 for the period 2006-2100 were simulated in SWAT with input data, the bias corrected rainfall, maximum and minimum temperature for climate scenarios RCP 2.6, RCP 4.5 and RCP 8.5 for the period 2006-2100, other meteorological data from SWAT.tamu website and optimized parameters for streamflow and sediment yield. The streamflow for climate scenarios RCP 2.6, RCP 4.5 and RCP 8.5 for the period 2006-2100 are presented in figures 6.13, 6.14 and 6.15 respectively. The average monthly streamflow for the climate scenarios RCP 2.6, RCP 4.5 and RCP 8.5 is given in Table 6.3. The sediment yield for climate scenarios RCP 2.6, RCP 4.5 and RCP 8.5 for the period 2006-2100 are presented in figures 6.16, 6.17 and 6.18 respectively. The average monthly sediment yield for the climate scenarios RCP 2.6, RCP 4.5 and RCP 8.5 is given in Table 6.4.

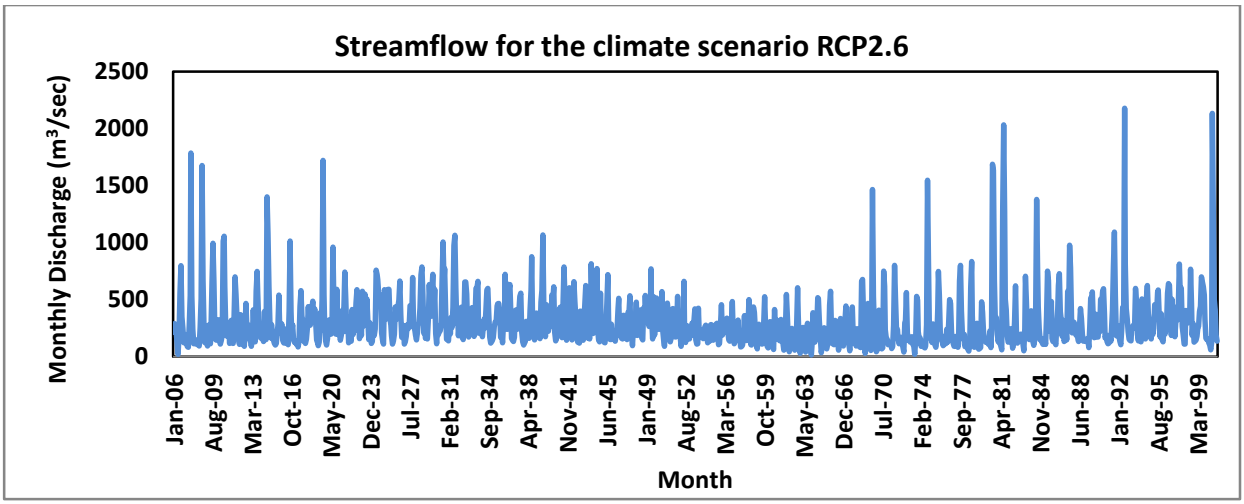

Fig. 6.13 Streamflow for climate scenario RCP2.6 for 2006-2100

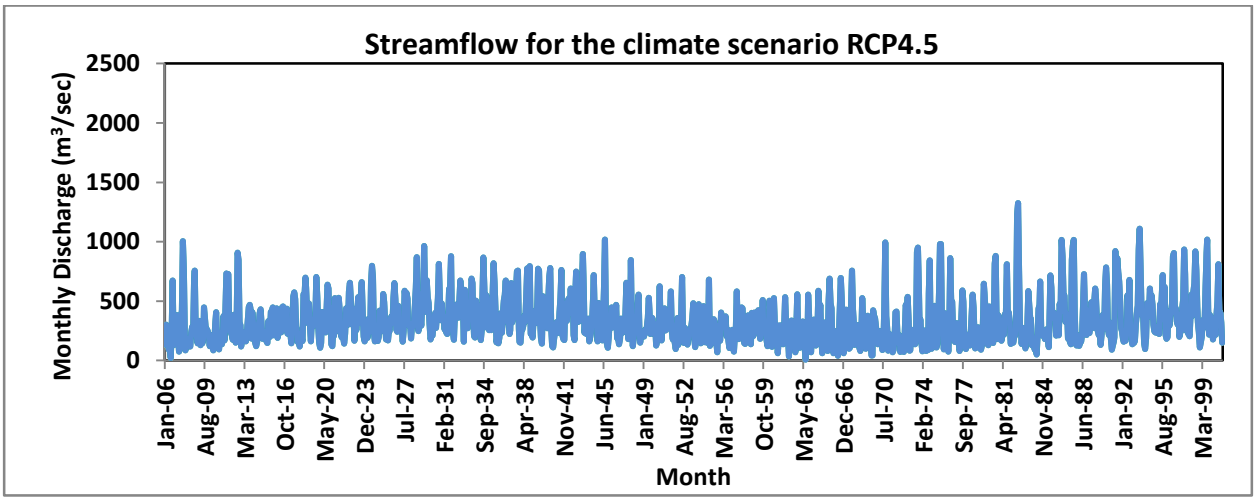

Fig. 6.14 Streamflow for climate scenario RCP4.5 for 2006-2100

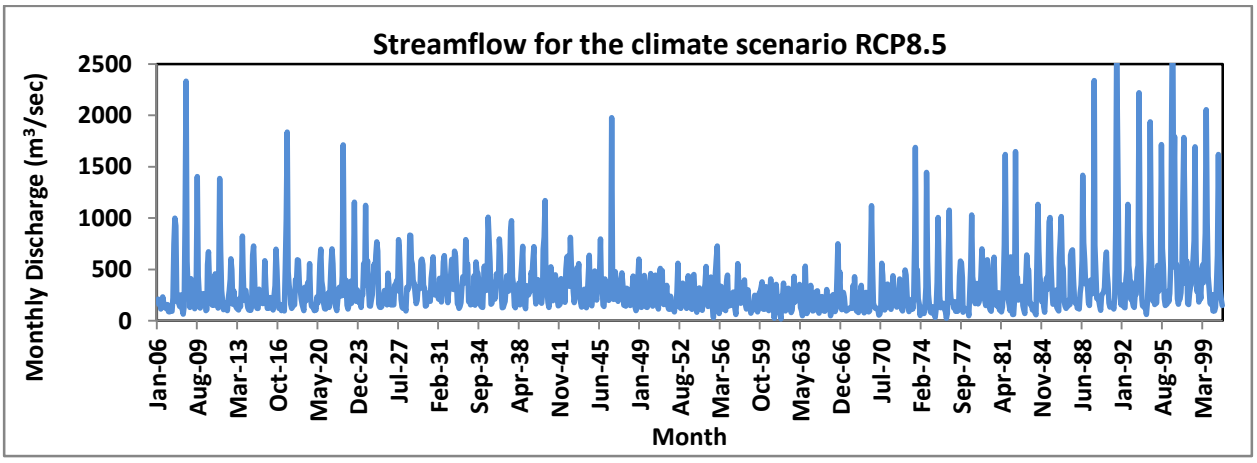

Fig. 6.15 Streamflow for climate scenario RCP8.5 for 2006-2100

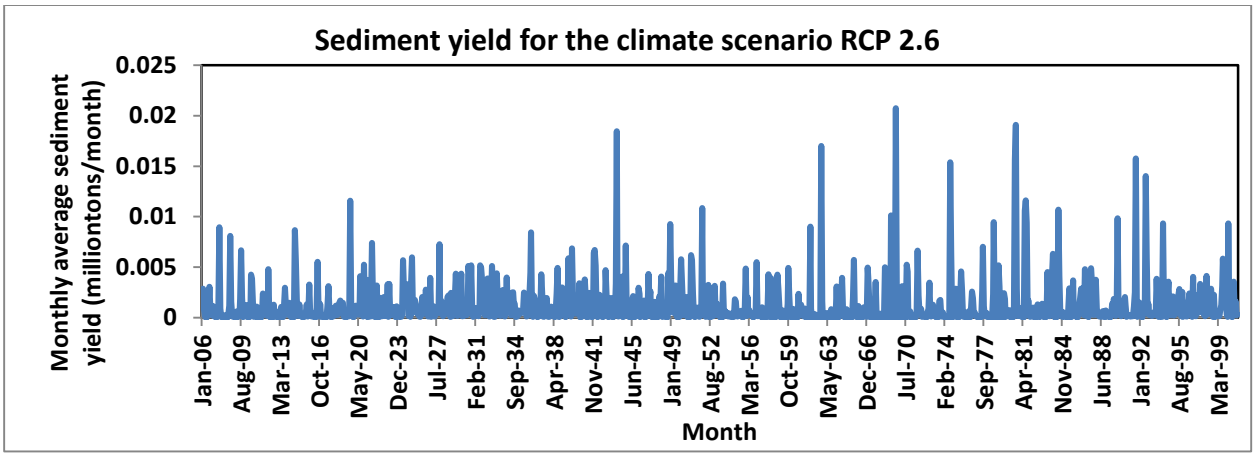

Fig. 6.16 Sediment yield for climate scenario RCP2.6 for 2006-2100

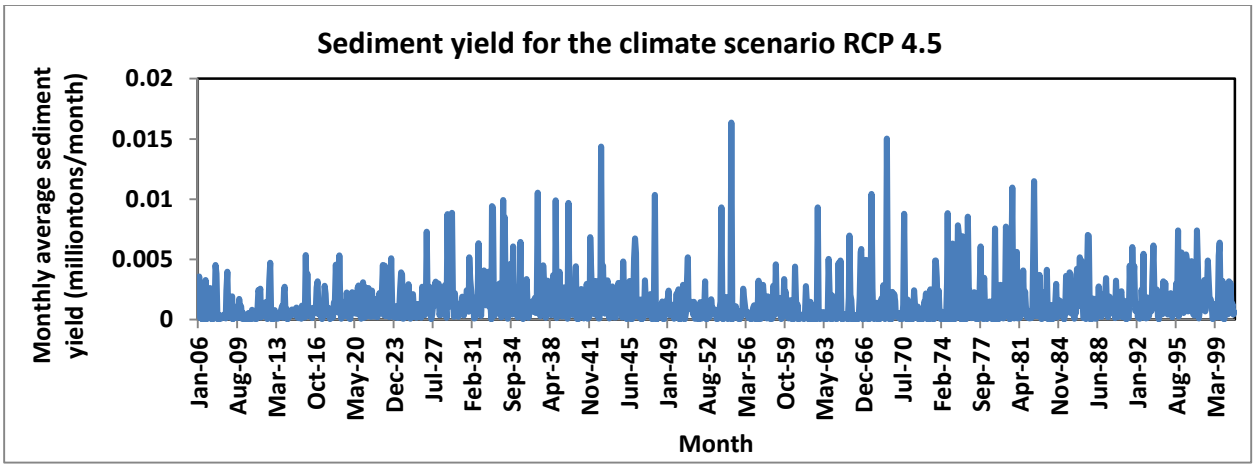

Fig. 6.17 Sediment yield for climate scenario RCP4.5 for 2006-2100

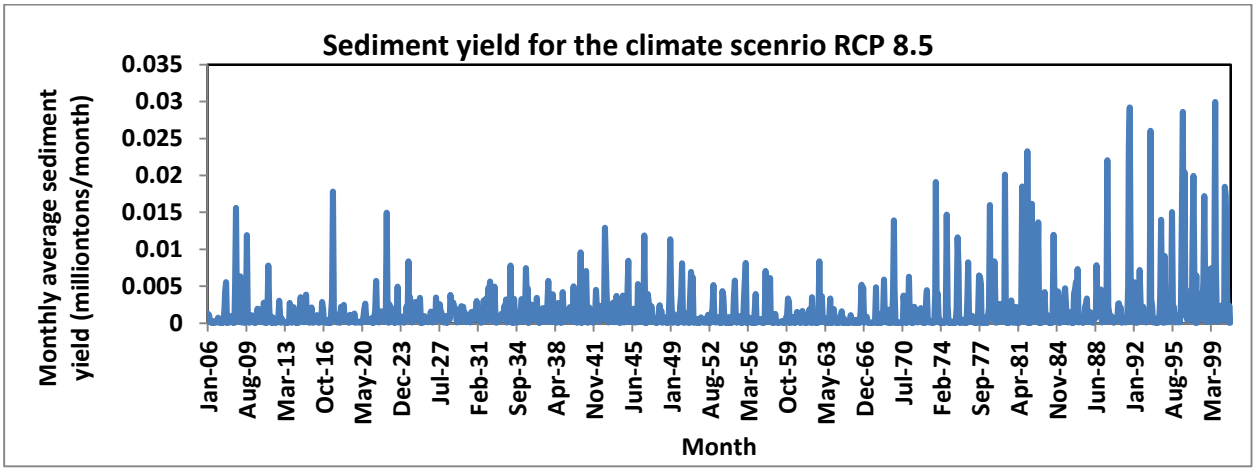

Fig. 6.15 Sediment yield for climate scenario RCP8.5 for 2006-2100

Table 6.3 Average monthly streamflow (m^3/sec) for the scenarios RCP 2.6, RCP 4.5 and RCP 8.5

Month	RCP 2.6	RCP 4.5	RCP 8.5
Jan	196.26	220.62	198.02
Feb	201.72	242.94	203.12
Mar	236.57	262.75	220.68
Apr	227.77	275.43	241.59
May	225.96	279.73	236.52
Jun	312.33	363.45	359.57
Jul	537.79	502.15	667.82
Aug	604.71	550.90	668.95
Sep	394.06	449.08	414.75
Oct	265.26	294.96	279.56
Nov	239.49	268.38	243.41
Dec	195.23	244.07	207.16

Table 6.4 Average monthly sediment yield (tons) for the scenarios RCP 2.6, RCP 4.5 and RCP 8.5

Month	RCP 2.6	RCP 4.5	RCP 8.5
Jan	41649.1	43079.5	47766.9
Feb	31611.9	46649.3	39175.7
Mar	26365.3	27478.7	21771.5
Apr	13656.5	20277.9	13635.6
May	10595.4	16048.0	12714.2
Jun	24272.7	25879.1	38196.4
Jul	61779.0	54166.3	124878.0
Aug	97140.4	72237.3	122390.7
Sep	38301.9	59208.8	49322.5
Oct	35835.5	40298.4	38448.2
Nov	34775.3	44197.5	39782.3
Dec	38069.0	57953.1	40807.5

6.5 Computation of Unit Weight of Sediment

The suspended sediment concentration observed at Nadaun bridge is a mixture of coarse sediment (above 0.2 *mm*), medium sediment (0.075 to 0.2 *mm*) and fine sediment (below 0.075 *mm*). According to the soil classification by American Geophysical Union, the observation of sediment at Nadaun bridge has only silt and sand. The method suggested by Lara and Pemberton

(1987) of USBR was used to compute unit weight of sediment by considering the percentages of silt and sand for daily data from 1987 to 2005 and the average unit weight for each year is given in Table 6.5. The average unit weight of sediment for the period from 1987 to 2005 is 1166.740 kg/m^3.

Table 6.5 Average unit weight of sediment from particle size distribution

Year	Percentage		Unit weight kg/m3
	Silt	Sand	
1987	90.52	9.48	1177.302
1988	89.26	10.74	1182.576
1989	86.03	13.97	1196.017
1990	86.25	13.75	1195.093
1991	87.43	12.57	1190.210
1992	87.86	12.14	1188.410
1993	93.40	6.60	1165.297
1994	87.71	12.29	1189.009
1995	94.86	5.14	1159.231
1996	97.25	2.75	1149.275
1997	95.83	4.17	1155.203
1998	95.66	4.34	1155.910
1999	95.57	4.43	1156.286
2000	95.98	4.02	1154.572
2001	94.78	1.82	1159.542
2002	98.18	1.82	1145.382
2003	97.13	2.87	1149.796
2004	97.18	2.82	1149.578
2005	97.23	2.77	1149.374

The unit weight of the sediment was calculated from silt retained and silt volume settled by hydrographic survey from 1987 to 2005 and is presented in Table 6.6. The silt retained was obtained by deducting the measured sediment load at downstream of the reservoir from the measured sediment load at upstream of the reservoir. The average unit weight of the sediment from the observed data for the period from 1987 to 2005 is 1117.829 kg/m^3.

Table 6.6. Unit weight of sediment from hydrographic survey

Year	Silt retained *kg*	Silt volume settled m^3	Unit weight kg/m^3
1987-88	5950000000	22580000	263.508
1988-89	26215000000	25560000	1025.626
1989-90	10278800000	17740000	579.414
1990-91	18565400000	17930000	1035.438
1991-92	6756400000	10980000	615.337
1992-93	15843800000	8610000	1840.163
1993-94	10525200000	8040000	1309.104
1994-95	29181600000	21160000	1379.093
1995-96	24889200000	21160000	1176.238
1996-97	17669400000	18920000	933.901
1997-98	28929600000	21690000	1333.776
1998-99	29065400000	24370000	1192.671
1999-00	28659400000	22020000	1301.517
2000-01	11134200000	8620000	1291.671
2001-02	19437600000	15820000	1228.673
2002-03	24411800000	20690000	1179.884
2003-04	26916400000	21910000	1228.498
2004-05	19700800000	16330000	1206.418

6.6 Computation of consolidated unit weight of sediment

The consolidated unit weights of sediment for the unit weights obtained from particle size distribution and hydrographic survey of the sediment for 2025, 2050, 2075 and 2100 years were computed using the equation (5.1) given by Miller (1953) and are presented in Table 6.7. The consolidated unit weights of the sediment for the life period of the reservoir were computed by the equation (5.4) assuming initial and ultimate porosity of sediment as 0.523 and 0.355 (Swamee, 2001) and the values for 2025, 2050, 2075 and 2100 years are computed by linear interpolation and are given in Table 6.7. The life of Pong reservoir is estimated as 330 years if the present rate of sedimentation continues (Swamee, 2001). L-moment ratios such as L-coefficient of variation (τ), L-skewness (τ_3) and L-kurtosis (τ_4) were used to fit Kappa distribution to yearly average unit weights of sediment computed from the particle size distribution of suspended sediment concentration at Nadaun bridge. The fitted Kappa distribution was used to generate 500 realizations of the unit weights of the sediment. The generated 500 realizations were used to fit any one of the three parameter distributions such as

generalized logistic (*GLO*), Generalized extreme value (*GEV*), Generalized normal, Pearson type III and generalized Pareto for the purpose of quantile estimation. The goodness of fit estimate (*z*) for generalized logistic (*GLO*), Generalized extreme value (*GEV*), Generalized normal, Pearson type III and generalized Pareto distributions were -10.20, -10.77, -10.71, -10.75 and -11.89 respectively and desirable limit of *z* to declare the suitability of the distributions is less than or equal to ± 1.64. It was found that none of the distributions considered were suitable and in this case Wakebey distribution was selected as the suitable distribution for explaining the unit weights of the sediment. The parameter estimates for Wakebey distribution are ξ = 0.000, α =135.127, β =136.913, γ =0.009 and δ =0.541 and the quantile estimates of unit weights of sediment for 2025, 2050, 2075 and 2100 using the parameters are given Table 6.7.

Table 6.7 Consolidated unit weights of the sediment by different methods

Year	Consolidated unit weights of sediment (kg/m^3)			
	Particle size distribution	Porosity of uniform sediment	Hydrographic survey	Frequency Analysis
2025	1204.673	1326.108	1155.762	1230.257
2050	1217.704	1359.835	1168.793	1284.308
2075	1225.048	1393.563	1176.137	1325.404
2100	1230.196	1427.290	1181.285	1360.128

6.7 Projection of Sediment Volume

The trap efficiency of the reservoir was computed by the equation (5.15) for 2025, 2050, 2075 and 2100 years and is presented in Table 6.8. The sediment volumes were obtained by converting the sediment yield at Pong for 2025, 2050, 2075 and 2100 years using the corresponding consolidated unit weights of the sediment and trap efficiency. Before applying trap efficiency of the reservoir, sediment volume was increased by 15 percent for bed load and 30.34 percent for sediment load contribution from tributaries such as Baner Khad, Gaj Khad, Dehar Khad and Buhl Khad. The sediment volumes computed by different methods such as particle size distribution, porosity of uniform sediment, hydrographic survey and frequency analysis for 2025, 2050, 2075 and 2100 years for climate scenario RCP 2.6 along with the sediment volume computed by empirical formula proposed Swamee (2001) are given in Table 6.9. The sediment volumes computed by different methods such as particle size distribution,

porosity of uniform sediment, hydrographic survey and frequency analysis for 2025, 2050, 2075 and 2100 years for climate scenario RCP 4.5 along with the sediment volume computed by empirical formula are given in Table 6.10. The sediment volumes computed by different methods such as particle size distribution, porosity of uniform sediment, hydrographic survey and frequency analysis for 2025, 2050, 2075 and 2100 years for climate scenario RCP 8.5 along with the sediment volume computed by empirical formula are given in Table 6.11.

Table 6.8. Trap efficiency of the reservoir by empirical formula

Year	Trap efficiency %
2025	100
2050	99
2075	98
2100	96

Table 6.9 Projection of sediment volume by different methods for RCP 2.6

Year	Sediment volume (Mm^3)				
	Particle size Distribution	Porosity of uniform Sediment	Hydrographic survey	Frequency analysis	Empirical formula
2025	775.951	775.073	776.359	775.951	1195.47
2050	792.379	789.659	793.471	792.379	1843.11
2075	802.862	798.433	804.384	802.862	2485.56
2100	816.831	809.859	818.926	816.831	3117.52

Table 6.10 Projection of sediment volume by different methods for RCP 4.5

Year	Sediment volume (Mm^3)				
	Particle size Distribution	Porosity of uniform Sediment	Hydrographic survey	Frequency analysis	Empirical formula
2025	775.416	774.587	775.801	775.416	1195.47
2050	794.940	791.953	796.140	794.940	1843.11
2075	806.558	801.681	808.234	806.558	2485.56
2100	822.767	814.976	825.109	822.767	3117.52

Table 6.11 Projection of sediment volume by different methods for RCP 8.5

Year	Sediment volume (Mm^3)				
	Particle size Distribution	Porosity of uniform Sediment	Hydrographic survey	Frequency analysis	Empirical formula
2025	776.133	775.238	776.548	776.133	1195.47
2050	792.554	789.816	793.653	792.554	1843.11
2075	803.196	798.727	804.732	803.196	2485.56
2100	831.804	822.765	834.521	831.804	3117.52

The consolidated sediment volume computed by hydrographic survey was considered to be the realistic since the unit weight of the sediment was computed from observed sediment load and the volume of the silt retained in the reservoir during 1987 to 2005. The sediment volumes computed by Empirical formula for 2025, 2050, 2075 and 2100 years for climate scenario RCP 2.6 are 53.98%, 132.28%, 209.00% and 280.00% higher than the sediment volumes computed by hydrographic survey. The sediment volumes for higher prediction periods are much higher than the lower prediction periods. The sediment volumes computed by particle size distribution for 2025, 2050, 2075 and 2100 years for the climate scenario RCP 2.6 are 0.05%, 0.14%, 0.19% and 0.25% lower than the sediment volume computed by hydrographic survey. The sediment volumes computed by porosity of uniform sediment for 2025, 2050, 2075 and 2100 years for climate scenario RCP 2.6 are 0.16%, 0.48%, 0.73% and 1.11% lower than the sediment volume computed by hydrographic survey. The sediment volumes computed by frequency analysis of particle size distribution for 2025, 2050, 2075 and 2100 years for the climate scenario RCP 2.6 are 0.07%, 0.31%, 0.53% and 0.84% lower than the sediment volume computed by hydrographic survey. The sediment volumes computed by particle size distribution for 2025, 2050, 2075 and 2100 years for the climate scenario RCP 2.6 are very close to sediment volumes computed by hydrographic survey. The projected reservoir capacity for 2025, 2050, 2075 and 2100 years for the climate scenario RCP 2.6 by different methods are given in Table 6.12. The percentage loss in reservoir capacity for 2025, 2050, 2075 and 2100 years for the climate scenario RCP 2.6 by different methods are given in Table 6.13. The percentage loss in reservoir capacity by empirical formula for higher projection period 2100 is much higher than the lower projection period 2025. The percentage loss in reservoir capacity by all other methods for 2025, 2050, 2075 and 2100 years are comparable.

Table 6.12 Projection of reservoir capacity by different methods for RCP 2.6

Year	Reservoir capacity (Mm^3)				
	Particle size Distribution	Porosity of uniform Sediment	Hydrographic survey	Frequency analysis	Empirical formula
2025	7803.039	7803.917	7802.631	7803.235	7383.52
2050	7786.611	7789.331	7785.519	7787.95	6735.88
2075	7776.128	7780.557	7774.606	7778.886	6093.44
2100	7762.159	7769.131	7760.064	7766.987	5461.48

Table 6.13 Percentage loss in reservoir capacity by different methods for RCP 2.6

Year	Loss in reservoir capacity (percent)				
	Particle size Distribution	Porosity of uniform Sediment	Hydrographic survey	Frequency analysis	Empirical formula
2025	9.04	9.03	9.05	9.04	13.93
2050	9.24	9.20	9.25	9.22	21.48
2075	9.36	9.31	9.38	9.33	28.97
2100	9.52	9.44	9.55	9.47	36.34

The sediment volumes computed by Empirical formula for 2025, 2050, 2075 and 2100 years for climate scenario RCP 4.5 are 54.09%, 131.51%, 207.53% and 277.83% higher than the sediment volumes computed by hydrographic survey. The sediment volumes for higher prediction periods are much higher than the lower prediction periods. The sediment volumes computed by particle size distribution for 2025, 2050, 2075 and 2100 years for the climate scenario RCP 4.5 are 0.05%, 0.15%, 0.21% and 0.28% lower than the sediment volume computed by hydrographic survey. The sediment volumes computed by porosity of uniform sediment for 2025, 2050, 2075 and 2100 years for climate scenario RCP 4.5 are 0.16%, 0.53%, 0.81% and 1.23% lower than the sediment volume computed by hydrographic survey. The sediment volumes computed by frequency analysis of particle size distribution for 2025, 2050, 2075 and 2100 years for the climate scenario RCP 4.5 are 0.07%, 0.34%, 0.58% and 0.94% lower than the sediment volume computed by hydrographic survey. The sediment volumes computed by particle size distribution for 2025, 2050, 2075 and 2100 years for the climate scenario RCP 4.5 are very close to sediment volumes computed by hydrographic survey. The projected reservoir capacity for 2025, 2050, 2075 and 2100 years for the climate scenario RCP 4.5 by different methods are given in Table 6.14. The percentage loss in reservoir capacity for 2025, 2050, 2075 and 2100 years for the climate scenario RCP 4.5 by different methods are given in Table 6.15. The percentage loss in reservoir capacity by empirical formula for higher projection period 2100 is much higher than the lower projection period 2025. The percentage loss in reservoir capacity by all other methods for 2025, 2050, 2075 and 2100 years are comparable.

Table 6.14 Projection of reservoir capacity by different methods for RCP 4.5

Year	Reservoir capacity (Mm^3)				
	Particle size Distribution	Porosity of uniform Sediment	Hydrographic survey	Frequency analysis	Empirical formula
2025	7803.574	7804.403	7803.189	7803.758	7383.52
2050	7784.05	7787.037	7782.85	7785.52	6735.88
2075	7772.432	7777.309	7770.756	7775.468	6093.44
2100	7756.223	7764.014	7753.881	7761.617	5461.48

Table 6.15 Percentage loss in reservoir capacity by different methods for RCP 4.5

Year	Loss in reservoir capacity (percent)				
	Particle size Distribution	Porosity of uniform Sediment	Hydrographic survey	Frequency analysis	Empirical formula
2025	9.04	9.03	9.04	9.04	13.93
2050	9.27	9.23	9.28	9.25	21.48
2075	9.40	9.34	9.42	9.37	28.97
2100	9.59	9.50	9.62	9.53	36.34

The sediment volumes computed by Empirical formula for 2025, 2050, 2075 and 2100 years for climate scenario RCP 8.5 are 53.95%, 132.23%, 208.87% and 273.57% higher than the sediment volumes computed by hydrographic survey. The sediment volumes for higher prediction periods are much higher than the lower prediction periods. The sediment volumes computed by particle size distribution for 2025, 2050, 2075 and 2100 years for the climate scenario RCP 8.5 are 0.05%, 0.14%, 0.19% and 0.32% lower than the sediment volume computed by hydrographic survey. The sediment volumes computed by porosity of uniform sediment for 2025, 2050, 2075 and 2100 years for climate scenario RCP 8.5 are 0.17%, 0.48%, 0.74% and 1.41% lower than the sediment volume computed by hydrographic survey. The sediment volumes computed by frequency analysis of particle size distribution for 2025, 2050, 2075 and 2100 years for the climate scenario RCP 8.5 are 0.08%, 0.31%, 0.54% and 1.08% lower than the sediment volume computed by hydrographic survey. The sediment volumes computed by particle size distribution for 2025, 2050, 2075 and 2100 years for the climate scenario RCP 8.5 are very close to sediment volumes computed by hydrographic survey. The projected reservoir capacity for 2025, 2050, 2075 and 2100 years for the climate scenario RCP 8.5 by different methods are given in Table

6.16. The percentage loss in reservoir capacity for 2025, 2050, 2075 and 2100 years for the climate scenario RCP 8.5 by different methods are given in Table 6.17. The percentage loss in reservoir capacity by empirical formula for higher projection period 2100 is much higher than the lower projection period 2025. The percentage loss in reservoir capacity by all other methods for 2025, 2050, 2075 and 2100 years are comparable.

Table 6.16 Projection of reservoir capacity by different methods for RCP 8.5

Year	Reservoir capacity (Mm^3)				
	Particle size Distribution	Porosity of uniform Sediment	Hydrographic survey	Frequency analysis	Empirical formula
2025	7802.857	7803.752	7802.442	7803.057	7383.52
2050	7786.436	7789.174	7785.337	7787.784	6735.88
2075	7775.794	7780.263	7774.258	7778.576	6093.44
2100	7747.186	7756.225	7744.469	7753.444	5461.48

Table 6.17 Percentage loss in reservoir capacity by different methods for RCP 8.5

Year	Loss in reservoir capacity (percent)				
	Particle size Distribution	Porosity of uniform Sediment	Hydrographic survey	Frequency analysis	Empirical formula
2025	9.05	9.04	9.05	9.04	13.93
2050	9.24	9.21	9.25	9.22	21.48
2075	9.36	9.31	9.38	9.33	28.97
2100	9.70	9.59	9.73	9.62	36.34

The comparison of results show that the sediment volume can be computed for 2025, 2050, 2075 and 2100 for the climate scenarios RCP 2.6, RCP 4.5 and RCP 8.5 by consolidated unit weights of sediment by particle size distribution, porosity of uniformly distributed sediment and frequency analysis in the absence of data from hydrographic survey.

The projected settled sediment rates for 2025, 2050, 2075 and 2100 years for climate scenario RCP 2.6 by different methods are given Table 6.18. The projected settled sediment rates vary from 0.437 to 0.603 Mm^3 for the methods such as particle size distribution, porosity of uniform sediment, hydrographic survey and frequency analysis. The projected settled sediment rate varies from 25.70 to 25.98 Mm^3. The projected settled sediment rates for 2025, 2050, 2075 and 2100 years for climate scenario RCP 4.5 by different methods are given Table 6.19. The projected settled sediment rates vary from 0.413 to 0.662 Mm^3 for the methods such as particle

size distribution, porosity of uniform sediment, hydrographic survey and frequency analysis. The projected settled sediment rates for 2025, 2050, 2075 and 2100 years for climate scenario RCP 8.5 by different methods are given Table 6.20. The projected settled sediment rates vary from 0.445 to 0.718 Mm^3 for the methods such as particle size distribution, porosity of uniform sediment, hydrographic survey and frequency analysis.

Table 6.18 Projected settled sediment rate by different methods for RCP 2.6

Year	Sediment rate (Mm^3)				
	Particle size Distribution	Porosity of uniform Sediment	Hydrographic survey	Frequency analysis	Empirical formula
2025	0.481	0.437	0.501	0.471	25.98
2050	0.579	0.518	0.603	0.549	25.94
2075	0.522	0.459	0.544	0.482	25.85
2100	0.532	0.458	0.554	0.481	25.70

Table 6.19 Projected settled sediment rate by different methods for RCP 4.5

Year	Sediment rate (Mm^3)				
	Particle size Distribution	Porosity of uniform Sediment	Hydrographic survey	Frequency analysis	Empirical formula
2025	0.454	0.413	0.474	0.445	25.98
2050	0.636	0.569	0.662	0.603	25.94
2075	0.575	0.505	0.599	0.531	25.85
2100	0.594	0.512	0.619	0.537	25.70

Table 6.20 Projected settled sediment rate by different methods for RCP 8.5

Year	Sediment rate (Mm^3)				
	Particle size Distribution	Porosity of uniform Sediment	Hydrographic survey	Frequency analysis	Empirical formula
2025	0.490	0.445	0.511	0.480	25.98
2050	0.583	0.522	0.607	0.553	25.94
2075	0.527	0.463	0.549	0.487	25.85
2100	0.689	0.594	0.718	0.623	25.70

The observed settled sediment rate from hydrographic survey for the period from 1974 to 2004-05 is given in Table 6.21. The average sediment rate for the period from 1974 to 2004-05 by hydrographic survey is 21.705 Mm^3 which is very close the projected settled sediment rate by empirical formula. The projected settled sediment rates by different methods for the climate

scenarios RCP 2.6, RCP 4.5 and RCP 8.5 are much lower than the observed settled sediment rate from hydrographic survey for the period from 1974 to 2004-05. The higher observed settled sediment rate may be due to the anthropogenic activity in the catchment.

Table 6.21 Settled sediment rate from hydrographic survey

Sl. no.	Survey year	Reservoir capacity (Mm^3)	Sedimentation volume (Mm^3)	Sedimentation rate (Mm^3)
1	1974	8578.99	0	0
2	1974-80	8408.05	170.94	28.49
3	1980-82	8347.46	60.59	30.295
4	1982-84	8257.65	89.81	44.905
5	1984-86	8159.38	98.27	49.135
6	1986-88	8114.22	45.16	22.58
7	1988-89	8088.66	25.56	25.56
8	1989-90	8070.92	17.74	17.74
9	1990-91	8052.99	17.93	17.93
10	1991-92	8042.01	10.98	10.98
11	1992-93	8033.4	8.61	8.61
12	1993-94	8025.36	8.04	8.04
13	1994-96	7983.04	42.32	21.16
14	1996-97	7964.12	18.92	18.92
15	1997-98	7942.43	21.69	21.69
16	1998-99	7918.06	24.37	24.37
17	1999-00	7896.04	22.02	22.02
18	2000-01	7887.42	8.62	8.62
19	2001-02	7871.6	15.82	15.82
20	2002-03	7850.9	20.7	20.7
21	2003-04	7828.99	21.91	21.91
22	2004-05	7812.66	16.33	16.33

Chapter 7.0 Conclusion

Soil erosion is the major cause of land degradation and reservoir sedimentation. The performance of the reservoirs gets reduced mainly due to the high sediment flow resulting from the unpredicted activities in the catchment of the reservoirs. The estimation of sediment yield from watershed is very important for ascertaining the useful life of reservoir for meeting its intended purposes. IPPC predicts more number of high intensity rainfalls due to increased anthropogenic emissions of green house gases and thus the soil erosion and sedimentation will also aggravated during the next century. It is imperative to study the effect of climate change on sediment yield to Pong reservoir as the Himalayan watersheds generate more sediment in general.

In this study, SWAT (Soil and Water Assessment Tool) was used to simulate the runoff and sediment from the catchment of Beas up to Nadaun Bridge. The input data such as DEM, LULC and soil type were generated from different sources such as National Aeronautics and Space Administration (NASA), USA, Landsat 8 OLI, USGS and National Bureau of Soil Survey and Land Use Planning (NBSSLUP), India. Grid based meteorological data such as daily rainfall, minimum and maximum temperatures were obtained from Indian Meteorological Department (IMD). The model was calibrated using the data of stream flow and sediment yield for the period from 1987 to 1995 and validated with data for the period from 1996 to 2005. The sensitive parameters for streamflow and sediment yield were optimized by SUFI2 algorithm (Sequential Uncertainty Fitting version 2). The simulated values of sediment yield were found to be in good agreement with the observed values. The performance of the model was evaluated on the basis of statistical parameters. The values of coefficient of determination (R^2) for streamflow and sediment yield were found to be 0.79 and 0.64 for calibration period and 0.76 and 0.61 for validation period.

The statistical downscaling model (SDSM) was used to downscale the daily rainfall, minimum and maximum temperature for the location, Nadaun Bridge, Himachal Pradesh from General Circulation Model (GCM) Coupled Model Intercomparison Project Phase 5 (CMIP5):

Canadian Earth System Model, CanESM2. In SDSM, the multiple linear regression (MLR) technique was used to derive the statistical relationships between observed small-scale variables and larger GCM scale. The daily rainfall, minimum temperature and maximum temperature data of Indian Meteorological Department (IMD) (1961-2005) of the Nadaun Bridge, Himachal Pradesh was considered as input to the model. This daily rainfall, minimum and maximum temperature data were predictands for the SDSM model. The MLR model was calibrated and validated with the daily rainfall, minimum and maximum temperature for the period of 1961 to1995 and 1996 to 2005 respectively. National Centre for Environmental Prediction (NCEP) reanalysis data (historical) were used as a predictor, which consists of 26 parameters. Monthly rainfall was predicted on the basis of future daily rainfall by MLR model with the predictors from CanESM2 for the period from 2006 to 2100 under the RCP 2.6, RCP 4.5and RCP 8.5 emission scenarios. The same procedure was adopted for the downscaling of the minimum and maximum temperature for the period from 2006 to 2100 under the RCP 2.6, RCP 4.5 and RCP 8.5 emission scenarios. The monthly streamflow and sediment yield for the period from 2006 to 2100 were projected using the monthly projected rainfall, minimum and maximum temperature under the RCP 2.6, RCP 4.5 and RCP 8.5 emission scenarios and the other meteorological data from SWAT website with optimized parameters for streamflow and sediment yield obtained from SWAT-CUP using the hydrometeorological data for the period from 1987 to 2005. The unit weight of deposited sediment in the reservoir was computed from particle size distribution of suspended sediment concentration and the method of reservoir operation by the procedure suggested by USBR, from the sediment volume observed by hydrographic survey and assuming porosity of uniformly distributed sediment in the reservoir. The consolidated unit weights of the sediment were computed by the equation proposed by Miller of USBR and frequency analysis of unit weights derived from particle size distribution. The consolidated unit weights computed by different methods were used to project the sediment volume and the life of the reservoir for the climate scenarios RCP 2.6, RCP 4.5 and RCP 8.5 for 2025, 2050, 2075 and 2100. The comparison of results shows that the sediment volume can be computed for 2025, 2050, 2075 and 2100 for the climate scenarios RCP 2.6, RCP 4.5 and RCP 8.5 by consolidated unit weights of sediment by particle size distribution, porosity of uniformly distributed sediment and frequency analysis in the absence of data from hydrographic survey. The average sediment rate for the period from 1974 to 2004-05 by hydrographic survey is 21.705 Mm^3 which is very close

the projected settled sediment rate by empirical formula. The projected settled sediment rates by different methods for the climate scenarios RCP 2.6, RCP 4.5 and RCP 8.5 are much lower than the observed settled sediment rate from hydrographic survey for the period from 1974 to 2004-05. The higher observed settled sediment rate may be due to the anthropogenic activity in the catchment.

Chapter 8 References

1. Arnold, J. G., Srinivasan, R., Muttiah, R. S., and Williams, J. R. (1998). "Large area Hydrologic modeling and assessment part I: Model development." Journal of the American water resources association, 34(1), 73-89, https://doi.org/10.1111/j.1752-1688.1998.tb05961.x.

2. Ayana, A.B., Edossa, D.C., and Kositsakulchi, E. (2012). "Simulation of sediment yield using SWAT model in Fincha watershed, Ethiopia." Kasetsart Journal Natural Sciences. 46, 283 – 297.

3. Awotwi, A., Kumi, M., Jansson, P.E.**,** Yeboah, F.**,** and Nti, I. K. (2015). **"**Predicting Hydrological Response to Climate Change in the White Volta Catchment, West Africa.**"** Journal of Earth Science and climate change, ISSN:2157-7617 JESCC, 6(1), https://doi:10.4172/2157-7617.1000249.

4. Azari, M., Moradi, H. R., Saghafian, B., and Faramarzi, M. et al. (2016). "Climate change impacts on streamflow and sediment yield in the North of Iran." Hydrological sciences journal, 61(1), 123–133, https://doi.org/10.1080/02626667.2014.967695.

5. Bagnold, R. A. (1977)." Bed load transport by natural rivers." Water Resources Research, 13(2), 303-312, https://doi.org/10.1029/WR013i002p00303.

6. Betrie, G. D., Mohamed, Y. A., Griensven, A. V., and Srinivasan, R. (2011). "Sediment management modelling in the Blue Nile Basin using SWAT model." Journal of Hydrology and Earth System Sciences, 15(3), 807-818, https://doi.org/10.5194/hess-15-807-2011.

7. Biggs, T. W., Gaur, A., Scott, C. A., et al (2007). "Closing of the Krishna Basin: Irrigation, stream flow depletion and macro scale hydrology." International Water Management Institute Research Report, Colombo, Sri Lanka.

8. Climate Change (2014). Impacts, Adaptation and Vulnerability: Summary for policy makers, IPPC WGII AR5 Phase I report, March 2014.

9. Chandra Prabhat , P. L. Patel, and P. D. Porey (2016). “Prediction of sediment erosion pattern in Upper Tapi Basin, India.” Research articles, Current Science, 110(6), 1038-1049.

10. Deasy, C., Brazier, R. E., Heathwaite, A. L., and Hodgkinson, R. (2009). “Pathways of runoff and sediment transfer in small agricultural catchments.” Hydrological Processes, 23(9), 1349-1358, https://doi.org/10.1002/hyp.7257.

11. Dugan, H. A., Lamoureux, S. F., Lafreniere, M. J., and Lewis, T. (2009). “Hydrological and sediment yield response to summer rainfall in a small high arctic watershed.” Hydrological Processes, 23(10), 1514-1526, https://doi.org/10.1002/hyp.7285.

12. Doomen, A. M. C., Wijma, E., Zwolsman, J. J. G., and Middelkoop, H. (2008). “Predicting suspended sediment concentrations in the Meuse River using a supply-based rating curve.” Hydrological Processes, 22(12), 1846-1856, https://doi.org/10.1002/hyp.6767.

13. Easton, Z. M., Fuka, D. R., White, E. D., Collick, A. S., Ashagre, B. B., McCartney, M., Awulachew, S. B., Ahmed, A. A., and Steenhuis, T. S. (2010). “A multi basin SWAT model analysis of runoff and sedimentation in the Blue Nile, Ethiopia.” Journal of Hydrology and Earth System Sciences, 14(10), 1827-1841, https://doi.org/10.5194/hess-14-1827-2010.

14. Fengping, L., Zhang, G., and Xu, Y. J. (2016). “Assessing Climate Change Impacts on Water Resources in the Songhua River Basin.” MDPI Water 2016, 8(10), 420; https://doi:10.3390/w8100420.

15. Gassman, P. W., Reyes, M. R., Green, C. H., & Arnold, J. G. (2007). “The Soil and Water Assessment Tool: Historical development, applications, and future research directions.” Journal of American Society of Agricultural and Biological Engineers, 50(4): 1211-1250.

16. Geza, M., and McCray, J. E. (2007). "Effects of soil data resolution on SWAT model stream flow and water quality predictions". Journal of Environmental Management, 88(3), 393–406, https://doi.org/10.1016/j.jenvman.2007.03.016.

17. Gupta, S. K., Jethoo, A. S., Tyagi, J. V., Gupta, N. K., and Gautam, P. K. (2015). "Application of Hydrological Models in Water resources: A Review." International Journal of Computer & Mathematical Sciences IJCMS ISSN 2347 – 8527.

18. Garde, R. J., and Rangaraju, K. G. (1985). Mechanics of sediment transportation and alluvial stream problems, Wiley Eastern Limited, New Delhi.

19. Gao, P., and Pasternack, G. (2007). "Dynamics of suspended sediment transport at field-scale drain channels of irrigation-dominated watersheds in the Sonoran Desert, southeastern California." Hydrological Processes, 21(16), 2081-2092, https://doi.org/10.1002/hyp.6398.

20. Gao, P., Deng J., Chai, X., Mu, X., Zhao, G., Shao, H., and Sun, W. (2017). "Dynamic sediment discharge in the Hekou-Longmen region of Yellow river and soil and water Conservation implications." Science of the Total Environment, 578, 56-66, https://doi.org/10.1016/j.scitotenv.2016.06.128.

21. Graf, W. H. (1984). Hydraulics of sediment transport, Water Resources Publications, P.O. Box 2481, Littleton, Colorado 80161, U.S.A.

22. Horowitz, A.J., Elrick, K. A., and Smith, J. J. (2008). "Monitoring urban impacts on suspended sediment, trace element, and nutrient fluxes within the city of Atlanta, Gerogia, USA: program design, methodological considerations, and initial results." Hydrological Processes, 22(10), 1473-1496, https://doi.org/10.1002/hyp.6699.

23. Janapriya, S., Santhana Bosu, S., and Kannan, B. (2016), "Impact of climate change on hydrology of Manjalar sub basin of river Vaigai in Tamil Nadu, India." Journal of Applied and Natural Science, 8 (3), 1670 – 1679, https://doi.org/10.31018/jans.v8i3.1021.

24. Jain, S. K., Tyagi, J., & Singh, V. (2010). “Simulation of runoff and sediment yield for a Himalayan watershed using SWAT model.” Journal of Water Resource and Protection, 2(3), 267, doi:10.4236/jwarp.2010.23031.

25. Lin, S., Jing, C., Chaplot, V., Yu, X., Zhang, Z., Moore, V., and Wu, J. (2010) “Effect of DEM resolution on SWAT outputs of runoff, sediment and nutrients.” Journal of Hydrology and Earth System Sciences. 7, 4411– 4435, https://doi.org/10.5194/hessd-7-4411-2010.

26. Mano, V., Nemery, J., Belleudy, P., and Poirel, A. (2009). “Assessment of suspended sediment transport in four alpine watersheds (France): influence of the climate regime.” Hydrological Processes, 23(5), 777-792, https://doi.org/10.1002/hyp.7178.

27. Mathlothi, M., and Lebdi, F. (2018). “Estimation of sediment deposits in the Ghezala reservoir in Northern Tunisia.” Proc. IAHS, 377, 35-40, https://doi.org/10.5194/piahs-377-35-2018.

28. Morris, G. L., and Fan, J. (1997). Reservoir sedimentation handbook – Design and Management of Dams, Reservoirs, and Watersheds for Sustainable Use, McGraw-Hill, New Delhi.

29. Moriasi, D. N., Arnold, J. G., Van Liew, M. W., Bingner, R. L., Harmel, T. L., and Veith, R. D.(2007). “Model evaluation guidelines for systematic quantification of accuracy in watershed simulations.” Soil & Water Division of American Society of Agricultural and Biological Engineers, 50(3), 885−900.

30. Monteclos-Zamora, Y., Cavazos, T., Kretzschmar, T., Vivoni, E. R., Corzo, G., and Molina-Navarro, E., (2018). “Hydrological Modeling of Climate Change Impacts in a Tropical River Basin: A Case Study of the Cauto River, Cuba” MDPI Water 2018, 10(9), 1135; https://doi.org/10.3390/w10091135.

31. Nagle, G. N., Fahey, T. J., Ritchie, J. C., and Woodbury, P.B. (2007). "Variations in sediment sources and yields in the Finger Lakes and Catskills regions of New York." Hydrological Processes, 21(6), 828-838, https://doi.org/10.1002/hyp.6611.

32. Nagy, H. M., Watanabe, K., and Hirano, M. (2002). "Prediction of sediment load concentration in rivers using artificial neural networks." Journal of Hydraulic Engineering, 128(6), 588-595, https://doi.org/10.1061/(ASCE)0733-9429(2002)128:6(588).

33. Neitsch, S. L., Arnold, J.G., Kiniry, J. R., and Williams J. R. (2005). Soil and Water Assessment Tool Theoretical Documentation – Version 2005, Grassland, Soil and Water Research Laboratory, Agricultural Research Service, 808 East Blackland Road, Temple, Texas 76502.

34. Omani, N., Tajrishy, M., and Abrishamch, A. (2000). "Modeling of a River Basin Using SWAT Model and SUFI-2." Fourth International Conference of SWAT Model, Delft, Netherlands.

35. Patil, N. S., Raikar, R. V., and Manoj, S. (2014). "Runoff Modelling for Bhima River using Swat Hydrological Model." International Journal of Engineering Research & Technology, (IJERT) ISSN: 2278-0181 3(7) 923-928.

36. Parajuli, P. B., Nelson, N. O., Frees, L. D., and Mankin, K. R. (2009). "Comparison of AnnAGNPS and SWAT model simulation results in USDA-CEAP agricultural watersheds in south-central Kansas." Hydrological Processes, 23(5), 748-763, https://doi.org/10.1002/hyp.7174.

37. Papanicolaou, A, N., Elahakeem, M., Krallis, G., Prakash, S., and Edinger, J. (2008). "Sediment transport modelling review-Current and Future developments." Journal of Hydraulic Engineering, 134(1), 1-14, https://doi.org/10.1061/(ASCE)0733-9429(2008)134:1(1).

38. Pandey, A., Chowdhary, V. M., Mal, B. C., and Billib, M. (2009). "Application of the WEPP model for prioritization and evaluation of best management practices in an Indian watershed." Hydrological Processes, 23(21), 2997-3005, https://doi.org/10.1002/hyp.7411.
39. Paul, P. K., and Mishra, A. (2014). "Uncertainty of climate change impacts on sediment yield in Brahmani river basin in India" National Conference on Emerging Technology Trends in Agricultural Engineering, ETTAE 2014, NERIST, Nirjuli (Itanagar).
40. Principe, J. A. (2012). "Exploring climate change effects on watershed sediment yield and land cover-based mitigation measures using SWAT model, RS and GIS: Case of Cagayan River basin, Philippines." International Archives of the Photogrammetry, Remote Sensing and Spatial Information Sciences, Vol XXXIX-B8, 193-198.
41. Raneesh, K., Surya, T.V., and Thampi, S. G. (2010). "Prediction of Stream flow and Sediment Yield in the Chaliyar River Basin, Kerala, India." International Journal of Earth Sciences and Engineering, 3(5), 654 – 661.
42. Refsgaard, J. C. (1997). "Parameterization, calibration and validation of distributed hydrological models". Journal of Hydrology, 198(1-4), 69-97, https://doi.org/10.1016/S0022-1694(96)03329-X.
43. Rijn, L. C. (1984a). "Sediment transport, Part I: Bed load transport." Journal of Hydraulic Engineering, 110(10), 1431-1456, https://doi.org/10.1061/(ASCE)0733-9429(1984)110:10(1431).
44. Rijn, L. C. (1984b). "Sediment transport, Part II: Suspended load transport." Journal of Hydraulic Engineering, 110(11), 1613-1641, https://doi.org/10.1061/(ASCE)0733-9429(1984)110:11(1613).
45. Rijn, L. C. (1984c). "Sediment transport, Part III: Bed forms and alluvial roughness." Journal of Hydraulic Engineering., 110(12), 1733-1754, https://doi.org/10.1061/(ASCE)0733-9429(1984)110:12(1733).

46. Rodriguez-Blanco et al (2016). "Potential Impact of Climate Change on Suspended Sediment Yield in NW Spain: A Case Study on the Corbeira Catchment." MDPI Water 2016, 8, 444; https://doi.org/10.3390/w8100444.

47. Kumar, S., and Mishra, A. (2015). "Critical Erosion Area Identification Based on Hydrological Response Unit Level for Effective Sedimentation Control in a River Basin." Water Resources Management, 29(6), 1749-1765, https://doi.org/10.1007/s11269-014-0909-3.

48. Sangroula, D. P. (2005). "Sedimentation and sustainability of the Kulekhani reservoir. A Himalayan case." Doctoral Thesis at NTNU-Trondheim, Norwegian University of Science and Technology.

49. Setegn, S. G., Srinivasan, R., and Dargahi, B. (2008). "Hydrological modelling in the Lake Tana Basin, Ethiopia using SWAT model." The Open Hydrology Journal, 2, 49-62.

50. Singh, G., Babu, R., Pratap, N., Bhushan, L. S., and Abrol, I. P. (1992)."Soil erosion rate in India." Journal of Soil and Water Conservation, 47(1), 97–99.

51. Singh, R., and Phadke, V.S. (2006). "Assessing soil loss by water erosion in Jamni River Basin, Bundelkhand region, India, adopting universal soil loss equation using GIS." Current Science, 90(10), 1431-1435.

52. Shrivastava, P. K., Tripathi, M. P., and Das, N.S.(2004). "Hydrological modelling of small watershed using satellite data and GIS technique." Journal of the Indian Society of Remote Sensing, 32(2), 145-157, https://doi.org/10.1007/BF03030871.

53. Smith, H. G. (2008). "Estimation of suspended sediment loads and delivery in an incised upland headwater catchment, south-eastern Australia." Hydrological Processes, 22(16), 3135-3148, https://doi.org/10.1002/hyp.6898.

54. Schwab, G. O., Fangmeier, D. D., Elliot, W. J., and Frevert, R. K. (1993). Soil and water conservation engineering, John Wiley & Sons, Inc, New York.

55. Shahin, M. M. A. (1993). “An overview of reservoir sedimentation in some African river basins.” Sediment Problems: Strategies for Monitoring, Prediction and Control (Proceedings of the Yokohama Symposium, July 1993), IAHS Publ. No. 217, 93-100.

56. Shrestha, B., Babel, M. S., Maskey, S., Griensven, A. V., Uhlenbrook, S., Green, A., and Akkharath, I. (2013). “Impact of climate change on sediment yield in the Mekong River basin: a case study of the Nam Ou basin, Lao PDR.” Hydrology and Earth System Sciences, 17, 1–20, https://doi.org/10.5194/hess-17-1-2013.

57. Sharanya, T. M., Mudbhatkal, A., and Mahesha, A. (2018). “Assessing climate change impacts on river hydrology – A case study in the Western Ghats of India.” Journal of Earth System Science, 127(6), Article 78, https://doi.org/10.1007/s12040-018-0979-3.

58. Soil and Water Assessment Tool Theoretical Documentation, Version 2009. (2011). TR-406, Texas Water Resources Institute, Texas A&M University, USA.

59. Suresh, R. (1997). Soil and Water Conservation Engineering, Second edition, Standard Publisher Distributors, Delhi, India.

60. SWAT 2012, Input/Output Documentation. (2012). TR-439, Texas Water Resources Institute, Texas A&M University, USA.

61. Tayfur, G. (2002). “Applicability of sediment transport capacity models for nonsteady state erosion from steep slopes.” Journal of Hydrologic Engineering, 7(3), 252-259, https://doi.org/10.1061/(ASCE)1084-0699(2002)7:3(252).

62. Tejwani, K.G. (1984). “Reservoir sedimentation in India-Its causes, Control, and Future course of action.” *Water International*, 9, 150-154, https://doi.org/10.1080/02508068408686525.

63. Tomas D. Reyes, JR. (2017). “Application of Soil and Water Assessment Tool (SWAT) Model to predict streamflow and sediment yield in Wahig-Inabanga watershed, Bohol,

Philippines." International Journal of Environmental and Rural Development, 8(1), 104-110, https://doi.org/10.32115/ijerd.8.1_104.

64. Tripathi, M. P., Raghuwanshi, N. S., and Rao, G. P. (2006). "Effect of watershed subdivision on simulation of water balance components." Hydrological Processes, 20(5), 1137-1156, https://doi.org/10.1002/hyp.5927.

65. Tyagi, J. V., Rai, S. P., Qazi, N., and Singh, M. P. (2014). "Assessment of discharge and sediment transport from different forest cover types in lower Himalaya using Soil and Water Assessment Tool (SWAT)." International Journal of Water Resources and Environmental Engineering, 6(1), 49-66, https://doi.org/10.5897/IJWREE2013.0448.

66. Thawait, A. K., and Chauhan, M. S. (2015) "Sediment Yield Modelling of Mohgaon Watershed of Narmada River Basin using SWAT Model." International Journal of Engineering and Technical Research (IJETR) ISSN: 2321-0869.

67. Williams, J. R., Nicks, A. D., and Arnold, J. G. (1985). "Simulator for water resources in rural basins." Journal of Hydraulic Engineering, 111(6), 970-986, https://doi.org/10.1061/(ASCE)0733-9429(1985)111:6(970).

68. Wischmeier, W.H., and Smith, D.D. (1965). "Predicting rainfall-erosion losses from crop land east of the Rocky mountainous." Agriculture Handbook No 282, USDA-ARS, Washington, USA.

69. Woodward, J.C., and Walling, D. E. (2007). "Composite suspended sediment particles in river systems: their incidence, dynamics and physical characteristics." Hydrological Processes, 21(26), 3601-3614, https://doi.org/10.1002/hyp.6586.

70. Xu, Z. X., Pang, J. P., Liu, C. M., and Li, J. Y. (2009). "Assessment of runoff and sediment yield in the Miyun Reservoir catchment by using SWAT model." Hydrological Processes, 23(25), 3619 – 3630, https://doi.org/10.1002/hyp.7475.